McHendry, Pauline (1998) TEM studies of the crystal growth of indanthrone pigments. PhD thesis

http://theses.gla.ac.uk/6575/

TEM STUDIES OF THE
CRYSTAL GROWTH OF
INDANTHRONE PIGMENTS

Pauline McHendry

submitted for the degree of Doctor of Philosophy at the Department of Physics and Astronomy, University of Glasgow

May, 1998

For my mum and dad
and Barry

DECLARATION

This thesis is a record of work carried out by me in the Department of Physics and Astronomy at the University of Glasgow and also at Zeneca Grangemouth. The work described herein is my own, apart from the preparation of drowned out indanthrone and a few selected samples. These samples were supplied by Zeneca. Some of the work contained in this thesis has been published in the following paper:

P McHendry, A J Craven, L J Murphy, 1997, in "Electron Microscopy and Analysis 1997", (Ed. J Rodenburg), IOP Conference Series 153, 671- 674

This thesis has not been previously submitted for a higher degree.

CONTENTS

Chapter 8 - Conclusions and Further Work

List of References

SUMMARY

The aim of this work was to study the crystal growth of indanthrone during the pigmentation process. The colouring properties of a pigment are dependant on the chemical and crystallographic structure of the pigment. However, other factors are known to affect these properties including particle size, particle size distribution and level of dispersion in the chosen application medium. The parameters which affect the growth of the pigment particles were investigated with the emphasis placed on the mechanism by which growth took place. The final form of the crystals after growth was also investigated in some detail. Various electron microscopy techniques were employed in the investigations in this thesis. High and low magnification imaging and diffraction were studied on the CTEM (conventional transmission electron microscope) whilst PEELS (parallel electron energy loss spectroscopy) and DPC (differential phase contrast) studies took place on the VG HB5 STEM (scanning transmission electron microscope). In addition to these studies, x-ray diffraction and surface area analysis techniques were employed.

The low magnification CTEM work gave good information on the size, shape and size distribution of the pigment particles and enabled detailed analysis of the level of growth attained under varied reaction conditions. Parameters varied during these reactions included choice of solvent, solvent concentration, reaction time and the method used for

removing the solvent. Methyl benzoate and nitrobenzene were found to be effective in promoting crystal growth in indanthrone whilst isopropanol proved to be extremely ineffective. The rate of growth was found to be affected by, among other things, the concentration of the solvent and the time it was in contact with the pigment. The most likely method of growth has been identified as ripening followed by coalescence. Initially, larger particles grow at the expense of the smaller particles – the smaller ones go into solution and are then able to aid the growth of the larger particles. As they increase in size coalescence is more likely as the surface area along the side of the particles is greater – therefore adhesion by the adjoining particle is more likely. Heat is also an important factor as it promotes the ripening part of this process as this increases both solubility and energy leading to faster ripening.

Diffraction showed that growth is strongly promoted along the same direction (b-axis) in the majority of crystals. Lattice imaging studies confirmed this orientation as the most favoured and also gave detailed structural information. This technique also gave evidence for coalescence as a secondary growth mechanism and illustrated strained crystals.

Annular dark field (ADF) imaging on the VG HB5 indicated that some particles were not of uniform thickness. PEELS confirmed that thickness variations were present in numerous particles due to irregular growth and/or coalescence. Differential phase contrast (DPC) imaging was used to give a topographical image of certain samples and confirmed the presence of undulations on the surface of the particles.

ACKNOWLEDGEMENTS

LIST OF FIGURES

Chapter 3

Chapter 4

LIST OF TABLES

Chapter 1

Introduction

1.1 Organic Pigments

Organic pigments are intensely coloured, finely divided molecular crystals. They are

physically and chemically unaffected by, and thus essentially insoluble in, the

medium into which they are incorporated. The colouring properties of a pigment are

dependant on the chemical and crystallographic structure of the pigment. Other

factors which are known to affect these properties include particle size and shape,

particle size distribution and dispersion of the pigments in the chosen application

medium (McKay, 1988, 1989, Sappok, 1978). In contrast to dyestuffs, organic

pigments retain their crystalline or particulate structure throughout the colouration

process. Organic pigments are usually purer, brighter and richer in colour than inorganic pigments. However, they are also more expensive. They tend to be less resistant to external influences such as sunlight, chemicals and humidity.

The characteristic colour of a pigment is determined primarily by the chemical constitution of its molecules. Certain pigments can also exist in several different lattice arrangements producing pigments sufficiently different in colour that they can be marketed as commercially distinct types of pigment (Fryer, 1981).

Colour strength in a pigment is brought about by the selective absorption and/or scattering of visible electromagnetic radiation by the pigment particles. Absorption of this radiation increases markedly with decrease in particle size in the submicron region and thus the colour strength is also improved. This is due to the fact that indanthrone is a strong absorber and the radiation penetration depth is short. A small depth near the surface of the particle is thus where the majority of the absorption takes place. Therefore, for a certain mass of pigment, a smaller average particle size increases the total surface area available to assist in the absorption and/or scattering of electromagnetic radiation. However, particles that are too small will tend to flocculate in the final ink or paint resin system hence reducing the available surface area (Carr, 1978). Thus, with many pigments, the colour strength does not increase continuously with decrease in particle size unless the pigment has been fully dispersed. In the majority of cases, colour strength appears to be maximised when pigment particles are of the order of 10-100nm in size. At this level, the particles are

finely divided and the interiors of the particles are able to absorb light as effectively as the surfaces.

Since the pigments are insoluble in their application medium, dispersion of the pigment usually takes place by mechanical means. The degree of this dispersion affects how well a pigment can impart colour to application systems such as printing inks, paints, surface coatings, plastics and artificial fibres (Carr, 1978, 1982, Cowley, 1987). The ideal pigment would consist entirely of primary particles, also known as single crystals. However, these primary particles are very often attached at their surfaces forming aggregates. This is due to the fact that primary particles are relatively small and thus their centres of gravity are situated close together. The particles then cling to one another due to short range attractive forces such as Van der Waals and London forces forming aggregates. Obviously these aggregates will have a smaller surface area than the sum of the surfaces of the primary particles and this will have implications on the colour strength of the pigment. Agglomerates are loose arrangements of primary particles or aggregates or a mixture of the two together. They are not bound together as with aggregates, and will therefore have a surface area equal to the sum of the surfaces of the contributing components. The degree of cohesion of such agglomerates will affect the texture of the powder, how dusty it is and will also have an effect on the dispersibility.

It can be seen that the final size and shape of particles in a pigment powder play a large rôle in determining the pigment properties. Crystal growth is thus an important parameter in the pigmentation process and methods of controlling the degree of

3

growth are being studied in order that the optimum crystal size may be obtained. The pthalocyanine pigments have been studied extensively by electron microscopy (Smith, 1997, Fryer, 1981, 1993, 1980) to gain information on their crystal properties. However, indanthrone has not been subjected to detailed study and thus further information on this organic pigment would be highly desirable.

1.2 Indanthrone

Indanthrone (figure 1.1) is a complex organic molecule which is of great interest due to its commercial significance in the pigments industry.
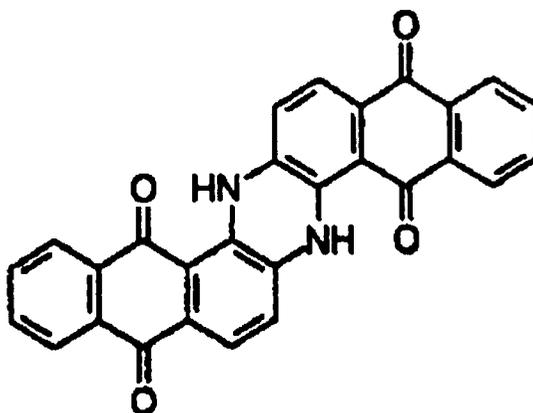
Figure 1.1 : Indanthrone

It is known to exist in several polymorphic forms with the crystal structure of the stable α form being as follows:-

Monoclinic; a = 3.083nm; b = 0.3833nm; c = 0.7845nm; β=91°55'; Space group P2$_1$/a (Bailey 1955). There are two molecules in the unit cell. Indanthrone was

4

discovered in 1901 at Badische Anilin-und-Soda-Fabrik (BASF) by René Bohn whilst attempting to produce an anthraquinone substance similar to indigo. He showed that it was possible to produce indanthrone by alkaline fusion of 2-aminoanthraquinone (Swan & Felton, 1957). Indanthrone, or 5,6,9,14,15,18-hexahydroanthrazine-5,9,14,18-tetrone has the formula $C_{28}H_{14}O_4N_2$ showing that it is formed by the loss of 4 hydrogen atoms from 2 molecules of 2-aminoanthraquinone. It contains no free amino groups. Indanthrone is known in the pigments industry as Pigment Blue 60 and has excellent stability and colour fastness. Zeneca manufacture indanthrone which is subsequently marketed under the trade name Monolite Blue 3R.

Crystal growth in indanthrone is usually promoted along the b-axis of the crystal (Bailey, 1955) implying that molecules are most likely to attach themselves to the crystal on the (010) face where they lie flat.
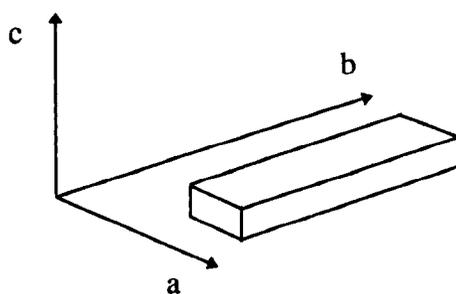
Figure 1.2: A schematic diagram of an indanthrone particle after typical solvent conditioning.

It has been suggested (Wyman, 1956) that the noteworthy stability of indanthrone and its deep blue colour are more readily explained on the basis of the fully conjugated structure as shown in figure 1.3.
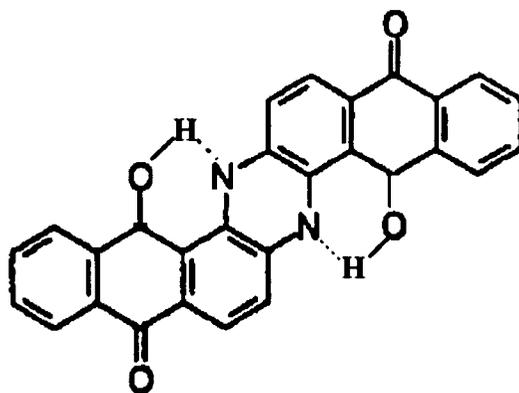
Figure 1.3: Fully conjugated indanthrone

Indanthrone, like most organic material, is damaged by the electron beam leading to loss of crystallinity. The consequences of radiation damage in indanthrone is discussed in section 3.11.

Molecular modelling simulations of indanthrone were carried out in the Chemistry Department of Glasgow University using the Cerius software package. Such simulations give useful information on the orientation of the molecules within the unit cells and how they fit together as the molecule undergoes a growth process. Figures 1.4 to 1.6 show simulations of indanthrone for an observer looking along the b, c and a axes. This order was chosen to assist visualisation. These simulations are particularly useful when considering which constituents of the molecule are exposed in an indanthrone crystal and thereby assisting in the determination of active sites in the molecule.
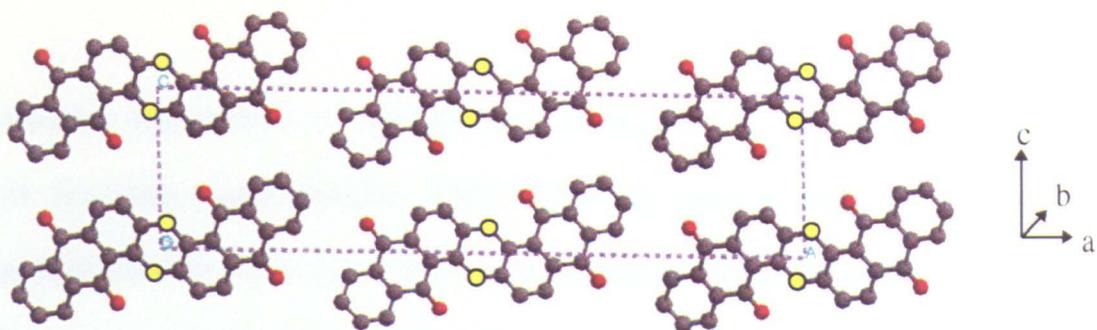
Figure 1.4
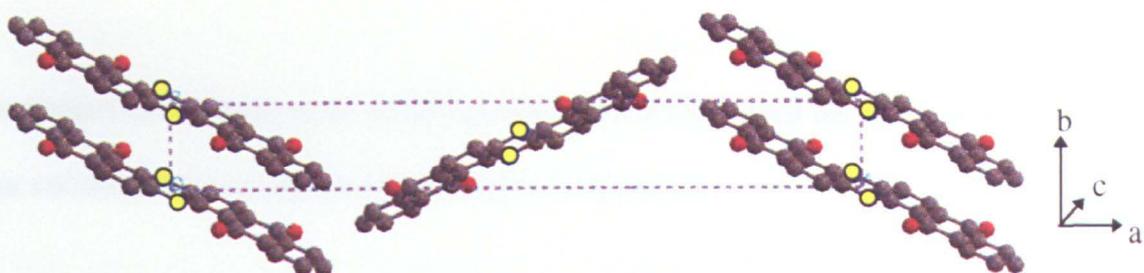
Figure 1.5
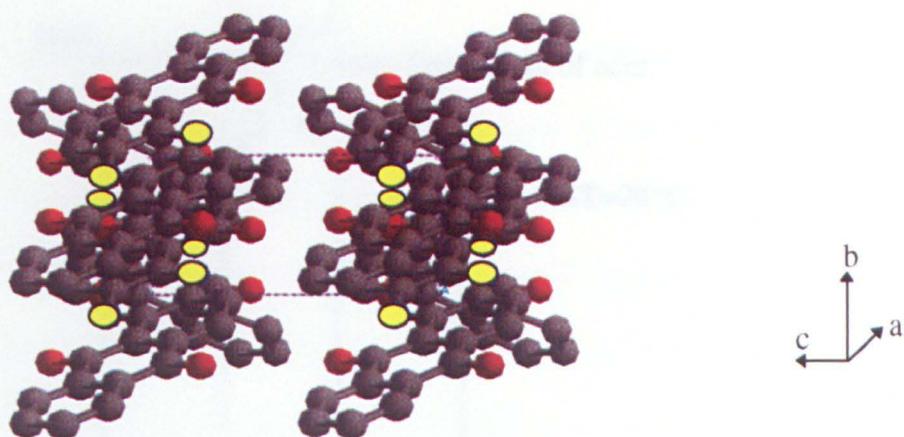
Figure 1.6

Figures 1.4 to 1.6 show Cerius Molecular Modelling Simulations for indanthrone looking along the b, c and a directions respectively. Red balls simulate oxygen molecules whilst yellow balls simulate nitrogen molecules.

1.3 Industrial Pigmentation of Indanthrone

The industrial pigmentation of indanthrone or manufacture of Monolite Blue 3R, involves two main stages (Murphy, 1995). The first stage is size reduction by milling, acid turbulent drown out (ATDO) or acid pasting of the crude indanthrone to produce the non-crystalline, amorphous, drowned-out form of the pigment. This can be followed by solvent conditioning to promote crystal growth thereby producing the final form of the pigment with the desired properties.

This project has focused on an ATDO process. ATDO is carried out at a pressure of 2 bar and the process is shown schematically in figure 1.7.
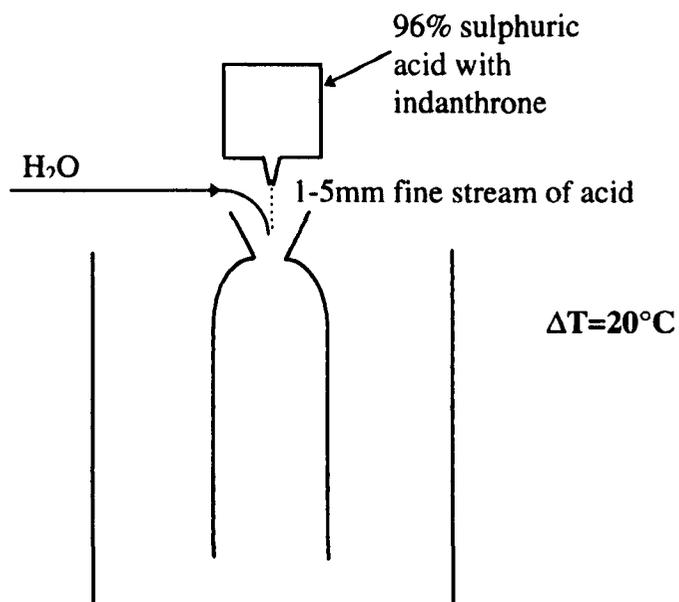
Figure 1.7 : Schematic diagram showing ATDO

ΔT is defined as the difference in temperature of the water before and after addition of acid and is a controlling factor in the exothermic reaction.

Solvent conditioning is then carried out on the drowned-out indanthrone. Details of solvents used are given in section 2.4. Indanthrone powder of known dry weight is combined with water weighing ten times this amount. Sodium sulphate and sodium bicarbonate are then added in quantities weighing 1/20th of the dry weight of indanthrone powder, ensuring the reaction mixture has the required pH. This mixture is heated in a large reaction vessel on the plant and is constantly agitated. Once the mixture has increased sufficiently in temperature, the solvent is added into the reaction vessel and the reflux process begins. Solvent concentration and reflux time are both parameters which affect the rate of growth and are therefore monitored carefully to ensure that the desired level of growth is achieved. More detailed discussion of parameters affecting crystal growth in indanthrone is given in section 2.3. After reflux, the solvent is recovered by distillation and can be re-used. This has obvious environmental benefits especially when the toxicity of the solvents are considered. Once solvent removal is complete, the pigment powder is dried and then milled to break down agglomerates and large aggregates. Primary particles are only present in small proportions in pigment powders. The pigment is now in its final form and is ready for transfer to the desired application medium.

1.4 Specimen Preparation

In order to examine the physical properties of the pigment which affect its performance, it is necessary to use a preparation technique which presents the pigments as they would appear in their application medium. Fortunately, like many pigments, indanthrone is insoluble in almost all solvents apart from concentrated sulphuric acid. The pigment particles may therefore be dispersed in a liquid without it affecting their structure. The technique used was similar to that used by Drummond (1985), McColgan (1990) and Smith (1997), although small adaptations have been made. A small amount of indanthrone powder was mixed with a few drops of a dispersing agent, Dispersol T. This was sodium based and was supplied by Zeneca. The mixture was then rubbed out several hundred times on a glass plate using a flexible palette knife. A small amount of a 35% ethanol/water solution was added drop-wise during rubbing out to prevent drying of the mixture. This same ethanol/water solution was placed in a small glass bottle. The pigment mixture was added to this until a transparent blue dispersion with a good colour strength was attained. The experimental apparatus used to produce specimens for use in the electron microscope is shown in figure 1.8. A lid with a hole in the centre was placed on the glass bottle which contained the blue dispersion. Spray tubes were prepared by heating capillary tubes over a Bunsen burner. The end of the tube was bent and then stretched out to give a small diameter at the spraying end. Any surplus glass at this end was cut off to ensure the tube would produce a fine spray. The tube was inserted into the hole in the lid of the glass bottle which was clamped in place. Nitrogen gas fed from a standard gas cylinder created a region of low pressure above
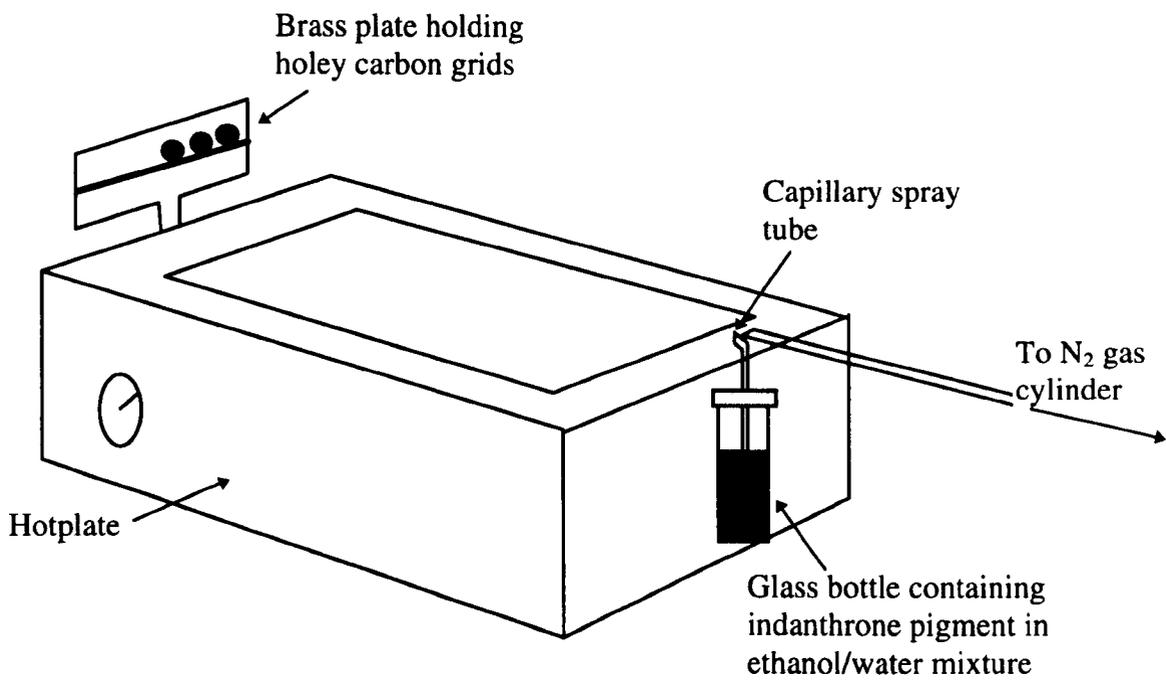
Figure 1.8 : A schematic diagram showing the apparatus used to prepare the indanthrone specimens. During operation, the equipment was encased within a framed metal box with transparent walls and enclosed in a fume cupboard.

the capillary tube, causing liquid to be drawn up the tube forming a spray. The emergent spray was directed across an electrical hot plate. The speed of the spray from the tube was adjusted to be as low as was possible, allowing the ethanol/water mixture to evaporate. This ensured that the pigment particles reaching the grids on the other side of the hotplate were as dry as possible. White paper was fixed directly behind the grids so that the particle density on the grids could be monitored. The optimum level of colour ensured a reasonable amount of particles were deposited on the grid. The grids in use were 300 mesh copper or nickel grids covered by a layer of holey carbon.

1.5 Aims of this Project

The aim of this project is to investigate crystal growth during the pigmentation process of indanthrone using various electron microscopy techniques. Methods used for analysis of the pigments at various stages of the pigmentation process have included conventional transmission electron microscopy, EELS (electron energy loss spectroscopy), DPC imaging (differential phase contrast), XRD (X-ray diffraction), surface area measurement and paint tests.

XRD measurements, carried out at Zeneca Grangemouth, are useful in determining which polymorphic form of indanthrone is present while paint tests show the colour strength and transparency of the pigment. Surface area analysis can be useful in determining the amount of growth which has occurred. This information is most effective when used in conjunction with electron microscopy. The techniques carried

out at Zeneca are described in chapter 2. Also included in this chapter are details of experimental techniques used at Zeneca to produce samples for study and the results of discussions on solvents used in an attempt to promote crystal growth. The reader is introduced to the concept of crystal growth in pigments in section 2.1, where relevant literature is reviewed to provide information on possible growth processes for indanthrone.

Chapter 2 also introduces the samples studied throughout the course of this research. Three different solvents were used to produce these samples. Nitrobenzene, methyl benzoate and isopropanol are discussed and the samples prepared are itemised.

Electron microscopy (carried out at Glasgow University) encompasses a wide range of techniques such as high resolution imaging, diffraction and lattice imaging. These are useful for gaining information on size, shape and size distribution of the particles. Information on the structure and growth direction can also be obtained. EELS and DPC were also carried out at Glasgow University and with these methods it is possible to analyse single particles at room temperature and glean topographic and structural information. These techniques are described in chapter 3.

The results from these experiments are presented in chapters 4, 5, 6 and 7. Chapter 4 gives results obtained from low magnification and surface area studies of indanthrone. Diffraction studies of indanthrone are discussed in chapter 5 whilst lattice imaging results are presented in chapter 6. Chapter 7 is dedicated to results

obtained using the VG HB5 STEM. Here, images obtained using the DPC and PEELS techniques are shown and their significance is discussed.

Finally, in chapter 8 the observations and conclusions from the preceding chapters are reviewed and discussed in terms of the study as a whole. Also included is a discussion on the possibilities for further work in this area.

Chapter 2

Sample Preparation and Characterisation

2.1 Introduction

The aim of this chapter is to describe work carried out at Zeneca Grangemouth over the course of the project. This discussion is opened in section 2.2, where the concept of crystal growth in pigments is considered. Continuing from this into section 2.3, the parameters affecting crystal growth in indanthrone are detailed. Section 2.4 contains a more in-depth discussion of the solvents used in an attempt to promote crystal growth. Three solvents in particular will be examined along with a discussion on their possible effects on indanthrone. As described in section 1.3, the solvent used to promote crystal growth must be removed after the solvent treatment stage. This project studied three techniques for removing this solvent and they are detailed in section 2.5. Some samples

were also investigated at Zeneca Grangemouth using x-ray diffraction and surface area analysis. Both these techniques proved very useful in characterising samples and they are discussed in sections 2.6 and 2.7.

2.2 Crystal Growth in Pigments

Many industries, including the pigment industry, involve the manufacture of stable suspensions which must have particular properties. It is therefore beneficial to have an understanding of the mechanisms which give rise to the formation of such particles and to have a degree of control over their size and shape.

It has long been believed that, in particle growth, the early stages involve nucleation in which the first minute particles are generated from "embryos" (Rideal, 1972). During nucleation, embryos that are smaller than a certain critical size will have a higher solubility and hence a tendency to dissolve, whilst embryos that are larger than this critical size will have a smaller solubility and therefore a tendency to grow. These embryo continue to grow into a macroscopic crystal, until supersaturation collapses; embryos at this stage are known as nuclei. It should be pointed out however, that this nucleation stage is not relevant to the pigments being studied in this project. This is due to the fact that crystal growth on the plant is preceded by acid turbulent drown out or ATDO as discussed in section 1.3. This is a rapid process which results in a large number of nucleation sites to favour the subsequent growth process. Either stage is followed by the growth of these nuclei into microcrystals. There is also the possibility

that such nuclei may revert rather than grow. A microcrystal will have characteristic planes, surfaces and ledges which are bounded by the edges and corners. The rate at which it will grow is determined by the difference between the rate at which constituent molecules arrive and the rate at which they are lost. However, the difference between these values must not be too great otherwise a molecule arriving will not have enough time to fit into the lattice, resulting in lattice dislocations and other imperfections in the crystal. The first-born crystals will be both the largest and the most numerous as they have been exposed to growth conditions for a longer period of time. This is followed by a stage where growth occurs by ripening via the solution. In growth processes such as that described by Ostwald ripening (Dunning, 1972, Honigmann and Horn, 1972), it is known that larger particles tend to grow at the expense of the smaller particles. Molecules from the smaller particles are dissolved in the solution and are then able to attach to larger particles to facilitate growth. Another growth process is also common to many systems. This involves the smaller particles which tend to have more Brownian movement and therefore will suffer frequent collisions with the larger particles. Some of these collisions will result in the particles adhering if the small particle has multi-point contact with the larger one. After some molecular surface migration, the small crystal becomes incorporated into the receiver (Rideal, 1972). This growth process is defined as coalescence and both processes will be discussed further in the results/discussion sections of this thesis.

Another area of interest is whether the crystal form can be modified by adsorption of surfactants. The growth process can be impeded by a solute which can lower the interfacial energy between the crystal and the solution. Where crystals of organic compounds are being grown, as is often the case with pigment growth, surfaces may expose polar or apolar groups. Using selective adsorption of a material with suitable reactive groups, it may be possible to alter the growth. If the impurity added is topologically compatible with the crystal face, but presents a reverse side onto which further molecules of the host material cannot adsorb, then growth perpendicular to that face would be inhibited (Wright, 1995).

2.3 Parameters affecting crystal growth in pigments

During the course of this work, certain parameters affecting crystal growth have been altered to investigate their significance in the crystal growth process. The parameters studied include the solvent used for reflux, the concentration of the solvent, the time allowed for reflux to occur and the method by which the solvent was removed from the reflux mixture. Crystal growth is affected by the use of different solvents due to the way in which they interact with the indanthrone molecules. It is not fully understood why such differences occur but it is thought that it may be connected with the polarity of the solvent in relation to the active sites of the indanthrone molecule. Nitrobenzene, isopropanol and methyl benzoate were studied. These solvents are described in section 2.4. The concentration of solvent in the reflux mixture was also varied. Variation of

solvent concentration in this way will obviously have a major effect on the rate of growth. The reasons for this will be discussed later in this thesis but one factor is likely to be the variation in the amount of solvent molecules which are available for interaction with indanthrone molecules. The time for which reflux was allowed to proceed also has an effect on the level of growth which occurs. This effect appears to be less important than solvent concentration. This may be due to "saturation" since the growth rate drops as particles grow. It is obviously beneficial from an industrial point of view to obtain more information on these growth parameters. Preparations were carried out for varying times to gain an understanding of the growth process as it progresses. With certain preparations, 'sampling' was carried out, i.e. a small amount of reflux mixture was removed at timed intervals. This method removed any discrepancies by ensuring all other factors were kept the same and only time was varied. Finally, the solvent was removed by three different methods. The first and most common was removal by steam distillation, as this is the current method used industrially. As a contrast to this method, one of the solvents was removed by hydrolysis and the effects of this are compared to removal by steam distillation. Different results might be expected due to the fact that steam distillation entails the solvent being held in the reflux mixture at high temperature for some of the removal time whilst with hydrolysis, we assume that the effect of the solvent is negated almost instantaneously. However, hydrolysis is still allowed to continue for 4 hours to ensure complete hydrolysis of the solvent. Steam distillation therefore allows a degree of crystal growth to occur after the reflux stage is over. The final method of removal was by filtration using acetone. This negated any effects of

heat-induced growth as the sample is removed from the oil bath and the solvent is washed off in much cooler apparatus. Due to its simplicity, this method was particularly useful when using the 'sampling' technique which was described earlier in this section. All methods of removal are discussed fully in section 2.5.

2.4 Solvents used in growth of indanthrone

During the pigmentation process, solvents are used to promote crystal growth. Solvent conditioning follows the stage where the initial form of the pigment is broken down. The pigments studied here were all broken down using acid turbulent drown out (ATDO) as discussed in section 1.3. The solvent conditioning process was simulated in the lab using scaled-down apparatus. This is carried out in a fume cupboard using the apparatus set-up shown in figure 2.1.
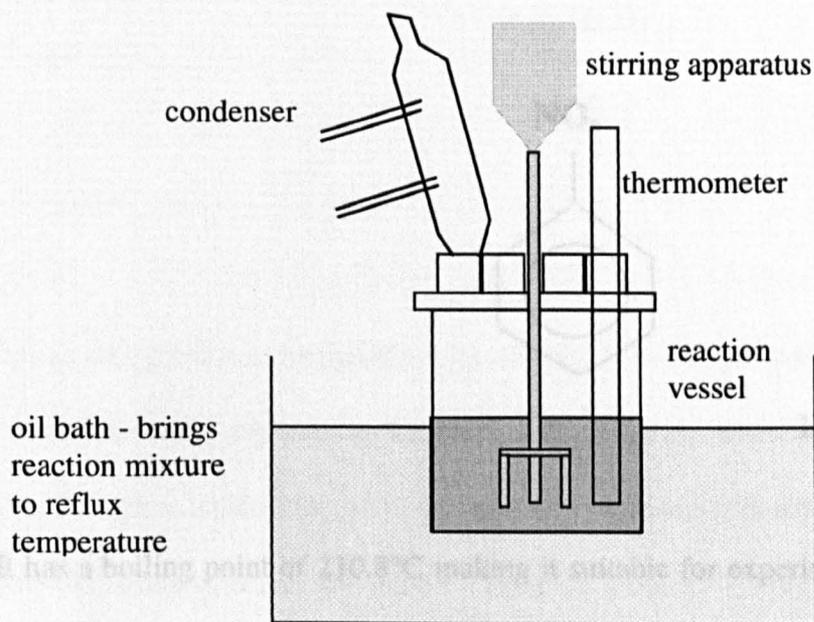
Figure 2.1 : Reflux apparatus

The mixture is brought up to reflux temperature and this is maintained for the desired time whilst the mixture is kept agitated by a mechanical stirrer. In the majority of cases (except those where no water was present, i.e. 100% solvent) the solvent was added once the mixture had reached 80°C. The speed of this stirring motion was kept constant throughout each experiment.

In the industrial preparation of indanthrone pigment at Zeneca Grangemouth, the chosen solvent is used in relatively low concentrations and is known to be an effective growth promoter in indanthrone. The solvents selected for study in this project were chosen after studying the literature and via private communications (Murphy, 1995, Fryer 1996).

Nitrobenzene, $C_6H_5NO_2$, is an aromatic compound as shown in figure 2.2:
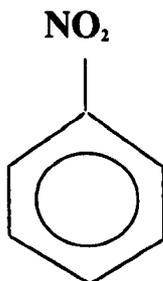
Figure 2.2 : Nitrobenzene

It has a boiling point of 210.8°C making it suitable for experiments at high temperature and when mixed with water the mixture undergoes reflux at 96°C. Nitrobenzene is good

19

for producing growth along the b-axis in indanthrone whilst simultaneously giving the required tinctorial changes (Murphy, 1995). Indanthrone grown in this way would therefore perform well when imparting colour to an application medium. A possible reason for favourable growth occurring with nitrobenzene is that indanthrone has carbons at its growth end which may favour a solvent with a certain polarity. Polarity is defined here as the presence of a dipole moment in a compound when it is not subjected to an electric field. This fact was important in choosing alternative solvents for study.

Isopropanol, shown in figure 2.3, was chosen for study in this project after considering how a solvent such as nitrobenzene promoted crystal growth along the b-axis (Fryer, 1996). Its polarity is somewhat different to that of nitrobenzene.

$$CH_3CHCH_3$$
$$|$$
$$OH$$
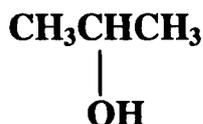
Figure 2.3 : Isopropanol

It was thought that isopropanol might not favour b-axis growth so readily and would thus be an interesting contrast to the work carried out on nitrobenzene. Ideally, if growth could be promoted along another axis, this knowledge could then be used to produce particles quite different in shape to standard indanthrone pigment particles. Although isobutanol had been studied previously, it has a higher boiling point and slightly

different polarity compared to isopropanol. The results of this work are shown in chapter 4.

The final solvent selected was methyl-benzoate which is shown in figure 2.4. This had the advantage that removal was possible by hydrolysis in sodium hydroxide producing two water soluble products (Gerson et al, 1993). This removal procedure is detailed in section 2.5.
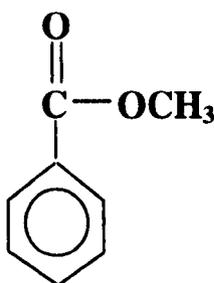
Figure 2.4 : Methylbenzoate

However, like nitrobenzene it is an aromatic compound and it was hoped this might be instrumental in promoting growth. However, its polarity is different to that of nitrobenzene and it was thought that this may affect the conditioning properties of the solvent. Again, such a property could modify the direction of growth in the crystal or simply affect the rate of growth. The results of work carried out with methyl benzoate are detailed in chapter 4.

2.5 Methods of solvent removal

During the course of this project the solvent was removed by either steam distillation, hydrolysis, or removal using acetone with filtration apparatus. As described in section 1.3, the current industrial process removes the solvent from the solvent-pigment mixture by steam distillation (Murphy, 1995). This has the obvious advantage that the solvent used can be recovered and recycled which is extremely environmentally beneficial in the case of solvents such as nitrobenzene and methyl benzoate. This industrial process was simulated in the lab using scaled-down apparatus. At the end of the reflux process, apparatus was set up in order that a steam distillation could be performed. This involved the use of a steam generator to supply steam to the reflux vessel. Whilst waiting for the pressure to reach 50 psi, the apparatus was adjusted to the following set-up:

stirring apparatus

condenser

steam inlet

reaction vessel   to boiler

collecting vessel

oil bath
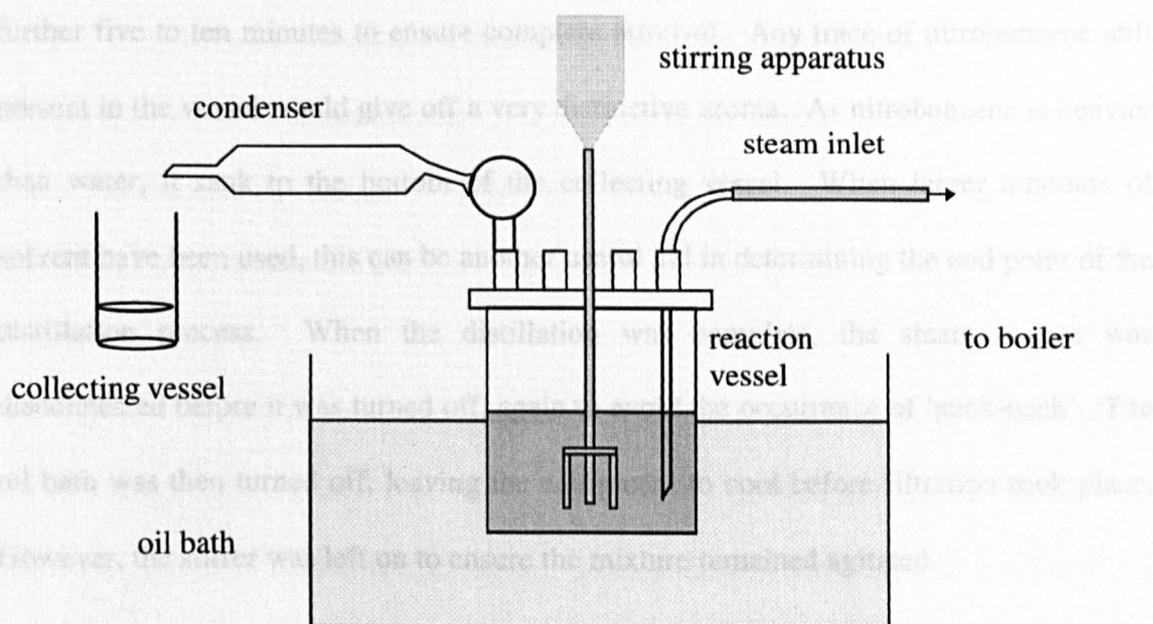
Figure 2.5: Steam Distillation Apparatus

22

All vessels were clamped securely and, with the condensers still on, the steam source was attached. Care had to be taken to avoid collision of the steam source with the stirrer or any thermometer that may also be inserted into the vessel. The level of steam was adjusted to ensure that no 'suck-back' occurred and the distillation process soon began. (During suck-back, liquid is drawn from the reaction vessel towards the boiler due to a difference in pressure caused by condensation of the steam in the cool liquid.) This is obviously highly undesirable, but can be avoided if caution is exercised. Each steam distillation usually lasted approximately 45 minutes, with the distilled off liquid emerging from the condenser. At the beginning of the distillation, this liquid was cloudy but it became clear as the distillation process neared its end. This was a good indication that all the solvent had been removed but the distillation would be left to continue for a further five to ten minutes to ensure complete removal. Any trace of nitrobenzene still present in the vessel would give off a very distinctive aroma. As nitrobenzene is heavier than water, it sank to the bottom of the collecting vessel. When larger amounts of solvent have been used, this can be another useful aid in determining the end point of the distillation process. When the distillation was complete, the steam source was disconnected before it was turned off, again to avoid the occurrence of 'suck-back'. The oil bath was then turned off, leaving the equipment to cool before filtration took place. However, the stirrer was left on to ensure the mixture remained agitated.

The hydrolysis method of removal was used only in the case of methyl benzoate (Gerson et al, 1993). After the reflux time was complete, the indanthrone-methyl benzoate mixture was removed from the oil bath and cooled rapidly using cold water and ice. Aqueous sodium hydroxide (NaOH, 50%) was then added to hydrolyse the methyl benzoate and the mixture was placed back in the oil bath to increase the temperature to 90°C. The vessel remained at temperature for 4 hours to ensure complete hydrolysis of the solvent. The reaction occurs as follows:

$$R\text{-}C(\text{=}O)\text{-}O\text{-}CH_3 + {}^-OH \longrightarrow R\text{-}C(\text{=}O)\text{-}O^- + CH_3OH$$

Hydrogen from aqueous solution
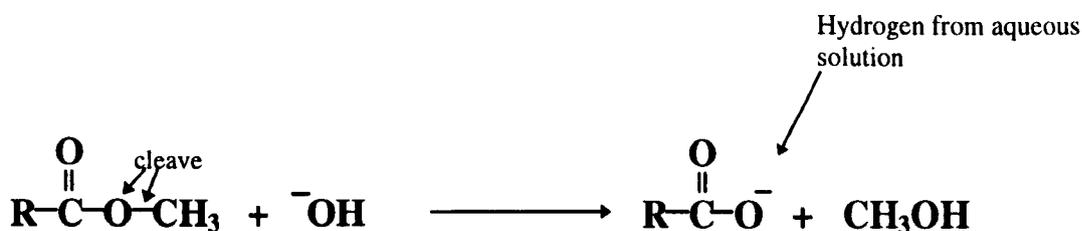
By replacing the **R** substituent for the benzene ring in methyl benzoate we can see that sodium benzoate and methanol are produced in the hydrolysis of methyl benzoate with sodium hydroxide. Sodium benzoate is formed easily as there are many hydrogen atoms present in the aqueous solution. Both products can easily be washed away during the filtration process as they are soluble in water.

The simplest method of solvent removal was used whilst sampling small amounts from the solvent-pigment mixture. The sample of the reflux mixture (usually 50-60ml in this case) was placed in a Buchner funnel and washed through with acetone to remove the solvent from the sample. After this was complete and no further solvent could be detected in the sample, the pigment powder was emptied onto a clock glass and dried in

an oven. Since this method required only basic filtration apparatus, it was possible to have a number of filtrations running simultaneously. This enabled samples to be taken at set time intervals which would have been impossible with other more complicated methods of removal. This method was also viable here because only small amounts of solvent were being removed at a time due to the amount being sampled - other methods are preferable where more solvent is being removed.

2.6 Samples

The samples studied during this project were, in the majority of cases, produced by growth of a small amount of indanthrone from the same batch of drowned-out material. This ensured that differences apparent after crystal growth could not be attributed to any differences in the starting material. However, a small number of samples, particularly in the earlier stages of the project, were produced in the laboratories and on the plant at Zeneca. These did not originate from the same batch of drown-out material and therefore any comparisons made between these samples and those produced during project time spent at Zeneca must be made with a degree of caution.

Within this section the effects of several parameters on the final form of the pigment were investigated. This included varying the concentration of solvent added to the reflux mixture, varying the time spent in the solvent reflux mixture and using different methods to remove the solvent from the mixture as described in section 2.5. Reflux was also

carried out with and without water in the mixture and the consequences of this are discussed in the results section. Another factor which could potentially alter the final form of the pigment is described as "sampling" of the reflux mixture. This involved a small amount (~60ml) being removed from the heated reflux vessel using a glass thimble shaped vessel with a long glass handle. Solvent removal occurred immediately after removal in these cases with no time allowed for cooling of the mixture.

The amount of solvent added was measured with reference to the weight of dry indanthrone powder present in the sample. This originates from the way in which Zeneca categorize and label such reflux products in the laboratory. For example, 10g of solvent added to 40g dry weight of indanthrone would be described as 25% concentration of solvent. This would be added to a water : indanthrone mixture in a 10:1 ratio with reference to the dry weight of indanthrone. For example, in the above sample with 40g dry weight of indanthrone, water would be added until the total weight of water present was equal to 400g. A certain amount of water is present in the indanthrone paste so this must be calculated and subtracted from the weight of water required. Concentrations of solvent added varied from 5% up to 100%. However, in the cases where the solvent concentration is described as being "100%", this is not a strictly accurate description. In these cases, no water was present and solvent was added in a quantity weighing ten times the weight of dry indanthrone. This ensured that enough liquid was present in the sample and the stirrer was able to move freely round the vessel. Sodium sulphate and sodium bicarbonate were added to each preparation containing

water, in amounts equal to 5% of the dry weight of indanthrone present. The sodium sulphate is added to de-aggregate/de-flocculate small particles whilst the sodium bicarbonate is present to neutralise any acid that might still be present from acid drown out.

After solvent recovery by distillation, it is normal practice for laboratory sized preparations to be filtered and the indanthrone powder is then oven dried. However, oven drying tends to form a "cake" of indanthrone which must then be broken down into powder form. This is carried out by simply milling a specific weight of the powder in a coffee grinding machine.

Those samples refluxed in nitrobenzene are documented first. Nitrobenzene is an extremely effective growth promoter in indanthrone and its use is described in section 2.4. All samples refluxed with nitrobenzene are listed in Table 2.1 and a more comprehensive description is given of each sample below.

The batch of drowned-out indanthrone used for all the other samples was studied and labeled as PM01. This enabled true comparisons to be made between this sample and those which were subsequently solvent treated.

PM011,12 and 13 were all refluxed in a small amount of solvent but for different times. This isolated the effect of reflux time and allowed the growth process to be followed.

Table 2.1 - Samples prepared using nitrobenzene

Sample	Amount of solvent present*	Time spent in solvent	Solvent removal
PM011	5%	1 hour with heat; overnight without heat	distillation
PM012	5%	1.5 hours	distillation
PM013	5%	3 hours	distillation
PM014	20%	3 hours	distillation
PM021	30%	3 hours	distillation
PM022	30%	16.5 hours	distillation
PM031	0%	0	N/A
PM032	100%	Sampled at 80°C - after 20 minutes	filtration
PM033	100%	Sampled at 96°C - after 35 minutes	filtration
PM034	100%	Sampled at 96°C - after 45 minutes	filtration
PM035	100%	Sampled at 96°C - after 75 minutes	filtration
PM036	100%	Sampled at 96°C - after 120 minutes	filtration
PM037	100%	Sampled at 96°C - after 240 minutes	filtration
PM038	100%	Sampled at 96°C - after 335 minutes	filtration
PM039	100%	300 minutes (no heat present)	filtration
PM051	20%	30 minutes	filtration
PM052	20%	70 minutes	filtration
PM053	20%	110 minutes	filtration
PM054	20%	160 minutes	filtration
PM055	20%	200 minutes	filtration

The contrast between PM013 PM014 and PM021 allowed the effect of an increasing solvent concentration to be viewed since reflux time was kept constant for all three samples. Another comparison of fixed concentration with varying time can be made between PM021 and PM022. This allowed information to be gained on the effect of lengthening the reflux time substantially.

The series of samples from PM031 to PM038 are quite a contrast to previous samples. These samples (excluding PM031) all originate from one reflux experiment which was sampled at increasing time intervals. No water was added to the vessel so that the importance of water in the growth process could be determined. As described earlier, this meant that large amounts of solvent had to be added for there to be enough liquid present in the vessel. Otherwise, the pigment particles may flocculate and aggregate together which could severely hinder any growth which might take place. Also, as the solvent was of a very toxic nature, this called for great care to be taken whilst using relatively large quantities. As only small amounts of the mixture were removed at a time during sampling, it became obvious that removal of the solvent by distillation was not viable for practical purposes. The nitrobenzene was thus removed using acetone and water by filtration as described in section 2.5. However, treatment of the indanthrone with another chemical could theoretically also promote growth. In order to check this, some of the drowned-out indanthrone was filtered in exactly this way (although methanol was also used to remove any acidity) and this sample PM031 was studied for any such changes. Another problem with this series is the fact that the solvent and

indanthrone were together in the vessel as the mixture was being heated up as opposed to the solvent being added once the mixture temperature had reached 80°C. Unfortunately this is unavoidable and means some growth will occur before the reflux temperature is reached. It can be seen that samples were removed at various stages starting with the mixture reaching a temperature of 80°C approximately 15minutes after heating began. Sampling was repeated once the vessel had reached 96°C (reflux temperature when water is present) and after this at the time intervals shown in table 2.1.

An experiment was then carried out to verify the importance of heat during the growth of indanthrone. PM039 was produced by combining indanthrone with nitrobenzene in a beaker which was maintained at room temperature. This was agitated regularly and the solvent was removed after 5 hours. This enabled this sample to be compared with PM038 which was also refluxed for 5 hours but with the advantage of heat present.

Finally, the last nitrobenzene series, PM051 to PM055 is also shown in Table 2.1. These samples were taken, at the time intervals shown, from a vessel containing indanthrone, water and 20% nitrobenzene along with sodium sulphate and sodium bicarbonate. This is representative of a typical plant preparation and by sampling, it was hoped that the particles could be studied at a slightly earlier stage of the growth process. Again, solvent removal was by filtration with water and acetone.

We now discuss the samples grown using methyl benzoate. This solvent was described in section 2.4. Again, certain parameters were varied e.g. the method of removal, the time allowed for reflux to occur and the level of solvent present. The samples which were refluxed in methyl benzoate are listed in Table 2.2 and are discussed in detail below. The samples where methyl benzoate was refluxed with indanthrone and water were PM024, PM025 and PM026. The relatively high concentration of solvent (80%) was chosen in order that any effect the solvent had on the pigment would be exaggerated. This choice was also influenced by information from the literature (Gerson et al, 1993). PM024 and PM025 were refluxed in the same high concentrations of the solvent which was removed by hydrolysis although their reflux times were significantly different. This isolates the effect of reflux time on the sample. As it is also possible to remove methyl benzoate by distillation, sample PM026 was prepared in an identical manner to PM024, only solvent recovery was via distillation instead of hydrolysis. This allowed a direct comparison to be made between these removal methods.

Methyl benzoate showed itself to be an effective growth promoter and was therefore studied further to produce the series PM042 to PM048. Similar to the nitrobenzene series, this comprised of indanthrone and the solvent being refluxed without water in the presence of a heat source. Samples were removed at the time intervals shown and solvent removal was carried out by filtration.

Table 2.2 - Samples prepared using methyl benzoate

Sample	Amount of solvent present*	Time spent in solvent	Solvent removal
PM024	80%	3 hours	hydrolysis
PM025	80%	15 hours	hydrolysis
PM026	80%	3 hours	distillation
PM042	100%	Sampled at 80°C - after 25 minutes	filtration
PM043	100%	Sampled at 96°C - after 35 minutes	filtration
PM044	100%	Sampled at 96°C - after 45 minutes	filtration
PM045	100%	Sampled at 96°C - after 75 minutes	filtration
PM046	100%	Sampled at 96°C - after 125 minutes	filtration
PM047	100%	Sampled at 96°C - after 245 minutes	filtration
PM048	100%	Sampled at 96°C - after 335 minutes	filtration

Finally the sample produced via reflux in isopropanol solvent is documented. No variation of solvent concentration or other parameters was carried out since the first sample produced showed little or no growth. Sample PM023 was refluxed in 50% isopropanol for 5 hours to exaggerate any effects the solvent had on the growth of the particles. The isopropanol was removed via distillation although as this solvent is water soluble it was not as obvious that all the solvent has been removed. Extra care was taken when filtering the sample afterwards to ensure all traces of the solvent were removed.

Table 2.3 - Sample prepared in isopropanol

Sample	Amount of solvent present*	Time spent in solvent	Solvent removal
PM023	50%	5 hours	distillation

At various stages in the project, samples were studied which were produced in the laboratories and on the plant at Zeneca. These samples are listed in table 2.4 and are described in detail below.

In section 1.3 industrial pigmentation of indanthrone was covered in detail. The crude indanthrone is broken down by ATDO into the drown out form, which is the solvent treated to promote crystal growth. It was therefore useful to study the crude form of indanthrone for comparison.

Vynamon Blue 3RFW is a pigment used for colouring plastics and has a larger particle size that standard pigments. Manufacture involves growth in a high concentration of nitrobenzene (50%) for 20 hours. This sample was studied to view the effects of such treatment and it was also interesting to gain familiarity with a commercial product.

Samples SD1941 and SD1942 were studied to compare the effects of a smaller concentration of solvent refluxed with indanthrone for 16 hours with a sample which was refluxed in a higher concentration of solvent but for the much shorter time of 3 hours. Also it was expected that both these samples would grow sufficiently to enable lattice images and diffraction patterns to be obtained from a specimen which was typical of a commercial product.

An interesting study was carried out on samples SD1653 and SD1654. These samples were prepared in an identical fashion although SD1654 was additionally treated. This treatment was designed to control crystal growth and comparisons between the samples can be made to estimate the effectiveness of this growth control treatment.

Those samples in table 2.4 which underwent solvent treatment were distilled to enable solvent recovery.

Table 2.4 - Samples supplied by Zeneca

Sample	Details
Crude indanthrone	Indanthrone prior to ATDO and crystal growth
Vynamon	Indanthrone refluxed in 50% nitrobenzene for 20 hours
SD1941	Indanthrone refluxed in 30% nitrobenzene for 3 hours
SD1942	Indanthrone refluxed in 20% nitrobenzene for 16 hours
SD1653	A standard solvent treated sample
SD1654	As SD1653, but with additional surface treatment

2.7 Characterization by X-ray diffraction

It is thought that indanthrone exists in several different forms and X-ray diffraction (XRD) is a useful method for differentiating between these forms (Murphy, 1995, Honigmann, 1966). Also, since the form is also an indication of the level of growth (due to changes in crystallinity affecting peak widths in the spectra), XRD can indicate how successful a particular solvent has been in promoting growth, prior to electron microscopy (McKay, 1993). A typical drown-out sample gives rise to an XRD spectrum showing the broad, rounded peaks which would be expected from such a non-crystalline sample. This is illustrated in figure 2.6 where a spectrum obtained from the drown out batch used for most of the experiments is shown. In contrast to this, a spectrum from a sample which has undergone crystal growth will exhibit sharper, more defined peaks

Figure 2.6 : XRD spectrum of drowned out indanthrone
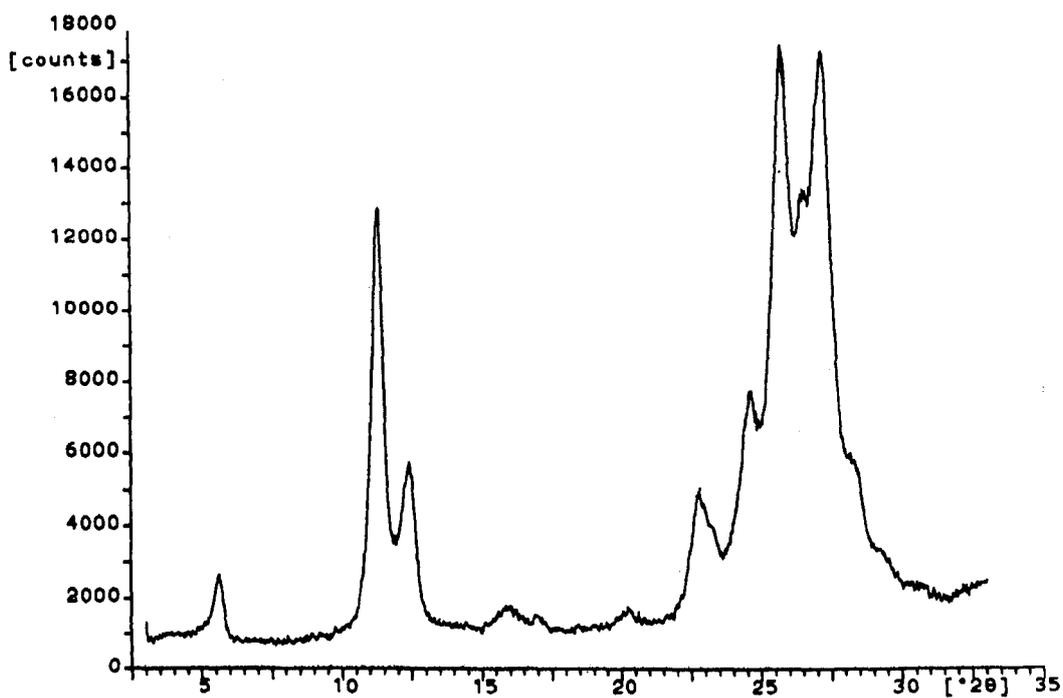
Figure 2.7 : XRD spectrum of indanthrone after growth by solvent treatment

which vary in appearance depending on the level of growth. Such a spectrum can be seen in figure 2.7. The sample giving rise to this spectrum was PM032 - indanthrone removed from pure nitrobenzene on reaching 80°C. It can be seen that this spectra has many more pronounced peaks than the spectrum arising from the drowned out indanthrone. The drown-out form is described as being the β-form of indanthrone, whilst solvent treated indanthrone which has undergone a reasonable amount of growth is described as being of the α form. XRD helps to identify which form is present thereby giving an indication of how much growth has occurred. XRD data can be used to provide information on the thickness of crystals by analysing the broadening of the profile along the [100] a-axis. It was thought that the length of the particle could be determined by studying the broadening of the [010] b-axis. However, (010) is a forbidden reflection and thus no precise length information can be gained from XRD spectra. For this purpose, it is thus preferable to use electron microscopy although XRD is still an extremely useful analysis technique for studying pigments. The theory and principles of XRD are detailed in this section.

An x-ray wavefront incident on a surface row of atoms in a crystal plane will be scattered by atoms in the crystal lattice (Wehr, Richards and Adair, 1984). For Bragg reflection to occur, two conditions must be satisfied in order that x-rays scattered from the Bragg planes will interfere constructively. The first condition is that the angle the incident beam makes with the planes must be equal to that made by the reflected beam. The second condition is that these reflections must satisfy the relation:

$$n\lambda = 2dsin\theta$$

where n is the spectrum order (1,2,3...), λ is the wavelength, d is the distance between successive planes and θ is the angle of incidence or angle of diffraction. This is shown schematically in figure 2.8.

In x-ray diffraction techniques, the crystal is used as a diffraction grating for a collimated beam of x-rays as shown in figure 2.9. The beam passes through the slit onto the crystal which is rotated about an axis parallel to the slit. Detection of Bragg reflection takes place at an angle 2θ from the incident beam of x-rays. Constructive interference of the rays at this position is an indication that the second Bragg condition has been fulfilled. Spectra from this technique therefore take the form of that shown in figure 2.6 and 2.7, with 2θ shown on the x-axis against intensity on the y-axis.

This work was carried out at Zeneca Grangemouth where the spectrometer in use is a Philips PW1840. Samples were prepared for x-ray diffraction by the following method: A small metal holder with a recess approximately 3cm by 2cm was used for each sample. The powder for analysis was placed in the recess, covered with cellophane and pressure was applied to compress the powder to prevent it from falling out whilst in the spectrometer. More powder was added if necessary in order to provide a flat surface of powder in the window for XRD. The cellophane was removed without disrupting the

powder compressed in the holder. The holder was inserted in its position and the
machine was switched on and usually left to operate overnight.

θ

α

Plane 1

d

θ
α

Plane 2

Plane 3

Figure 2.8 : Waves scattered by successive planes of atoms in a crystal

Detector

2θ

X-ray
source

Slit

θ

Crystal

Figure 2.9 : Crystal Spectrometer

powder compressed in the holder. The holders were stacked in a cartridge and the machine was switched on and usually left to operate overnight.

2.8 Surface Area Analysis

Brunauer, Emmet and Teller were the first to develop a theory for multilayer adsorption which was an extension of the well-known Langmuir adsorption isotherm (Shoemaker, Garland and Nibler, 1982). The Langmuir theory is only useful at low pressures where only monolayer adsorption is involved. They assumed that the surface of the adsorbent is composed of uniform, localised sites and that adsorption on one site does not affect adsorption on neighbouring sites. It is also assumed that there is no limit on the number of adsorbed layers that may form with the surface area available on the nth layer equal to the coverage of the $(n-1)^{th}$ layer. It is possible to derive an equation for the ratio of the volume V of gas adsorbed (under standard conditions) to the volume required to cover the entire surface with a complete monolayer, V_{mon}.

The BET isotherm is thus expressed as follows:

$$\frac{V}{V_{mon}} = \frac{cz}{(1-z)\{1-(1-c)z\}} \quad \text{where } z = \frac{p}{p^{*}}$$

where p^* is the vapour pressure above a macroscopically thick layer of pure liquid on the surface, V_{mon} the volume corresponding to monolayer coverage, and c is a constant which is large when the enthalpy of desorption from a monolayer is large compared with the enthalpy of vaporization of the liquid adsorbate (Alberty and Silbey, 1992). This equation can be reorganized into

$$\frac{z}{(1-z)V} = \frac{1}{cV_{mon}} + \frac{(c-1)z}{cV_{mon}}$$

Therefore, by plotting $z/(1-z)V$ against z, $(c-1)/cV_{mon}$ can be obtained from the gradient. Then, using the intercept to yield a value for cV_{mon}, the results can be combined to give both c and V_{mon}. V_{mon} can then be used to deduce how many nitrogen molecules would occupy this volume. By assuming each molecule is spherical and that they are close packed in the liquid, the cross sectional area for an adsorbed N_2 molecule can be taken to be around $0.16nm^2$. Thus from the value of V_{mon} obtained from the BET technique, if multilayer adsorption is involved, the surface area of the adsorbant can be calculated.

Adsorption isotherm curves can be plotted using the data collected experimentally by plotting V/V_{mon} against p/p^* (Fryer, 1981). The adsorption isotherm is simply the amount adsorbed as a function of the equilibrium gas pressure at a constant temperature. Adsorption increases rapidly at high pressures. The pressure p^*, as discussed earlier, is the saturation pressure of the gas, i.e. the vapour pressure of the liquid at that temperature. When $p/p^* = 1$, bulk condensation will occur to form a liquid film on the

surface. The isotherm also gives no clear indication of the formation of the first layer. Second and higher layers usually begin to form before the first layer is complete which meant that a value for V_{mon} could not be obtained from the adsorption isotherm. It was this that led to the development of the BET theory for multilayer adsorption.

The surface area calculations in this project were carried out using the S_{BET}, or Brunauer-Emmett-Teller (BET) gas adsorption technique. This method is widely used as a routine procedure for the determination of the surface area of organic pigments. Pigment crystals are usually grouped together in aggregates and it can be difficult to assess the total surface area by any method other than gas adsorption. However, as organic pigments have low surface energy the BET technique may not be a totally reliable method for quantitative surface area measurement (Fryer et al, 1981). For more detailed knowledge of the extent of face-to-face packing of crystals, the ratio S_{BET}/S could be studied where S_{BET} is the specific surface area of the pigment powder and S is the specific surface area of the crystals determined from electron micrographs and/or electron diffraction (McKay, 1989). Also, the BET isotherm fits experimental observations moderately well over a restricted pressure range, but it underestimates the extent of adsorption at low pressures and overestimates it at high pressures. Having said this, the BET method is still useful for comparison of specific surface areas between similar substances.

Pigment samples were placed in a stoppered tube overnight at 25°C with nitrogen gas on a Micrometrics VacPrep 061 prior to determination of the surface area. The nitrogen gas was fed to the sample via a needle and removes hydrocarbons etc from the surface of the particles. No adsorption of nitrogen will take place during this procedure due to the ambient temperature. The BET specific surface areas were then determined using data obtained from nitrogen gas adsorption at -196°C. A Micrometics Gemini III 2375 surface area analyser was used for this purpose. The nitrogen layer on the pigment surface is assumed to be monomolecular and the cross sectional area of the nitrogen molecule was taken to be $0.162nm^2$. We must also consider how the nitrogen molecules gain access to crystal surfaces in the interior of aggregate structures. It has been found that nitrogen molecules do not penetrate between crystals in face-to-face contact under the conditions used in the determination of the BET specific surface area (Mather, 1981, Mackay, 1988, Fryer et al, 1981). S_{BET} therefore gives a measure of the external surface of such an aggregate structure as well as that of single crystals. We must take this into consideration when considering the results obtained from this method. The results were obtained by performing the following technique :

A $10cm^3$ surface area tube was weighed and approximately ~0.5g of pigment powder was added depending on the density of the sample. Less dense samples were of a more 'fluffy' nature and it was difficult to fit as much powder into the tube. The glass tube was placed in the instrument and gas supply needle was inserted into the tube which was loosely stoppered. The tube was left overnight to "degas" at room temperature. The next morning, liquid nitrogen was poured into the instrument. Meanwhile, p^* was

calculated using the machine and samples which had degassed overnight were weighed. Each sample was then placed in the machine one at a time for adsorption of the nitrogen and subsequent calculation of the surface area. A typical print-out is shown in figure 2.10. This shows the data used by the machine to generate a value for the surface area. For sample PM053 this can be seen to be $65.3627 m^2 g^{-1}$ and this procedure was repeated for all the samples studied in this way. The instrument in use has been shown to produce reproducible results with variations being in the region of ±0.2 $m^2 g^{-1}$. For this reason, results are quoted to only one decimal place when presented in chapter 4.

Surface area can also be measured using electron micrographs. The length and width of many particles were measured for particle size distirbutions and knowledge of the thickness was gained from PEELS work. However, this illustrated variations in the thickness of particles in certain samples thus for ease of comparison, surface area was measured only by the BET technique. This topic is discussed further in the Future Work section of this thesis in Chapter 8.

Gemini 2375 V3.03
Instrument ID:
Setup Group: 2 - (used)

Sample ID: 053   Started: 18/09/97 11:44:54
Sample Weight: 0.5039 g   Completed: 18/09/97 12:25:09
Evacuation Rate: 500.0 mmHg/min   Evacuation Time: 1.0 min
Measured Free Space: -0.924 cc STP   Saturation Pressure: 799.46 mmHg
Analysis Mode: Equilibration   Equilibration Time: 5 sec

BET Multipoint Surface Area Report

Surface Area: 68.3627   sq. m/g
Slope: 0.062825
Y-Intercept: 0.000853
C: 74.649361
Vm: 15.704022
Correlation Coefficient: 9.9998e-001

Analysis Log

Relative Pressure	Pressure (mmHg)	Vol. Adsorbed (cc/g STP)	Elapsed Time,(h:m)	Surface Area Point
0.0500	39.98	13.275	0:23	*
0.0875	69.93	15.028	0:28	*
0.1250	99.90	16.373	0:31	*
0.1624	129.85	17.554	0:35	*
0.1999	159.84	18.643	0:39	*

Figure 2.10: Print-out from surface area analyser for sample PM053

Chapter 3

Microscopy Techniques Used to Study Indanthrone

3.1 Introduction

The aim of this chapter is to outline the main features of the conventional

transmission electron microscope (CTEM) and scanning transmission electron

microscope (STEM) and discuss the operational modes which were used in this

project. The JEOL 1200EX CTEM at the University of Glasgow is introduced in

section 3.2 with a description of the major components of the CTEM. The theory

and practice of electron diffraction in the electron microscope is discussed in

sections 3.3 and 3.4. Information obtainable from such diffraction patterns is then

considered in section 3.5. Examples of diffraction patterns obtained in this manner

are shown.

The major components of the STEM, and the basic principles of image formation in the STEM are introduced in section 3.6 as is the VG HB5 STEM at the University of Glasgow. (In these sections, it is shown that the STEM is capable of producing similar images to the CTEM when operated under conditions satisfying the reciprocity principle.) Annular Dark Field (ADF) imaging is detailed and a description is given of how this technique was implemented to yield high quality images. Section 3.7 gives a brief summary of the angular detectors. For certain imaging modes, such as standard lattice imaging, the STEM is markedly inferior in terms of efficiency of electron utilisation. This can be a problem when studying radiation sensitive materials as the achievement of high quality images requires irradiating the specimen with a greater dose of electrons than in the CTEM, leading to an increase in radiation damage to the specimen.

In section 3.8 and 3.9, Differential Phase Contrast (DPC) imaging is discussed including the principles of imaging formation using this technique along with a description of the quadrant detector in use. This technique is advantageous in that topographical images are produced and the efficient use of electrons is maximised. This technique can be useful when studying radiation sensitive samples.

Parallel Electron Energy Loss Spectroscopy (PEELS) is introduced in section 3.10. This section describes the detector used to acquire PEELS spectra along with a detailed description of how the HB5 STEM was aligned for PEELS. Some of the problems encountered during spectrum acquisition are reviewed at the end of this section.

Finally, in section 3.11 the concept of radiation sensitivity is discussed and how this was a factor in limiting the amount of information obtainable from an organic sample such as indanthrone which is prone to damage.

3.2 The Conventional Transmission Electron Microscope

A schematic diagram of the JEOL 1200EX conventional transmission electron microscope (CTEM) is shown in Fig. 3.1. Situated at the top of the microscope column is an electron gun. The cathode is a heated filament which acts as the electron source for the microscope. The diameter of the wire filament is approximately 125μm and it is bent like a hairpin with a V-shaped tip that is approximately 100μm at the widest point. The cathode is heated by passing a current directly through the filament wire and electrons are emitted thermionically from the filament. The filament is surrounded by a Wehnelt cylinder containing a small circular aperture which is centred on the bend in the hairpin filament. This filament is also connected to the Wehnelt by an auto-bias resistor to provide a stable operating point. A large negative potential, 100kV in this case, is applied between the Wehnelt and the anode which is at ground potential causing the acceleration of the emitted electrons.

The condenser lens system is the next component in the CTEM and is designed to focus the electron beam. This system consists of two condenser lenses, C1 and C2, and a variable aperture. C1 forms a de-magnified image of the gun crossover whilst

Filament

Condenser Lens 1

Condenser Lens 2

Condenser Aperture

Specimen

Objective Lens

Objective Aperture

Selected Area Aperture

1st Image

Projector Lens 1

2nd Image

Projector Lens 2

Final Image

Viewing Screen
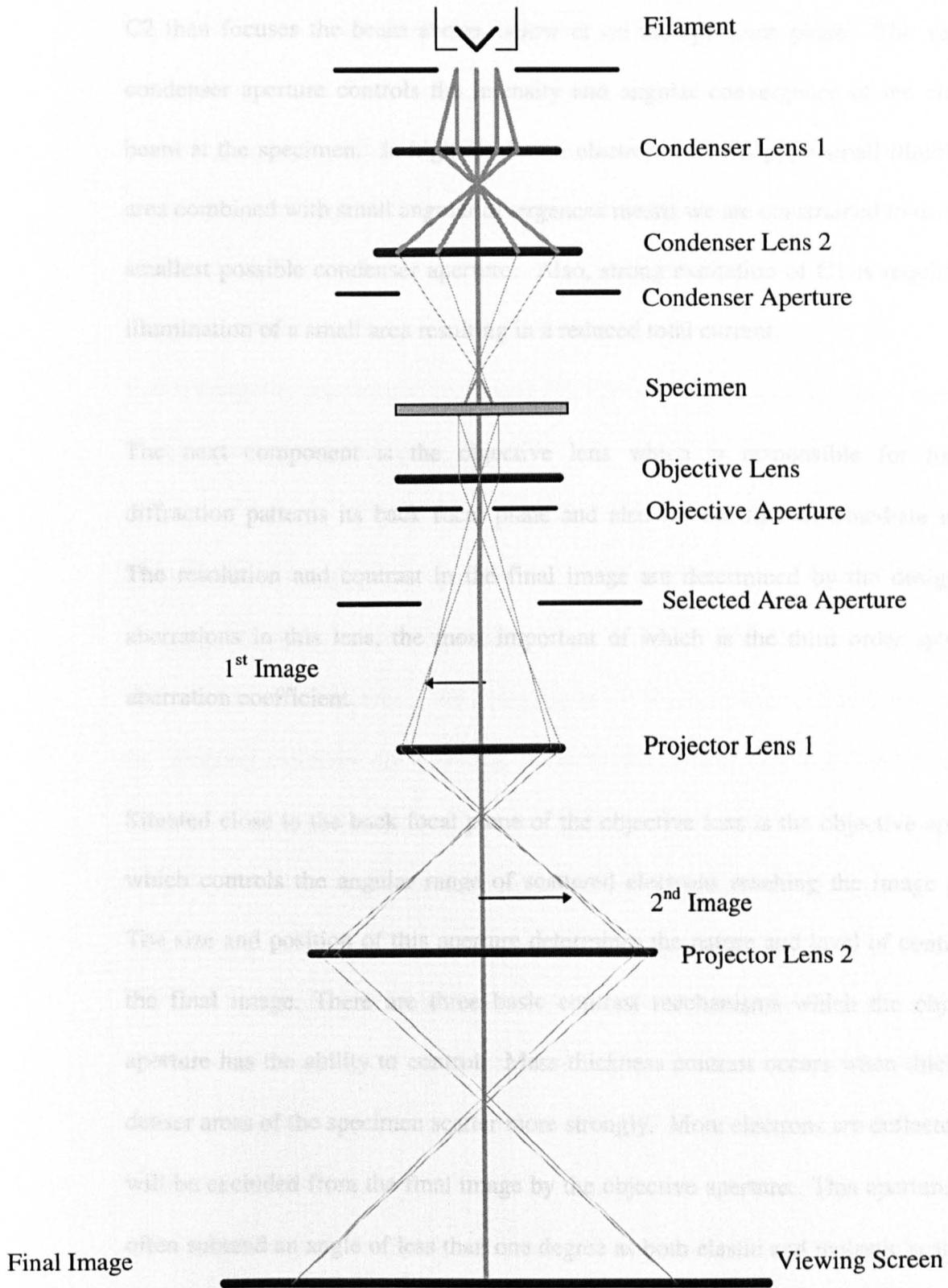
Figure 3.1 : Schematic diagram of a CTEM

C2 then focuses the beam above, below or on the specimen plane. The variable condenser aperture controls the intensity and angular convergence of the electron beam at the specimen. In high resolution electron microscopy, a small illuminated area combined with small angular divergences means we are constrained to using the smallest possible condenser aperture. Also, strong excitation of C1 is required for illumination of a small area resulting in a reduced total current.

The next component is the objective lens which is responsible for forming diffraction patterns its back focal plane and also for the first intermediate image. The resolution and contrast in the final image are determined by the design and aberrations in this lens, the most important of which is the third order spherical aberration coefficient.

Situated close to the back focal plane of the objective lens is the objective aperture which controls the angular range of scattered electrons reaching the image plane. The size and position of this aperture determines the nature and level of contrast in the final image. There are three basic contrast mechanisms which the objective aperture has the ability to control. Mass-thickness contrast occurs when thicker or denser areas of the specimen scatter more strongly. More electrons are deflected and will be excluded from the final image by the objective aperture. This aperture must often subtend an angle of less than one degree as both elastic and inelastic scattering are strongly 'forward peaked.' Diffraction contrast occurs when a crystalline specimen is being studied. Diffraction of the electron beam by the specimen means that, at particular angles, the intensity of scattering is greatly increased. The

objective aperture can then be used to prevent these diffracted beams from contributing to the final image. This gives dark contrast from regions that are scattering strongly. Both of these mechanisms have given rise to contrast when studying indanthrone whilst using an objective aperture. Phase contrast results whenever electrons of different phase are allowed to pass through the objective aperture. When two or more diffracted beams pass through it and interfere, a set of lattice fringes is produced in the image. A lattice image is then formed where each fringe represents a lattice plane.

In bright field imaging, the aperture is centred about the optic axis. In dark field imaging, the aperture must be positioned to exclude all beams except a particular diffracted beam of interest. This gives rise to a low resolution dark field image since the imaging electrons are traveling far from the optical axis and aberrations are introduced. It is preferable to tilt the primary electron beam in order that the chosen diffracted beam may pass along the optic axis and through the centred aperture.

The remaining lenses are the intermediate lens and the projector lenses, the purpose of which is to magnify the image produced by the objective lens and transfer it to the final viewing screen. In imaging mode, the intermediate lens is focused on the image plane of the objective lens with the final magnification being controlled by the strength of the projector lenses. In diffraction mode it is focused on the back focal plane of the objective lens with the diffraction pattern being projected onto the viewing screen. The projector lenses control the magnification of the diffraction

pattern though for diffraction, this magnification is usually described in terms of the camera length.

The recording device in a CTEM usually takes the form of photographic plates. In this work, two different types of film were used. Kodak 4489 photographic film was used for low magnification imaging and for some diffraction work. However, for high magnification lattice imaging and other diffraction work it was necessary to use CEA Reflex 15 also known as 'RX' film. This allowed much shorter exposure times when recording images which is a distinct advantage for studying a radiation sensitive sample such as indanthrone.

Low magnification (5kx to 75kx) bright field imaging was used to gain information about the size shape and size distribution of indanthrone particles. This was performed with an objective aperture positioned on the optic axis of the microscope to exclude diffracted electrons from the image and give enhanced contrast in the final image. The largest condenser aperture was used and the spot size was usually kept at the largest setting.

Bright field imaging was also used at high magnification (over 100kx) to view lattice fringes. The emphasis in this technique was to reduce the amount of radiation falling on the specimen whilst preserving a degree of intensity and contrast so that the lattice fringes could be viewed and recorded. In this case, the smallest condenser aperture was used with an objective aperture at the smallest spot size setting. In practice this results in a very low intensity image appearing on the fluorescent screen

and makes it difficult to view the lattice fringes before they fade due to radiation damage.

3.3 Electron Diffraction

When diffraction occurs in a crystalline specimen the scattering angle of the incident beam is $2\theta_B$ and the distance from the diffraction spot to the optic axis is known as D. If L is the camera length, by geometry,

$$tan(2\theta_B)=D/L$$

Braggs law states that

$$2d \sin \theta_B = n\lambda$$

where d is the crystal spacing and λ is the wavelength of the electrons. This indicates that strong scattering will only occur at angle θ_B which is known as the Bragg angle. Using a small angle approximation, θ_B can be substituted for both $tan\theta_B$ and $sin\theta_B$. Therefore,

$$Dd = \lambda L$$

The d-spacing of the lattice planes for a particular crystalline specimen can thus be easily determined if λ, D and L are known. It is advisable however to calibrate camera lengths regularly using a standard specimen for greater accuracy.

3.4 Electron Diffraction in the Electron Microscope

A beam of electrons incident on a crystalline specimen will be scattered by some of the constituent atoms. The beam will emerge from the sample either undeviated or having been diffracted by sets of suitably oriented lattice planes under Braggs Law. Both the scattered and unscattered beams are then focused on the back focal plane of the objective lens to form the diffraction pattern. As discussed in section 3.2 the strength of the intermediate and projector lenses can be altered to produce either the diffraction pattern or the image on the viewing screen.

In many cases, it is useful to limit the area of specimen giving rise to the diffraction pattern and there are two ways of doing this. One is by insertion of a selected area diffraction (SAD) aperture at the first intermediate image plane. A ray diagram of this is shown in figure 3.2 (Smith, 1997). A diffraction pattern from the entire illuminated area is formed in the back focal plane with the intermediate image being produced at D. By insertion of an aperture in this plane, the rays passing further down the column are limited. Therefore, the diffraction pattern formed by the intermediate lens, uses only electrons from the selected area. Electromagnetic lenses however, suffer from aberrations and spherical aberration of the objective lens in particular gives rise to error in SAD. This causes the electrons which pass through
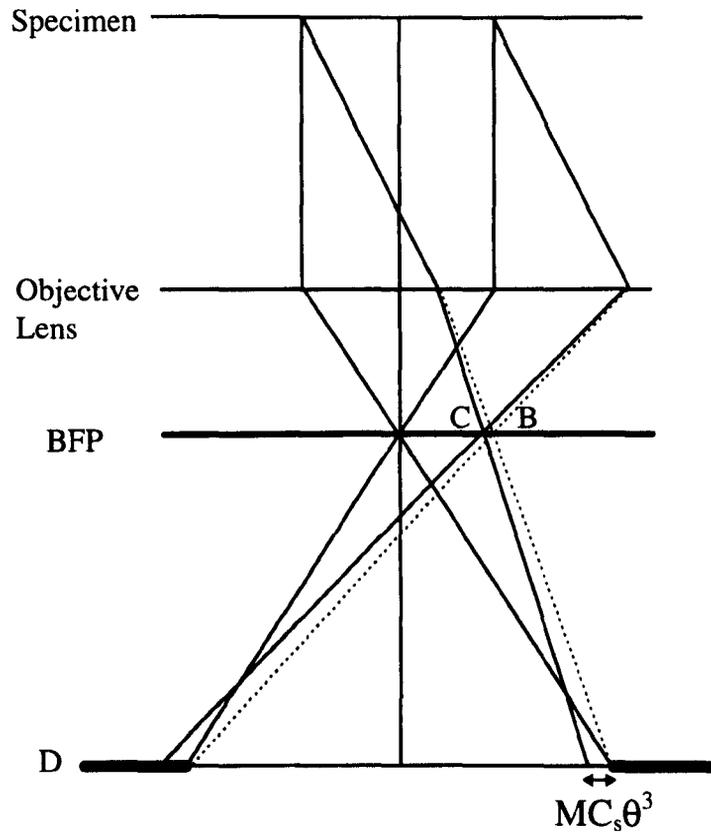
Figure 3.2 : Ray diagram illustrating Selected Area Diffraction (SAD)

the outer regions of the lens to be deviated more strongly than if they were under the influence of a perfect lens. Therefore, the image of an area of specimen formed using the unscattered beam is focused in the plane of the SAD whilst the image formed using the diffracted beam is focused in a plane some distance above the selected area aperture. Thus electrons coming from different areas of specimen will pass through the same points on the selected area aperture plane and vice versa. This displacement is given by

$$d = MC_s\theta^3$$

where M is the magnification, C_s is the spherical aberration coefficient and θ is the scattering angle (Williams and Carter, 1996). This is illustrated in figure 3.2. It can be seen that there is an error in selecting the area if the beams do not travel at the same angle to the optic axis. Position B is the diffraction spot position for a perfect lens (crossover of dotted lines) whilst position C is the spot position with spherical aberration (crossover of solid lines). The spatial resolution tends to be low using this technique and diffraction information can only be obtained from relatively large areas of the specimen. In the JEOL 1200EX for example, the smallest selected area aperture has a diameter equivalent to ~450nm at the image.

The alternative method used to record a diffraction pattern from a selected area of specimen is that of microdiffraction or convergent beam diffraction. The beam is condensed into a small spot so that the diffraction pattern comes from the whole of the illuminated area. The use of such a small probe size makes this technique very suitable for the study of small particles. A ray diagram for convergent beam

diffraction is shown in figure 3.3 (Williams and Carter, 1996). Convergent beam diffraction was performed in this work by insertion of the smallest condenser aperture in imaging mode at spot size 6. The area of interest was selected and the beam was focused onto it before changing to diffraction mode and ensuring the objective aperture was removed. Typical camera lengths used were 30cm and 50cm although calibration of these values showed them to be approximately 31.7cm and 47.2cm respectively. The resulting diffraction pattern was obtained from a region of specimen of around 80nm in diameter in the JEOL 1200EX. However, although the spatial resolution was increased, the angular resolution was reduced because of the increased convergence of the illumination.

3.5 Information from Electron Diffraction Patterns

The electron diffraction pattern from a thin perfect crystal is directly related to the crystal structure. A single crystal specimen oriented such that several sets of planes are parallel to the beam will give rise to a diffraction pattern consisting of a regular array of spots with the symmetry of the reciprocal lattice. The position of these spots are a function of the crystal lattice. By indexing them, various lattice plane spacings in the structure can be determined by measuring spot spacings on micrographs although an accurate measurement of the camera length is required. It is also possible to determine the orientation of the crystal from such a diffraction pattern. The intensity of the spots is dependent a number of factors. This includes the atom type, their arrangement within the unit cell, the crystal shape, exact orientation, thickness and therefore the number of unit cells contributing to the

C2 Aperture

C2 Lens

Upper objective lens

Specimen

Lower objective Lens

Diffraction pattern in
back focal plane

Figure 3.3 : Ray diagram illustrating convergent beam diffraction (CBED)

signal. The structure factor of a unit cell can be used to illustrate which diffracted beams will exist since not all reflections are necessarily allowed. Certain reciprocal lattice points have systematic absences and thus, zero intensity even though they are geometrically allowed by Bragg. The structure factor is given as follows,

$$F_g = \Sigma_j f_j \, (\underline{K}) \, exp(2\pi i\underline{K} \cdot \underline{r}_j)$$

where $f_j \, (\underline{K})$ is the atomic scattering factor of the jth atom positioned at $\underline{r}_j$.

When we are at the Bragg angle, $\underline{K}=\underline{g}$, where $\underline{g}$ is the reciprocal lattice vector. This is known as the kinematical theory of electron diffraction which is used to give a rough guide to which spots will appear (Williams and Carter, 1996), (Myers, 1990). However, spots that are forbidden kinematically can occur by double diffraction rendering the kinematical theory invalid. This occurs where the crystalline specimen is thicker than about one third of the extinction distance and as a result there is appreciable interaction between the electron beams as they travel through the solid. In such cases, it is better to use the dynamical theory of electron diffraction which is a much more mathematical method. This theory considers how the intensities of the incident beam and diffracted beam(s) vary as they pass through the sample.

Changes in intensity, position and shape of diffraction patterns including extra diffraction spots or streaked areas of the pattern can indicate a deviation from perfect crystallinity. The pattern can then be used to extract information about the type of defect causing these alterations.

3.6 The Scanning Transmission Electron Microscope (STEM)

The STEM in operation at the University of Glasgow is an extended VG HB5 which operates at 100kV. It has been modified by the addition of three post specimen lenses and a z-lift stage.

In the STEM, images are formed by scanning a focused electron probe across a specimen. Detectors are used to collect some portion of the transmitted electrons (either scattered or unscattered), x-rays or other signal. Each pixel in the resulting image is thus formed in a sequential manner as opposed to the CTEM where the whole image is acquired simultaneously.

The HB5 is equipped with a field emission source which gives a high brightness and hence a large current in a small spot. This field emission gun (FEG) consists of a single crystal tungsten cathode with a sharp point supported on a tungsten filament. Electrons are stripped from the surface when a potential of ~4kV is applied between the cathode and the extraction anode. A second anode accelerates the electrons up to energies of 100keV. However, the emission of electrons decreases with time due to a build up of gas on the tip making it necessary to 'flash' the tip every 15 to 20 minutes. This entails passing a high current through the support wire to heat the tip and therefore which removing contamination by desorption. In this way, damage is also annealed. The vacuum in the gun region of the STEM must be kept at around 10^{-11}mbar to prevent production of ions which might damage the tip whereas the column vacuum is kept at around 10^{-8}mbar.

The main components of the VG HB5 STEM are shown in figure 3.4 showing alignment for PEELS. The first component after the FEG is the virtual objective aperture (VOA) which defines the angular convergence of the probe. The size of this probe and therefore the spatial resolution is determined by a three lens system comprising the two condenser and objective lenses. The condenser lenses on the HB5 lenses allow for a greater degree of flexibility in both convergence and probe size. In this work only one condenser lens was used at a time. C_1 was used for ADF imaging and PEELS whilst C_2 was used in the DPC imaging mode. The total current in the probe is greater when using C_1. However, the use of C_2 enables the formation of a smaller probe on the specimen. In normal imaging mode, the condenser lens is used to transfer an image of the electron source to the plane of the selected area aperture (SAA). The objective lens, which is kept at almost constant excitation, then transfers the probe onto the specimen plane. This probe can either be held stationary on the specimen or scanned across it in a raster by the scan coils. The area of specimen being scanned in this way determines the magnification of the image.

The image can be focused using the z-lift mechanism which adjusts the height of the specimen. The objective current is then adjusted slightly but only to finely tune the focus. This method allows the objective lens excitation to remain standard. This gives a fixed post-specimen field and therefore a fixed angular compression.

PEELS detector

spectrometer aperture

annular dark field detector

collector aperture

large angle
annular dark field detector

post-specimen lens3

post-specimen lens 2

post-specimen lens 1

objective lens post-specimen field

specimen

objective aperture

objective lens pre-specimen field

selected area aperture

scan coils

condenser lens 2

condenser lens 1

virtual objective aperture

FEG electron source

Figure 3.4 : Schematic diagram of the HB5 STEM aligned for PEELS

The post specimen lenses (PSL) allow the angular distribution of the electrons transmitted through the specimen to be matched to the size and shape of the detectors. The PSL's may be used independently or in conjunction with one another.

The modified HB5 has three ADF detectors and one bright field detector. Two of the ADF detectors have different sized central holes and are situated at the same position as the bright field detector in the column. Preceding this in the optical column is the third ADF detector which has a large central hole. This can be used simultaneously with any of the other detectors. These detectors are annular scintillators and therefore on being hit by an electron they emit photons which are then detected by a photomultiplier tube. Some electrons pass through the annulus if they have been scattered through a solid angle which is less than that subtended by the ADF detector. These can then be detected by a parallel electron energy loss spectrometer which is described in section 3.10. The HB5 is also equipped with a quadrant photodiode detector for use in DPC (Differential Phase Contrast) imaging. These are discussed in sections 3.8 to 3.9.

3.7 Use of the Angular Detectors

Most images obtained from work carried out in the STEM were obtained using an annular dark field (ADF) detector. This detector collects a large fraction of the angular range of the electrons scattered outside the central electron beam resulting in a larger signal and therefore more efficient use of electrons than in a typical CTEM

dark field image. This does, however, result in lower contrast but allows all phases and orientations to be imaged.

The ADF detector was used to investigate properties of the particles which are difficult to study in a CTEM. Bright field imaging with a small defocus on the CTEM had indicated that some particles were not of uniform thickness. An asymmetric Fresnel fringe appeared even after careful correction of astigmatism. The HB5 STEM was then used to provide ADF images of the indanthrone particles to show thicker areas of the specimen as bright areas on the display. This gave a qualitative estimate of thickness so PEELS was then used give a quantitative value for the thickness of indanthrone particles. DPC was carried out to determine the topography of these particles and the nature of any thickness variations.

3.8 Use of the Quadrant Detectors

CTEM images of indanthrone provide information on the size and distribution of indanthrone pigment particles. However, neither CTEM images nor ADF images can provide topographic information on specimens. A technique based on the differential phase contrast (DPC) mode of microscopy can provide simultaneous topographic information and high contrast lattice images. This technique makes efficient use of the scattered electrons but radiation damage still imposes a limitation of the spatial resolution. The DPC image is formed by using the difference signals from a split or quadrant detector as the probe is scanned across the specimen. The aim of this section is to discuss the basic principles of DPC imaging with particular

reference to obtaining topographic and some structural information. However, this is not an exhaustive discussion and more detail can be found in the literature.

Dekkers and De Lang (1974, 1977) discussed the production of images from the difference in the signals falling on two halves of a circular detector as the electron beam was scanned across the specimen. These DPC images are linearly related to the phase gradient of the specimen transmittance in a direction perpendicular to the split in the detector.

Figure 3.5 shows how topographic contrast arises in the DPC imaging mode. Small shifts of the bright field cone away from the symmetry position are related to the thickness gradients in the specimen (McVitie, 1997). The electrons, focused to a small probe in the plane of the specimen, are deflected through an angle that is proportional to the thickness gradients integrated along an electron trajectory. Due to deflection by the specimen, the electron distribution on each quadrant is not the same and difference signals from opposite quadrants provide a quantitative measure of the components of the deflection angle. Images derived from pairs of difference signals can be regarded as maps of two orthogonal components of the thickness gradient.

To reveal the internal structure of the particles via lattice images, the diffracted beams emerging from the specimen must overlap with the unscattered primary beam. If the specimen is illuminated by a coherent probe, the electron wave leaving the specimen consists of an unscattered cone of angular radius α_s together with two

diffracted cones of the same angular radius but displaced from the primary beam by an angle $\lambda/\Lambda = \theta_B$, where λ is the electron wavelength and Λ is the periodicity. The condition $\alpha_o > \theta_B$ must be satisfied for overlap of the diffraction discs to occur (Chapman, McFadyen and McVitie 1990; Smith 1997). Only the areas involving overlap between the undiffracted and diffracted beams carry information in the difference image. This standard DPC imaging technique allowed topographical and lattice images to be achieved simultaneously (McColgan 1989). However, improved structure analysis can be achieved if this information can be separated.

3.5 The Modified DPC Imaging Mode

Chapman et al. (1990) have developed a modification to the DPC detector geometry which allows appreciable separation of the topographic and lattice information. This was achieved by dividing the detector into eight segments to take the form of an outer annular quadrant detector surrounding an inner solid quadrant detector as shown in figure 3.6.

The detector in use in the VG HB5 STEM is an Oxford Instruments eight quadrant silicon detector comprising two separate detectors with four p-n junction diodes fabricated on each piece of silicon. The upper set, in the shape of an annular quadrant, is mounted on top of, but electrically isolated from, the lower set which is in the form of a solid quadrant detector. The annular top quadrant has a diameter of 25mm and an inside diameter of 9.7mm.

Probe Forming Aperture

Electron Motion

**Specimen**

Quadrant Detector

Figure 3.5 : Differential Phase Contrast Imaging Mode (DPC)

diffracted cones of the same angular radius but displaced from the primary cone by an angle $\lambda/\Lambda=\theta_B$, where λ is the electron wavelength and Λ is the periodicity. The condition $\alpha_s>\theta_B$ must be satisfied for overlap of the diffraction discs to occur (Chapman, McFadyen and McVitie, 1990), (Smith, 1997). Only the areas involving overlap between the unscattered and diffracted beams carry information in a difference image. This standard DPC imaging technique allowed topographic and lattice images to be achieved simultaneously (McColgan 1989). However, improved structure analysis can be achieved if this information can be separated.

3.9 The Modified DPC Imaging Mode

Chapman et al (1990) have developed a modification to the DPC detector geometry which allows appreciable separation of the topographic and lattice information. This was achieved by dividing the detector into eight segments to take the form of an outer annular quadrant detector surrounding an inner solid quadrant detector as shown in figure 3.6.

The detector in use in the VG HB5 STEM is an Oxford Instruments eight quadrant silicon detector comprising two separate detectors with four pn junction diodes fabricated on each piece of silicon. The upper set in the shape of an annular quadrant, is mounted on top of, but electrically isolated from, the lower set which is in the form of a standard quadrant detector. The detector has an outside diameter of 23mm and an inside diameter of 9.7mm.
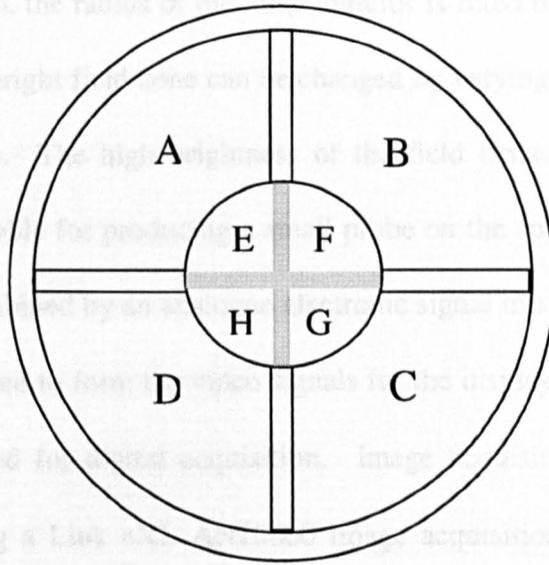
Figure 3.6 : Oxford Instruments Eight Segment Detector for DPC

During operation, the radius of the inner annulus is fixed but the area of the detector covered by the bright field cone can be changed by varying the excitation of the post specimen lenses. The high brightness of the field emission gun in the STEM is particularly suitable for producing a small probe on the specimen. Signals from the detector are combined by an analogue electronic signal mixing unit, the outputs from which can be used to form the video signals for the display monitors or alternatively they can be used for digital acquisition. Image acquisition on digital mode was performed using a Link eXL AN10000 image acquisition and processing system. The images were acquired with a resolution of 512x512 at 8 bits per pixel. Usually two images were acquired simultaneously. One image of each set was acquired from the difference signal (A - C) or (D - B) to yield a topographic image whilst the other was from (F - H) to provide images showing the internal structure of the particles although (E - G) could also have been used to obtain internal structure. The imaging condition used when acquiring was condenser lens C2 and a 30μm ROA.

3.10 Parallel Electron Energy Loss Spectroscopy (PEELS)

The theory behind this section is given in Chapter 7 of this thesis. In the pages that follow, details are given of the spectrometer in use, the alignment of the STEM for PEELS and the problems encountered during spectrum acquisition.

The spectrometer used in this work is a Gatan model 666 parallel-detection electron energy loss spectrometer. A schematic diagram is shown in figure 3.7 (MacKenzie,
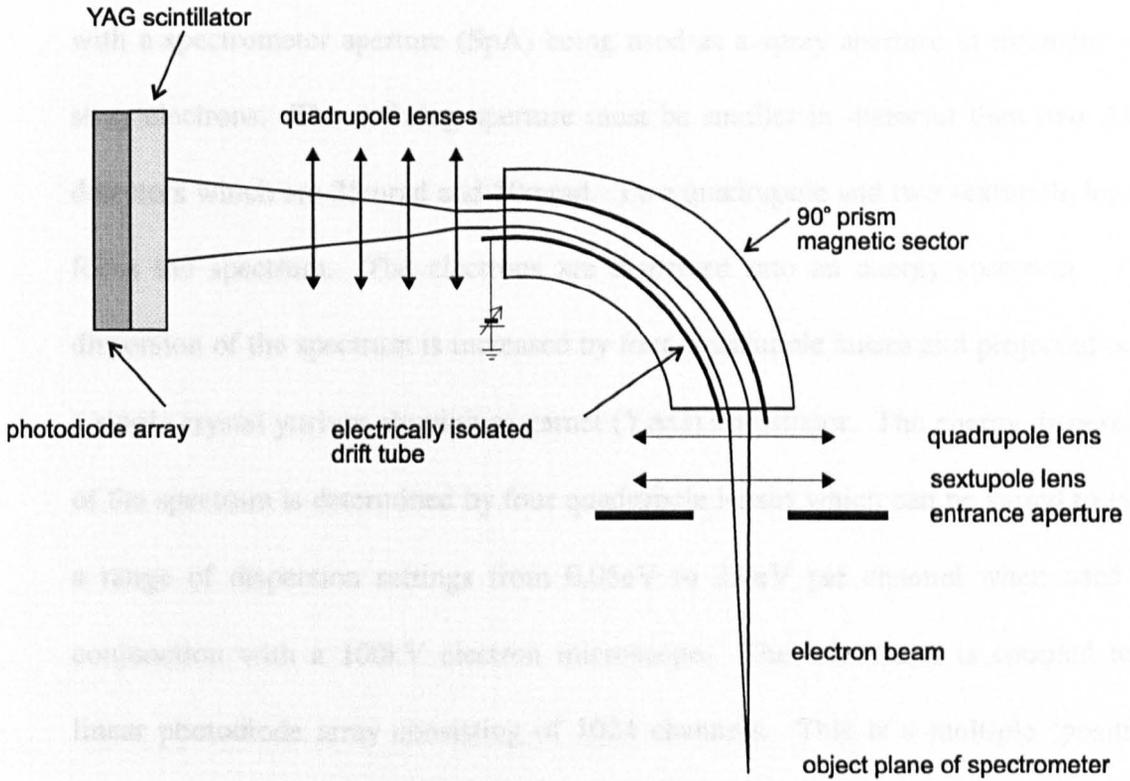
Figure 3.7 : Gatan 666 PEELS spectrometer

1997). Electrons enter the spectrometer through the entrance aperture. A collector aperture (CA) was used to define the collection angle of the PEELS spectrometer with a spectrometer aperture (SpA) being used as a spray aperture to intercept any stray electrons. The defining aperture must be smaller in diameter than two ADF detectors which are 25mrad and 50mrad. Two quadrupole and two sextupole lenses focus the spectrum. The electrons are dispersed into an energy spectrum. The dispersion of the spectrum is increased by four quadrupole lenses and projected onto a single crystal yttrium aluminium garnet (YAG) scintillator. The energy dispersion of the spectrum is determined by four quadrupole lenses which can be varied to give a range of dispersion settings from 0.05eV to 2.0eV per channel when used in conjunction with a 100kV electron microscope. The scintillator is coupled to a linear photodiode array consisting of 1024 channels. This is a multiple 'position sensitive' detector and enables parallel detection. This simply means the whole spectrum can obtained at once since electrons which have lost different amount of energy are collected simultaneously. The energy offset of the spectrum can be altered by applying a voltage to an electrically isolated drift tube.

For collection of PEELS spectra, the microscope column must be aligned in a particular way. The axis of the lower column of the microscope was defined by centring the objective aperture. This was carried out by wobbling the objective lens current and mechanically shifting the aperture until the image was stationary and 'pulsed' at approximately double the wobble frequency. The condenser lens wobble was also checked to ensure that the lower column was aligned with the necessary accuracy. Small adjustments can be made using the electrical trims whilst more

serious corrections require mechanical alignment. By the use of electrical shifts, it was possible to position the axis of the lower column on the spectrometer axis. The collector aperture was inserted on this common axis. Finally, the PSL's were excited individually and aligned mechanically to this axis. The objective aperture was used only to define the optic axis during alignment. For acquisition of data, the VOA was inserted and centred on the optic axis.

The majority of the data in this thesis was collected using a 1mm collector aperture and a 1.25mm spectrometer aperture. PSL1 was used for PEELS work and, in conjunction with these apertures, this gave a collection semi-angle of 12.5mrad. The use of the 70μm VOA to define the probe gave a convergence semi-angle of 8mrad whilst the 100μm VOA gave one of 11mrad.

Before acquiring data, it was necessary to flood the photodiode array for five to ten minutes to equalise the charge distribution in the YAG scintillator. This involved the removal of all apertures from the column except the 250μm VOA and use of the 0eV energy dispersion setting on the PEELS spectrometer. This spreads the illumination uniformly over the active area of the scintillator.

The apertures were then re-inserted and checks were made to ensure they were on axis. The EELS spectrum could then be finely focused by minimising the width of the zero loss peak. Since the optical conditions are essentially standard, only fine adjustments should be necessary. The presence of such a peak also confirms that the alignment of the microscope is acceptable. The energy dispersion and energy scale

of the spectrum was then calibrated using Gatan software and a voltage scan module (VSM).

It was then possible to collect spectra for specific areas of the indanthrone by focusing the probe on different areas of the sample. As discussed earlier, this work was concerned with the low loss area of the spectrum. A low loss spectrum was normally acquired by summing 100 acquisitions, each having an integration time of 0.04s. The zero loss peak caused saturation even at this minimum integration time. To prevent this, a beam blanking system was used. This reduced the number of counts reaching the spectrometer. Dark current spectra were also recorded in order that they could be removed from the low loss spectra for subsequent analysis. They were recorded with the same acquisition parameters as the low loss spectra but without the beam falling on the detector. The energy dispersion was typically 0.2 eV per channel which, in conjunction with the 1024 channel photodiode array this gave a range of around ~200eV for the spectrum.

One problem encountered during the acquisition and subsequent analysis of spectra was that of contamination. Carbon polymerised by the electron beam built up on the surface of the specimen thereby increasing its thickness. Obviously, this would render any thickness calculations invalid and therefore this problem had to be overcome. This was done usually by flooding the specimen. Flooding involved removing all the apertures and, starting at a low magnification, irradiating the specimen whilst slowly increasing the magnification over a period of a few minutes. This fixes the contamination in place so that it cannot spread. This method was

effective in the limitation of carbon build up on the sample. This does however have implications for the specimen in terms of radiation damage and this is discussed in section 3.11.

Another problem encountered was drift of the specimen. Any mechanical movement of the specimen resulted in a small residual drifting of the specimen for a period. As spectra were taken from certain points evenly spaced across a particle, this had to be carefully monitored. However, any slight movement can usually be corrected by adjusting the electric shifts without the microscope alignment being affected.

3.11 Radiation Sensitivity in Organic Specimens

While the majority of electrons traveling through a thin specimen are unaffected, the remainder can undergo elastic scattering or inelastic scattering. Elastic scattering occurs when the electron interacts with the atoms as a whole, transferring little energy to the atom. This can provide structural information about the specimen without inducing damage. In inelastic scattering the incident electron interacts with the orbital electrons in the structure. Due to their identical masses, the resulting energy transfer can be large and molecular excitation and ionization may occur.

A consequence of this energy transfer is that many specimens, particularly organic materials, experience damage upon irradiation by the electron beam. This damage is characterised by loss of crystallinity and/or mass loss with both effects becoming more pronounced as irradiation continues. As a result, for most beam sensitive

materials, the amount of information which can be obtained is limited by radiation damage rather than by instrumental performance.

Structural damage in crystalline samples can be observed by monitoring the change in the electron diffraction pattern of such a sample (Isaacson, 1979). Fading of the diffraction spots indicates the molecules have either suffered internal disruption or a change in their orientation with respect to one another. This occurrence implies reduced long range crystalline order but not necessarily a compositional alteration. The ease with which either inter or intra molecular bonds are broken will determine exactly which type of damage will take place. By measuring the rate at which high and low order diffraction spots disappear, one can gain information on the dose sustainable by a specimen before severe structural disorder occurs (Isaacson, 1979).

A decrease in electron scattering or other change relating to the electron transparency of the specimen is an indication of a loss in volatile components from the sample. It has been shown however that changes to electron diffraction patterns occur at doses an order of magnitude lower than other indicators (Isaacson, 1979).

A given incident electron dose is necessary in order that information is obtained with a given accuracy. However, this is only possible if actions are taken to prolong the useful lifetime of the specimen by ensuring it is not irradiated unnecessarily. As previously discussed, radiation damage can be considered to be a two stage process. Primary damage results in ionisation or excitation of the molecule. This may result

in the breaking of bonds leading to secondary damage processes such as diffusion. The consequences of this would be severe degradation of the structure.

There is evidence to show that primary damage may be reduced by increasing the accelerating voltage. The reasoning for this is that higher energy electrons will interact more weakly with the specimen thereby depositing less energy whilst traversing the specimen (P.McColgan, 1989). However at such incident electron energies, knock-on cascade collisions become more prevalent resulting in increased risk of damage (Isaacson, 1979).

Changes in structure and composition are thought to be dependent on the diffusion of highly reactive radicals following bond breaking. Therefore, secondary effects such as diffusion, which is a temperature dependent process, may be slowed down by temperature reduction. Whilst the lower temperatures may not prevent bond breakage, the mobility of the fragments will be retarded at low temperatures (Isaacson, 1979). Whilst such measures may improve compositional analysis, the crystalline order would still be destroyed resulting in degradation of the diffraction pattern.

Many techniques are employed in the attempt to limit the damage sustained by the specimen and to gain the maximum information possible from a radiation sensitive specimen. Included in these are low dose techniques, low temperature studies and specialised specimen preparation techniques (Fryer, 1993[1]), (Fryer 1993[2]).

During transmission electron microscopy studies of indanthrone, care was taken to reduce the illumination in order to minimise the amount of radiation falling onto the sample. Low magnification bright field TEM images (5K - 100Kx) gave the required information on size, shape and size distribution of the indanthrone pigment particles. Radiation damage was not particularly problematic during this technique as crystalline order was not being studied. The only occurrence which could have been caused by radiation damage was 'edge-rounding' of some particles, seen commonly in pthalocyanines (Fryer, 1980). The information from such low magnification images tends to be limited and for more detail, the particles were be studied at higher magnifications. High magnification lattice images (120Kx), although difficult to obtain in a radiation sensitive sample such as indanthrone, provided good information about the internal structure of the particles. These fringes, which represent the lattice planes, were usually viewed when the image was slightly underfocus at 120K x, using spot size 5 with the smallest condenser and objective apertures. The beam diameter was kept small in this way thus allowing fresh areas to be examined easily (Fryer, 1980). However, even with these measures to minimise the dose to the specimen, the fringes usually disappeared after 1-4 seconds. Similar effects have been seen with pthalocyanines but degradation usually takes approximately two to three times as long to occur (Fryer, 1980), (Smith, 1997). Diffraction patterns can give good structural information with the standard method used being convergent beam diffraction. This involved focusing the beam down to a small probe size and moving the sample to study different areas. Diffraction spot patterns of single crystals of indanthrone were recorded at camera lengths of 30cm and 50cm on the JEOL 1200EX TEM, again utilising the smallest condenser

aperture to reduce the radiation falling onto the specimen. The spots were not prone to fading as quickly as the lattice fringes, though the deterioration in the pattern was always visible with fading often occurring within 2 to 6 seconds. However, no obvious mass loss leading to holes in the particles occurred when the probe was focused on the specimen.

During scanning transmission electron microscopy (STEM) studies of indanthrone, contamination of the specimen was a common problem. The specimen thus had to be flooded as discussed in section 3.10. This would have had a destructive effect on the crystallinity of the indanthrone although this was less important for the work carried out in the STEM when compared with the high resolution TEM work. Although destruction of the crystalline order occurred quickly, there was no evidence of serious mass loss which would be caused by the focused probe drilling a hole through the sample. However, work carried out with the quadrant detector was hampered by this loss of crystallinity. Previous DPC work carried out on copper pthalocyanine (CPC) pigments (Smith, 1997) has enabled both topographic and lattice images to be recorded simultaneously. CPC's are much less radiation sensitive than indanthrone and it was therefore impossible to obtain the same level of detail in the images.

Chapter 4

Low Magnification Studies of Indanthrone

4.1 Introduction

As discussed in Chapter 1, the colouring properties of pigments are strongly dependent on the size, shape and distribution of the pigment particles and on their internal structure. This chapter describes the application of imaging techniques available on the CTEM to investigate various samples of indanthrone pigments. Surface area measurements obtained by the BET method described in Chapter 2 were also obtained for the majority of samples and are compared with the relevant micrographs. These micrographs were also used to measure the average particle size for selected samples enabling further comparisons to be made. It should be noted that when particle size is discussed, the length of the particle is the dimension of interest in indanthrone as growth is strongly promoted along this axis in most cases.

67

Section 4.2 reviews the production of pigmentary indanthrone and shows images corresponding to the three key stages in the pigmentation process. In section 4.3 results are presented from low magnification and surface area studies of indanthrone refluxed in nitrobenzene solvent. Analysis of these results is presented in section 4.4. Results obtained from indanthrone which was treated with isopropanol solvent are given in section 4.5. Similarly, the action of the methyl benzoate solvent is investigated in section 4.6, with further analysis presented in section 4.7. Conclusions about the investigations using low magnification imaging and diffraction are presented in section 4.8.

4.2 The pigmentation process

Organic pigments tend to be strongly coloured molecular crystals which are finely divided. Due to their insolubility, they must be dispersed in their application medium. The extent of this dispersion affects how well a pigment can impart colour to application systems. Colour strength increases markedly with decrease in particle size and ideally particles in the final ink or paint resin system should be individual crystals. However, flocculation will occur if the particles are too small leading to poor dispersion. With indanthrone, the average finished pigment particle size is usually ~80-100nm and, in a good pigment, the particle size distribution should be as narrow as possible.

As discussed in Chapter 1, indanthrone is converted from the non-pigmentary form to the pigmented form by a two stage process. Non-pigmented indanthrone takes the form of long, lath shaped particles (generally >500nm in length) as shown in figure 4.1. The first stage of the pigmentation process involved this crude form being dissolved and precipitated by acid turbulent drown out as detailed in section 1.3. This produces a non-crystalline, amorphous form illustrated in figure 4.2 which can be described as "post drown-out" indanthrone. The diffraction patterns from such a sample were found to fade more quickly than could be recorded and there were no defined spots to indicate the presence of any degree of crystallinity. The final stage involved solvent conditioning by reflux of the drowned out indanthrone to promote crystal growth producing the final form of the pigment. A typical solvent treated sample is shown in figure 4.3. The size of these final particles is dependent on (among other things) the type and percentage of solvent used to treat the drowned out indanthrone and the length of time over which reflux extends. This project is concerned with this final stage of pigmentation and the crystal growth resulting from solvent treatment of the particles.

4.3 Imaging and surface area results for indanthrone refluxed in nitrobenzene

A series of low magnification images were recorded for each sample in order that samples produced using different processes could be compared. In order that true comparisons may be made, samples produced by Zeneca will be studied separately from
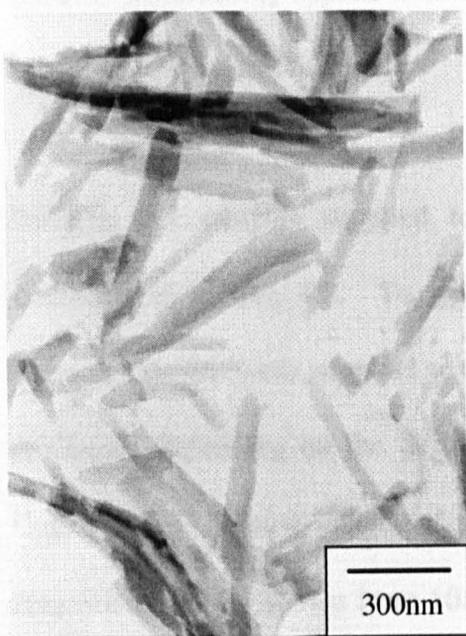
Figure 4.1 : Crude indanthrone
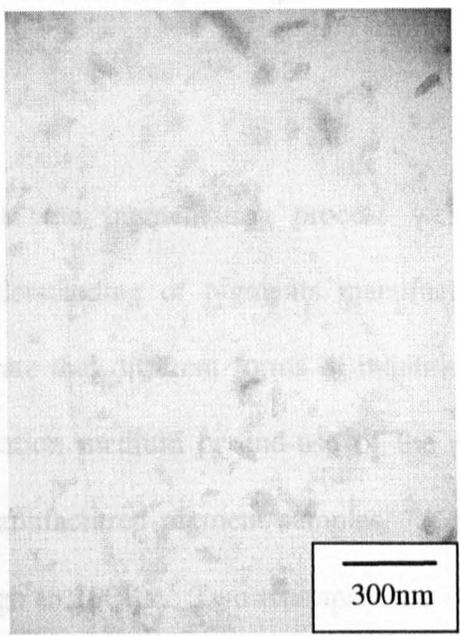


Figure 4.2 : Post drown-out indanthrone
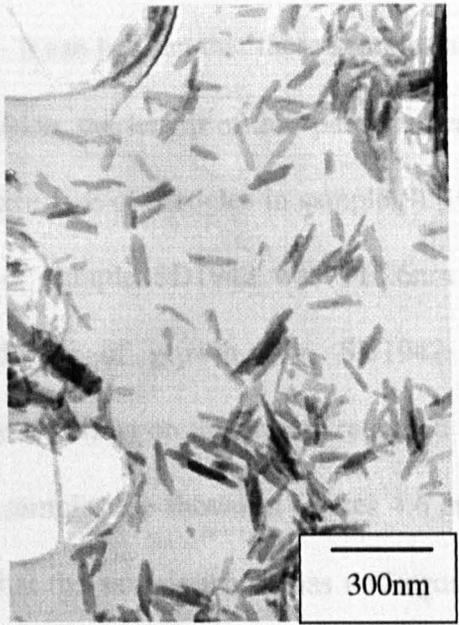
Figure 4.3 : Solvent treated indanthrone

samples produced by myself at Zeneca. These later samples originated from a single batch of drowned out material.

Initially, the samples supplied to illustrate the pigmentation process were those discussed in section 4.2. To gain an understanding of pigments manufactured by Zeneca, samples were supplied to demonstrate that different forms of indanthrone are produced, depending on the desired application medium or end-use of the pigment. Figures 4.4, 4.5 show images of typical manufactured pigment samples. A range of magnifications are shown from 10Kx through to 100Kx. Two examples are shown of 50Kx images as these give the best overall view of the pigment particle size, shape and distribution. Figure 4.4 shows sample SD1941 which was refluxed in 30% nitrobenzene for 3 hours and can be compared to SD1942 in figure 4.5 which underwent 20% solvent treatment for 16 hours. It can be seen that these samples are comparable in size and, for a more precise comparison, the length of 200 particles was measured for each sample. This revealed the average size of particles in sample SD1941 to be 129.6nm whilst the average particle size of sample SD1942 was 116.6nm indicating that SD1941 has achieved a greater degree of growth than SD1942. This shows that solvent concentration has a greater effect on the growth rate then reflux time. The particle size distributions for these samples are shown in figures 4.6 and 4.7. The structure of these histograms indicates that the sample which has undergone slightly more growth has a greater number of larger particles particularly in the 100-140nm range combined with a

Figure 4.4: SD1941 - 30% nitrobenzene for 3 hours
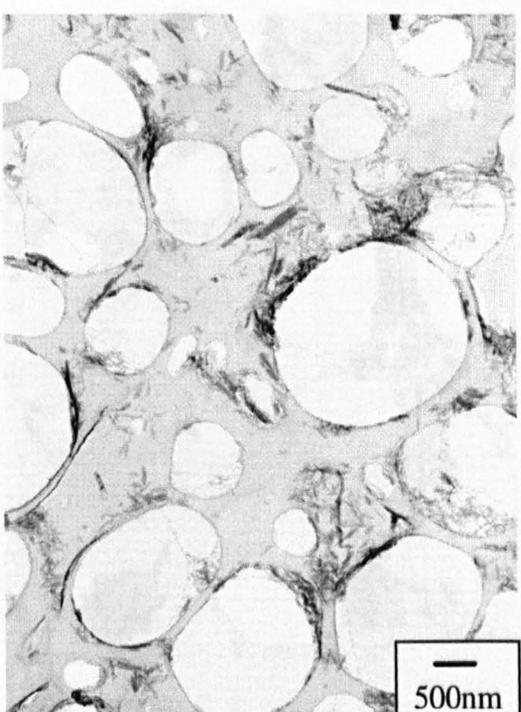
(a) 10K image of SD1941

(b) 100K image of SD1941
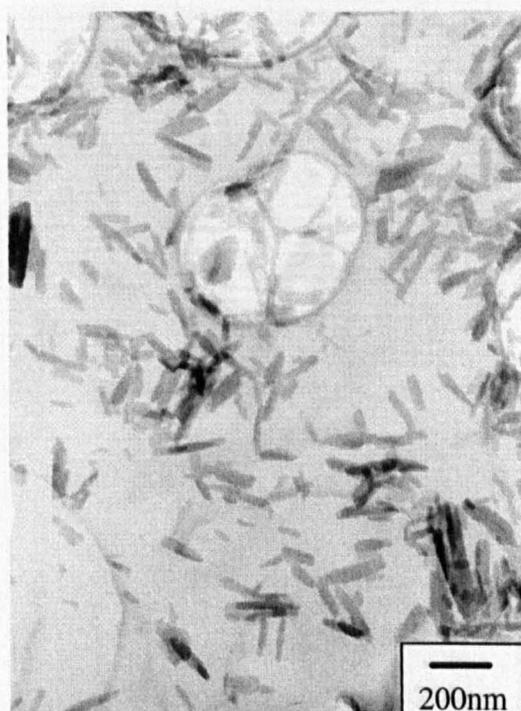
(c) 50K image of SD1941

(d) 50K image of SD1941

Figure 4.5 : SD1942 - 20% nitrobenzene for 16 hours
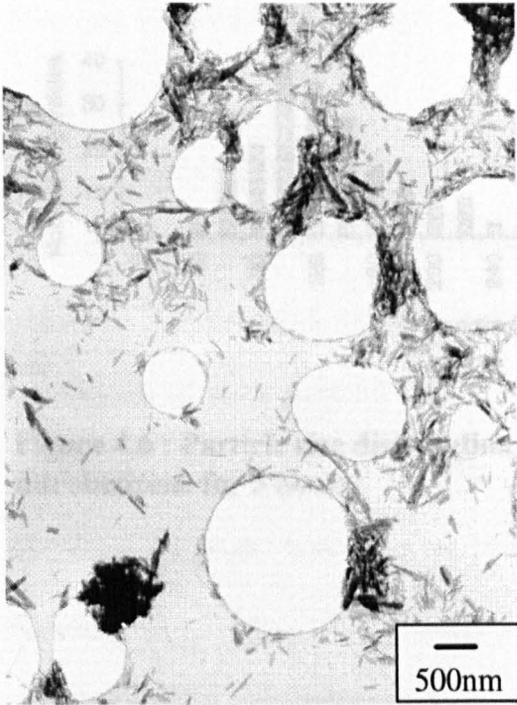
(a) 10K image of SD1942
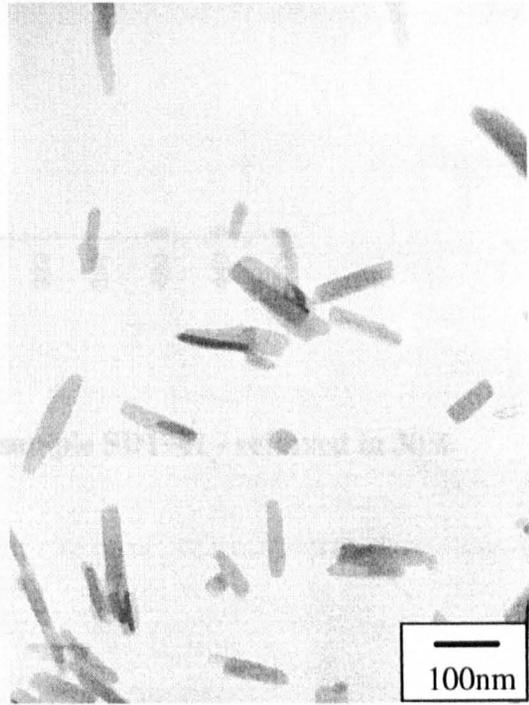
(b) 100K image of SD1942

(c) 50K image of SD1942

(d) 50K image of SD1942
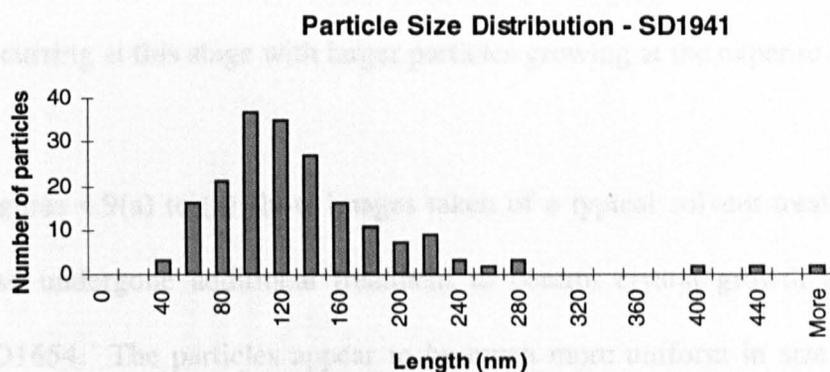
Figure 4.6 : Particle size distribution for sample SD1941 - refluxed in 30% nitrobenzene for 3 hours
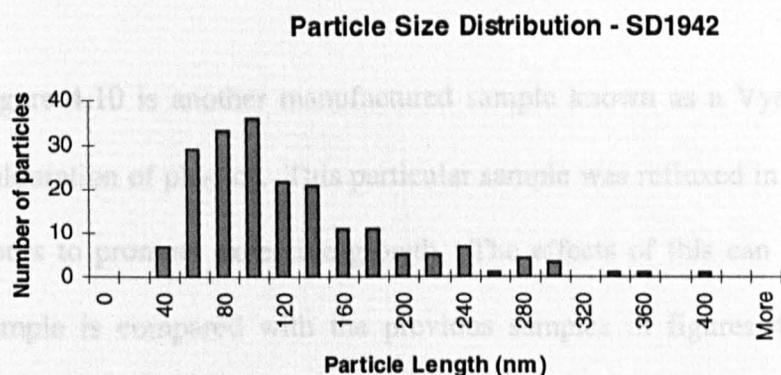
Figure 4.7 : Particle size distribution for sample SD1942 - refluxed in 20% nitrobenzene for 16 hours

smaller number of particles in the 40-80nm range. This suggests growth by ripening is occurring at this stage with larger particles growing at the expense of smaller particles.

Figures 4.9(a) to (c) show images taken of a typical solvent treated sample which has also undergone additional treatment to control crystal growth and is referred to as SD1654. The particles appear to be much more uniform in size and the particle size distribution of these particles which is shown in figure 4.8 reflects this. The curve of particle sizes is much tighter than the previous two samples indicating that the additional treatment was effective in inhibiting growth of larger particles whilst also lowering the number of very small particles. This gives rise to a high number of particles confined to a relatively small range in the centre.

Figure 4.10 is another manufactured sample known as a Vynamon which is used for colouration of plastics. This particular sample was refluxed in 50% nitrobenzene for 20 hours to promote excessive growth. The effects of this can easily be seen when this sample is compared with the previous samples in figures 4.4, 4.5 and 4.9. In the Vynamon sample there is further evidence to suggest that ripening has occurred - an increased number of large particles with a number of very small particles visible, particularly in figure 4.10(b).

Studies were then carried out at Zeneca to produce a series of samples from a single drown-out batch of indanthrone. The surface area values obtained for these samples are

Particle Size Distribution - SD1654

Figure 4.8 : Particle size distribution for sample SD1654 - solvent treated and additional treatment to control growth

Figure 4.9 : SD1654 - Solvent Treated with additional growth control treatment
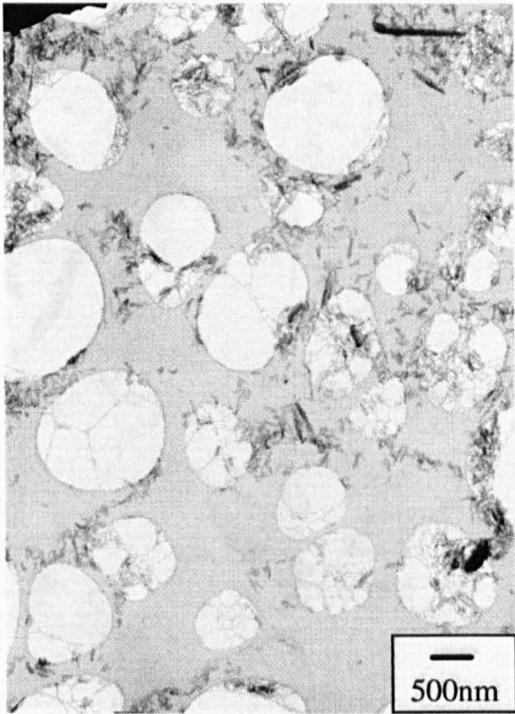
(a) 10K image of SD1654
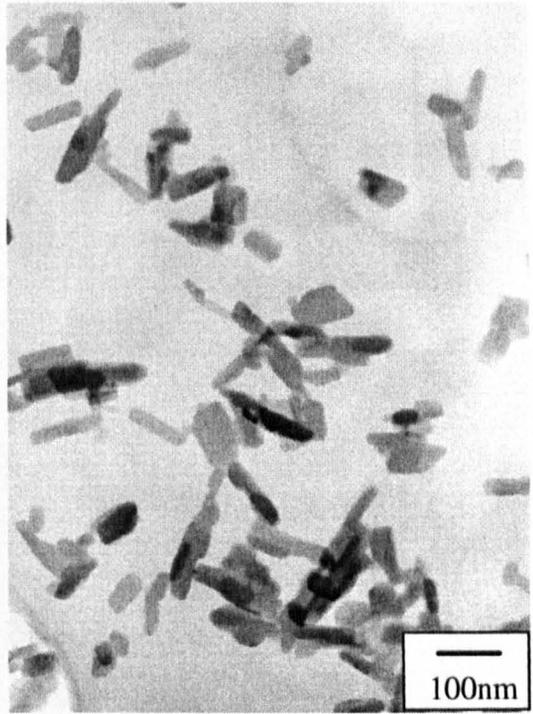
(b) 100K image of SD1654
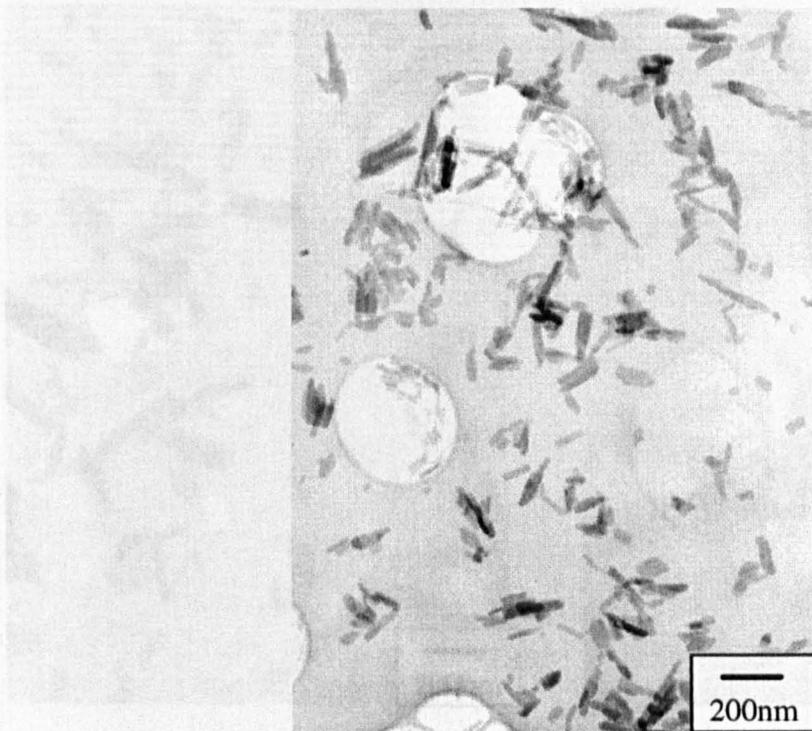
(c) 50K image of SD1654

**Figure 4.10 :** Vynamon Sample - 50% nitrobenzene for 20 hours on plant

(a) 10K image of Vynamon
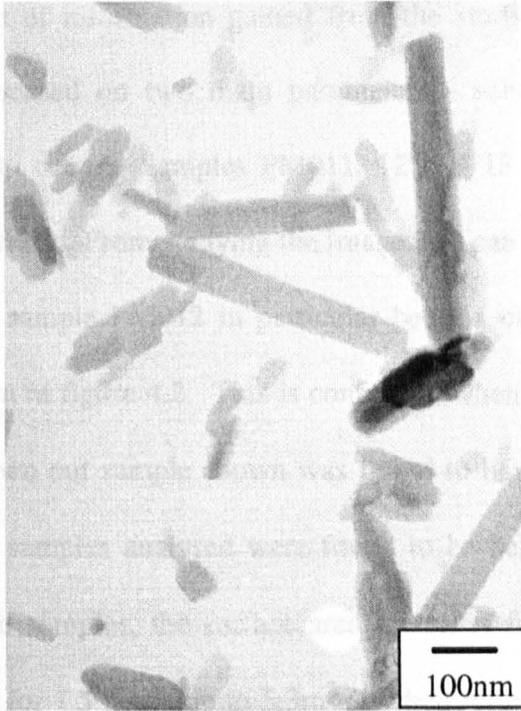
(b) 100K image of Vynamon

(c) 50K image of Vynamon
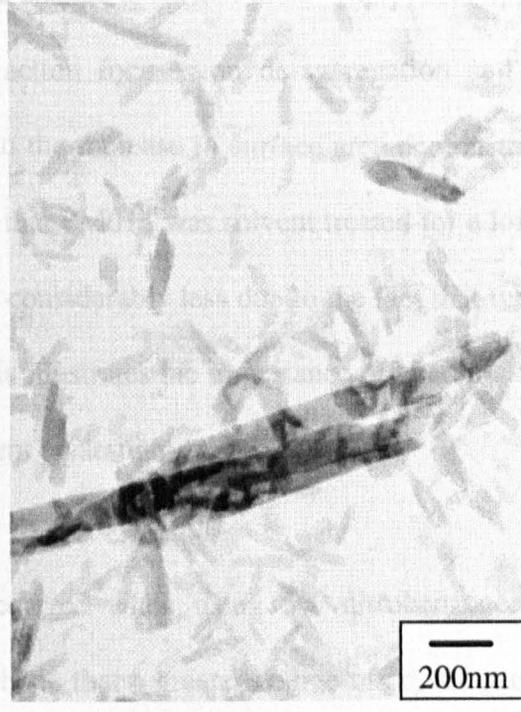
(d) 50K image of Vynamon

shown in Table 4.1 and will be referred to in discussions concerning the samples which were refluxed in nitrobenzene. In the light of information gained from the study of Zeneca supplied samples, initial studies focused on two main parameters - solvent concentration and time allowed for reflux to occur. Samples PM011, 12 and 13 are shown in figures 4.11, 4.12 and 4.13 respectively. From studying the images we can see that very little growth has taken place and sample PM012 in particular bears a close resemblance to the drown out material shown in figure 4.2. This is confirmed when we study the data shown in table 4.1. The drown out sample shown was found to have a surface area of $1.8m^2g^{-1}$ and all drown out samples analysed were found to be below $2m^2g^{-1}$. Turning now to the solvent treated samples, the surface area increases from $1.4m^2g^{-1}$ when refluxed in 5% nitrobenzene for 1.5 hours up to $5.3m^2g^{-1}$ when refluxed in the same concentration of solvent for three hours. However, the change in particle size on the image does not signify a four-fold change in surface area. This would appear to be due to the fact that initial solvent action focuses on de-aggregation and de-flocculation of the particles and this leads to the increase in surface area demonstrated by these samples. Also, considering the fact that PM011 was solvent treated for a longer time in total than PM013, its surface area is considerably less due to the fact that the oil bath was turned off after only one hour. This illustrates the importance of heat in aiding de-flocculation of the particles and subsequent crystal growth.

In view of the lack of growth which occurred when using 5% nitrobenzene, the concentration was increased to 20% in the hope that a greater degree of crystal growth

Table 4.1 - Surface areas for samples prepared using nitrobenzene

| Sample	Solvent present*	Time	Solvent removal	Surface area (m^2g^{-1}) ±0.2
PM01	0% - drown out batch	0	N/A	1.8
PM011	5%	1 hour with heat; overnight without	distillation	3.1
PM012	5%	1.5 hours	distillation	1.4
PM013	5%	3 hours	distillation	5.3
PM014	20%	3 hours	distillation	63.0
PM020	0% - drown out batch	0	N/A	1.2
PM021	30%	3 hours	distillation	67.2
PM022	30%	16.5 hours	distillation	59.4
PM031	0% - washed with acetone and methanol	0	N/A	3.8
PM032	100%	Sampled at 80°C after 20 minutes	filtration	79.5
PM033	100%	Sampled at 96°C after 35 minutes	filtration	67.2
PM034	100%	Sampled at 96°C after 45 minutes	filtration	53.3
PM035	100%	Sampled at 96°C after 75 minutes	filtration	42.6
PM036	100%	Sampled at 96°C after 120 minutes	filtration	39.1
PM037	100%	Sampled at 96°C after 240 minutes	filtration	35.5
PM038	100%	Sampled at 96°C after 335 minutes	filtration	20.3
PM039	100%	300 minutes (no heat present)	filtration	80.6
PM051	20%	30 minutes	filtration	72.7
PM052	20%	70 minutes	filtration	69.2
PM053	20%	110 minutes	filtration	68.3
PM054	20%	160 minutes	filtration	65.9
PM055	20%	200 minutes	filtration	64.0

Figure 4.11 : PM011 - 5% nitrobenzene with indanthrone refluxed 'overnight'

500nm
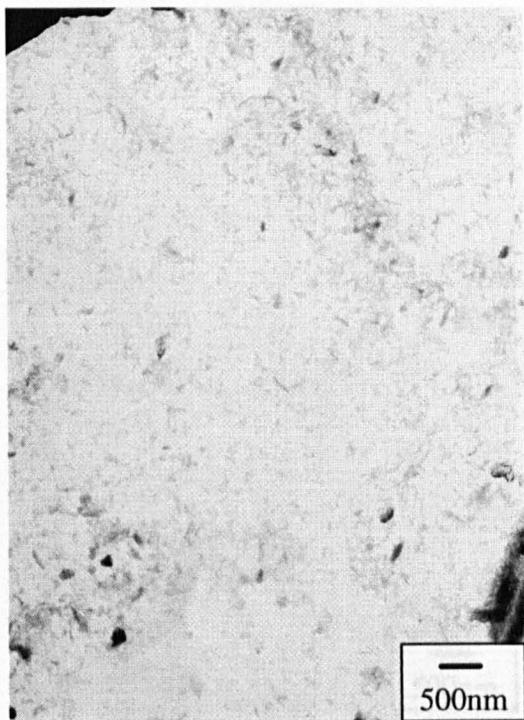
(a) 10K image of PM011

100nm
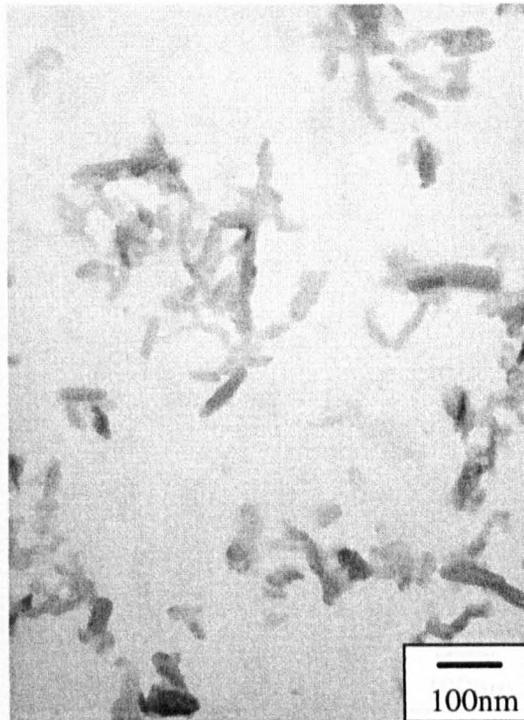
(b) 100K image of PM011

200nm
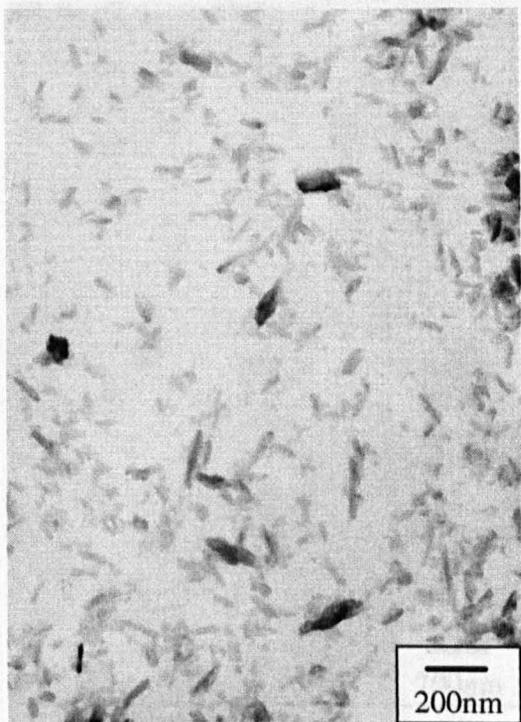
(c) 50K image of PM011

200nm
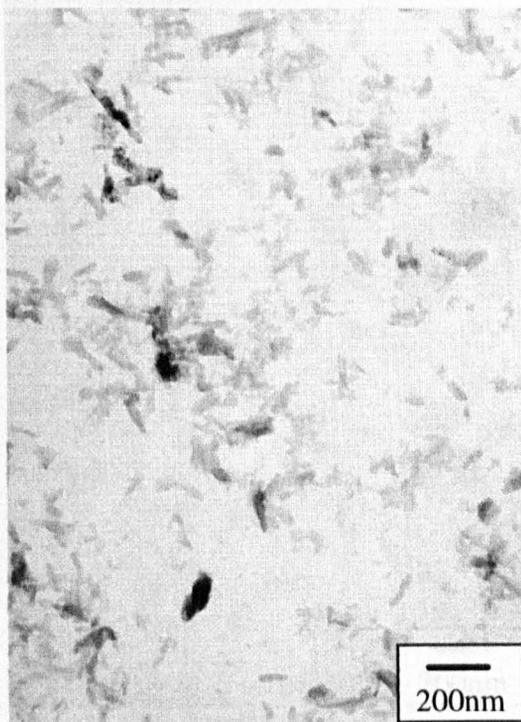
(d) 50K image of PM011

Figure 4.12 : PM012 - 5% nitrobenzene for 1.5 hours
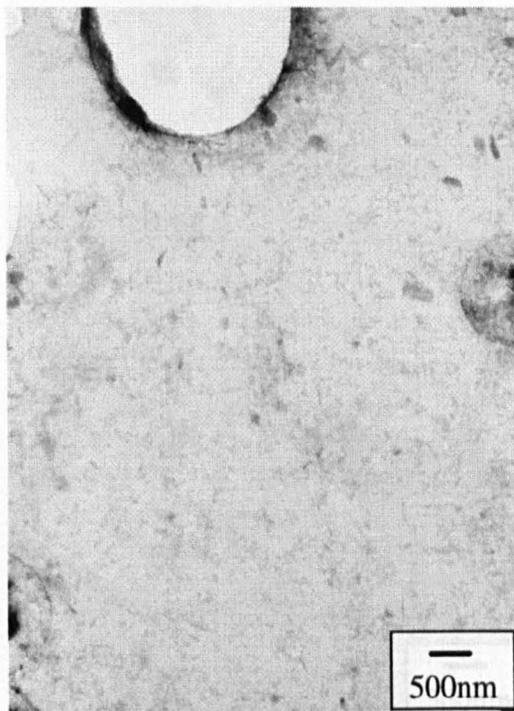


(a) 10K image of PM012
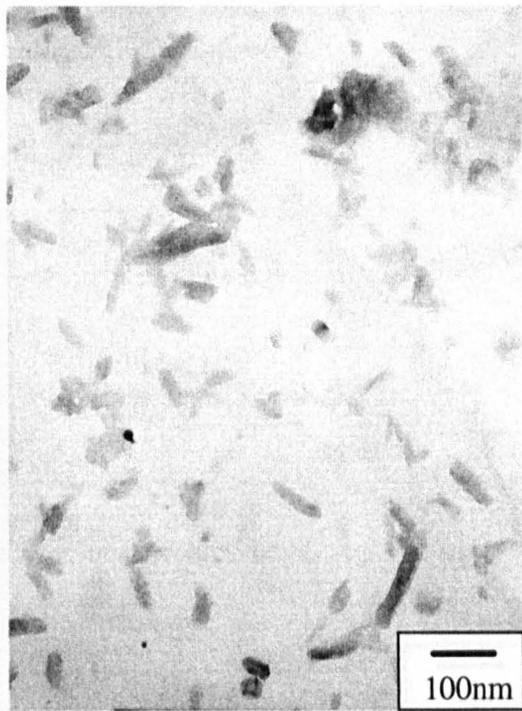
(b) 100K image of PM012
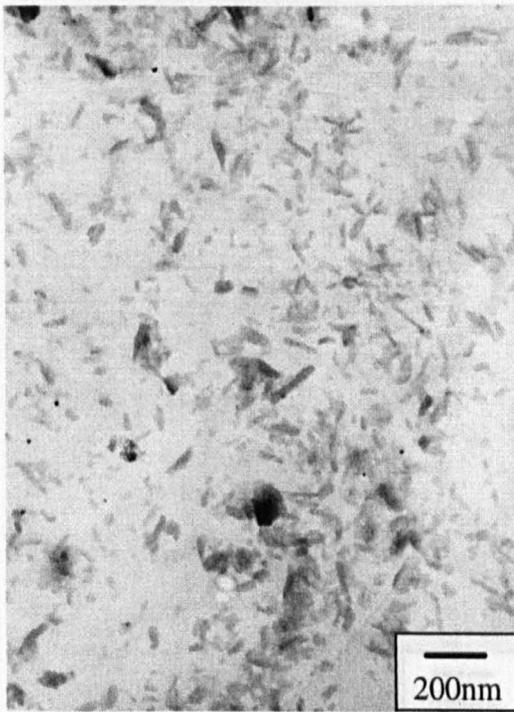
(c) 50K image of PM012
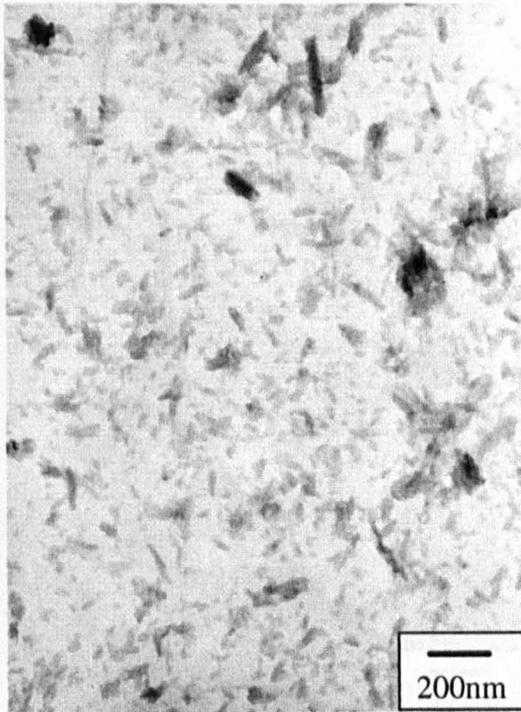
(d) 50K image of PM012

Figure 4.13 : PM013 - 5% nitrobenzene for 3 hours
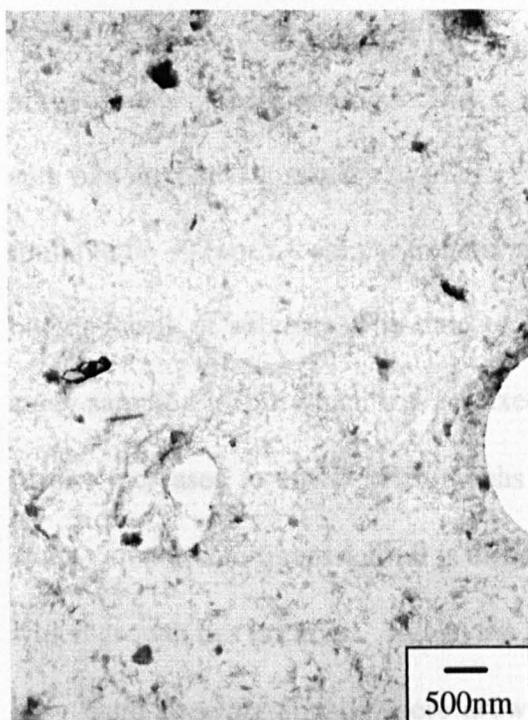

(a) 10K image of PM013
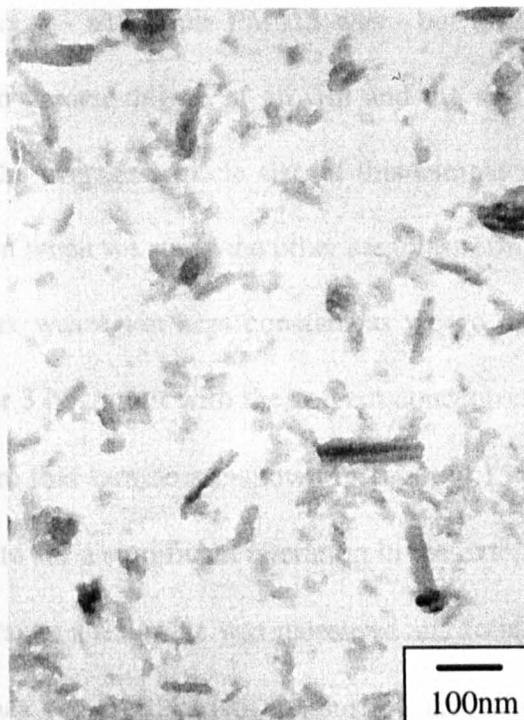
(b) 100K image of PM013
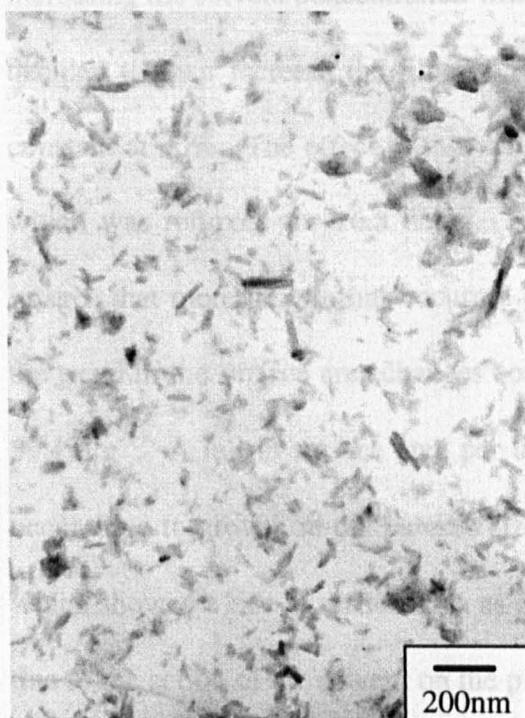
(c) 50K image of PM013
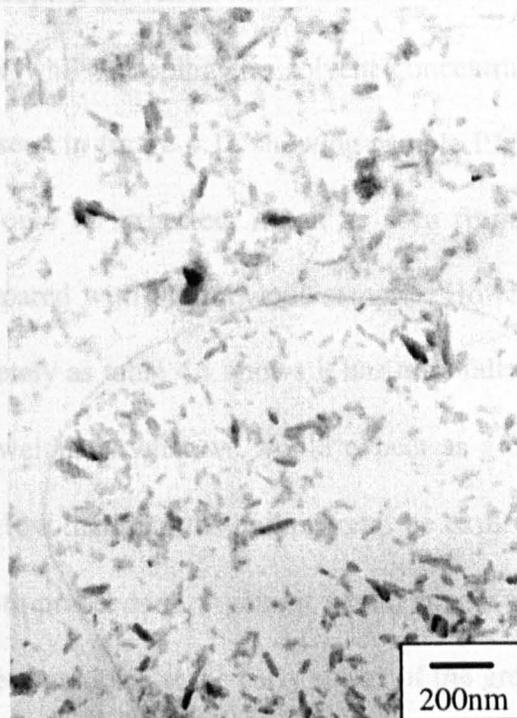
(d) 50K image of PM013

could be observed. The consequences of this are easily seen in figure 4.14 which shows sample PM014. This was refluxed for 3 hours - as sample PM013 was - but in 20% nitrobenzene. These particles show a much greater degree of growth and the surface area has increased markedly to $63m^2g^{-1}$. The average particle size of this sample was found to be ~92nm. A similar trend is shown when we study the other samples refluxed higher levels of solvent. The time of reflux was again kept constant as we go on to study sample PM021 which was refluxed for 3 hours but with the solvent concentration further increased to 30%. Micrographs from this sample are shown in figure 4.15 and when compared to figure 4.14, it is difficult to see a significant alteration in the extent to which growth has occurred. Again, the average particle size was measured and found to be ~99nm showing slightly more growth has occurred. Also, the surface area shows only a slight increase to $67.2m^2g^{-1}$. These samples clearly illustrate the effects of increasing the solvent concentration whilst keeping the reflux time constant. It was thus decided to then increase the time of reflux whilst keeping the solvent concentration constant at 30%. The effect of this can be seen in figure 4.16 showing sample PM022 which was refluxed for 16.5 hours. As would be expected, it can be seen from the images that more growth has occurred compared with the previous sample. However, the trend in the surface area changes completely as table 4.1 shows it has now fallen to $59.4m^2g^{-1}$. A fall in surface area per unit weight is what we would expect as growth occurs due to growth in the particle size. How then can the earlier trend be explained which showed a rise in surface area as growth proceeded? Again, it would appear to be due to the action of the solvent on the pigment particles at the early stages of the growth

Figure 4.14 : **PM014 - 20% nitrobenzene for 3 hours**
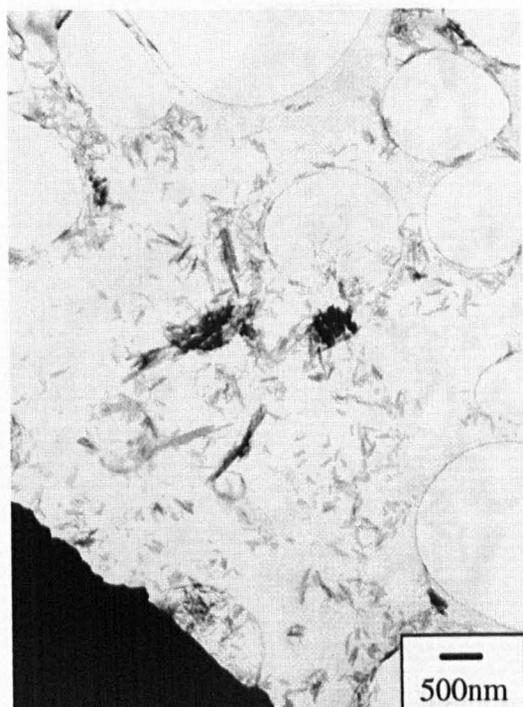
(a) 10K image of PM014
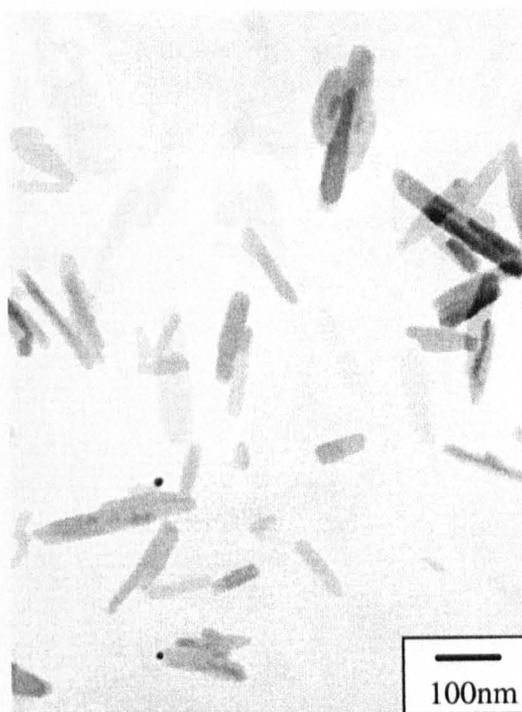
(b) 100K image of PM014
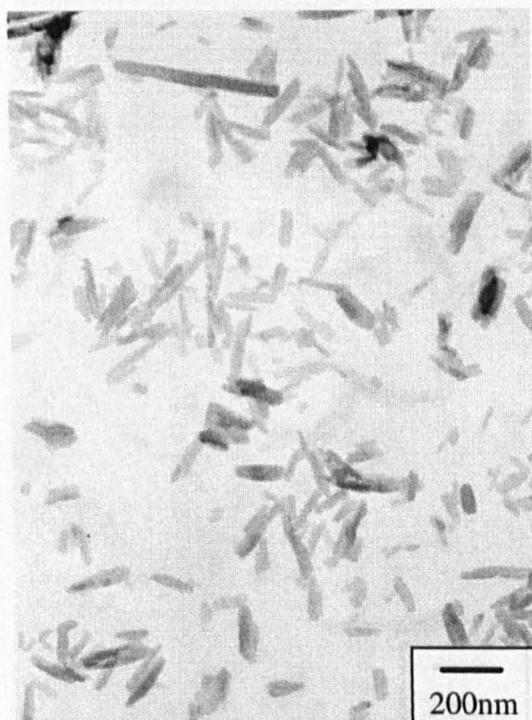
(c) 50K image of PM014
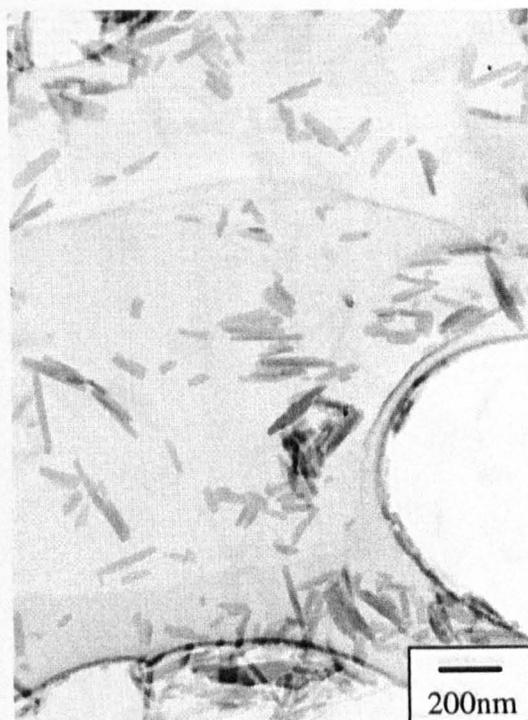
(d) 50K image of PM014

Figure 4.15 : PM021 - 30% nitrobenzene for 3 hours
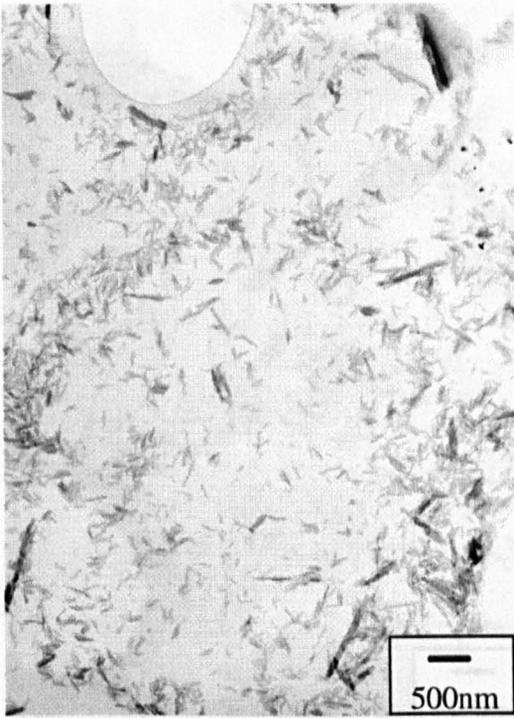
(a) 10K image of PM021

(b) 100K image of PM021

(c) 50K image of PM021

(d) 50K image of PM021

Figure 4.16 : PM022 - 30% nitrobenzene for 16.5 hours
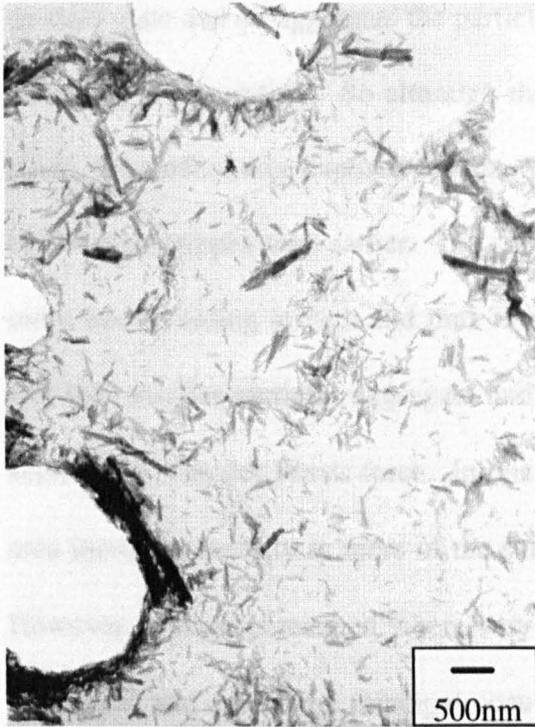
(a) 10K image of PM022
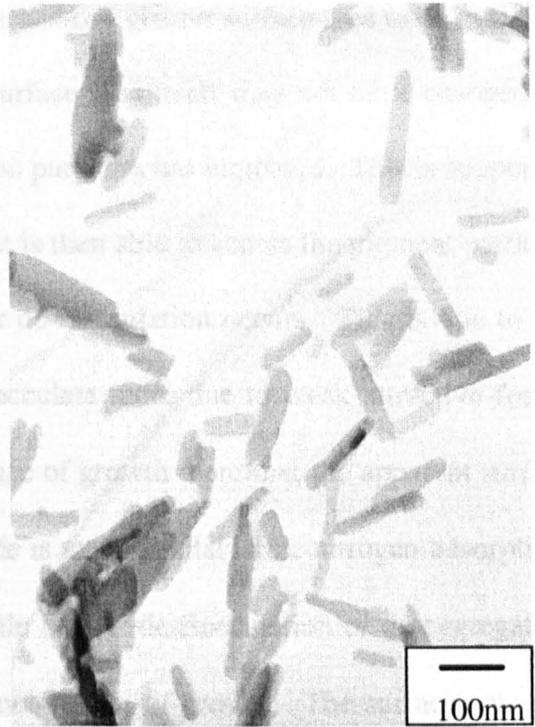
(b) 100K image of PM022

(c) 50K image of PM022

(d) 50K image of PM022

process combined with the method of surface area analysis. Initially the solvent acts to de-flocculate and de-aggregate the particles causing a greater surface area to be available for nitrogen adsorption. So although the surface area itself may not have changed by much, the surface area exposed for adsorption purposes has increased. This is supported by the micrographs seen earlier. The solvent is then able to access the pigment particles more easily, aiding growth and thus further de-flocculation occurs. This is due to the fact that smaller particles aggregate and flocculate more due to weak attractive forces such as the Van der Waals force. In this stage of growth therefore, the apparent surface area increases steadily as more of the surface is made available for nitrogen adsorption. However, a stage is reached where very little further de-flocculation or de-aggregation will occur and where the principal occurrence is that of growth. The surface area per unit weight then starts to decrease, as viewed in sample PM022.

In an attempt to gain a clearer picture of these particles as they undergo crystal growth, an experiment was carried out where a sample of the reflux mixture was removed from the vessel and the solvent removed immediately to prevent further crystal growth. This was carried out on a sample of indanthrone being refluxed in 20% nitrobenzene - a concentration already shown to promote a reasonable degree of crystal growth. The samples removed were studied and give rise to the series PM051 to PM055 as described in section 2.6. Surface areas are given in Table 4.1 for all of these samples and, in the light of this data, three were chosen for further study by microscopy. The surface areas can be seen to fall from $72.7m^2g^{-1}$ after 30 minutes in the solvent, steadily down to

$64m^2g^{-1}$ after more than three hours in the solvent. This agrees with the earlier statement that further growth will cause a reduction in the surface area. The micrographs for two of the samples, PM051 and PM055, are shown in figures 4.17 and 4.18 respectively. These were used to obtain an average particle size for the sample by measuring >60 particles per sample. The average length of pigment particles in sample PM051 was found to be 105nm and had increased to 109nm in sample PM055. Both the surface area data and the data obtained from micrographs shows that the vast majority of the growth had already taken place after only 30 minutes in the solvent. It had been expected that the surface area would have increased during de-flocculation and growth then decreased as only growth occurred as demonstrated earlier. However, the first 30 minutes of reflux with only 20% solvent present has encapsulated both the de-flocculation/de-aggregation and a relatively large degree of growth. A reduction in reflux time would obviously be beneficial from a manufacturing point of view so it is important to establish why longer reflux times such as in PM055 lead to an improvement in pigmentary qualities if the particles have completed a large amount of growth earlier in the reflux stage. Further study of the micrographs led to the belief that an investigation into the particle size distribution might be beneficial. The results of this are shown in figures 4.19 and 4.20. It can be seen that they differ significantly, with PM055 exhibiting a much tighter, more symmetrical and even distribution which would, in turn, lead to improved performance. This is also significant in terms of growth mechanisms. As growth continues, it is clear that more particles tend towards the average particle size which would also point towards ripening as being the main source

75

Figure 4.17 : PM051 - 20% nitrobenzene
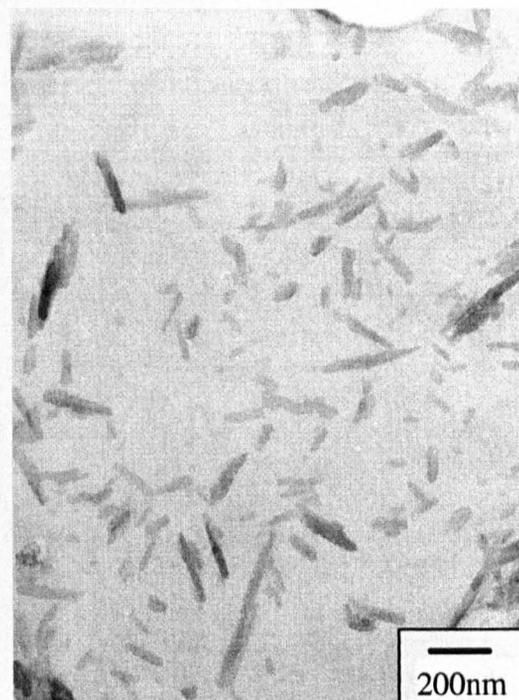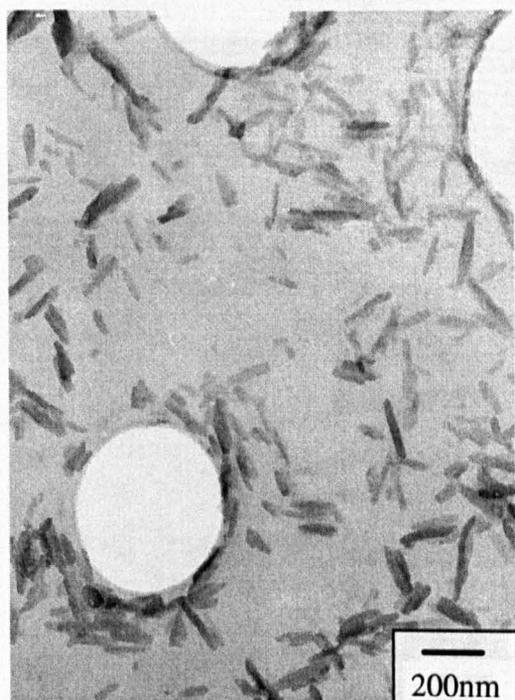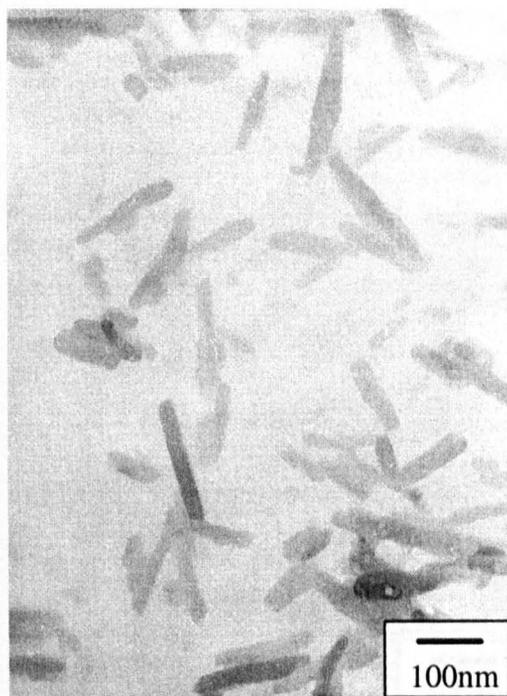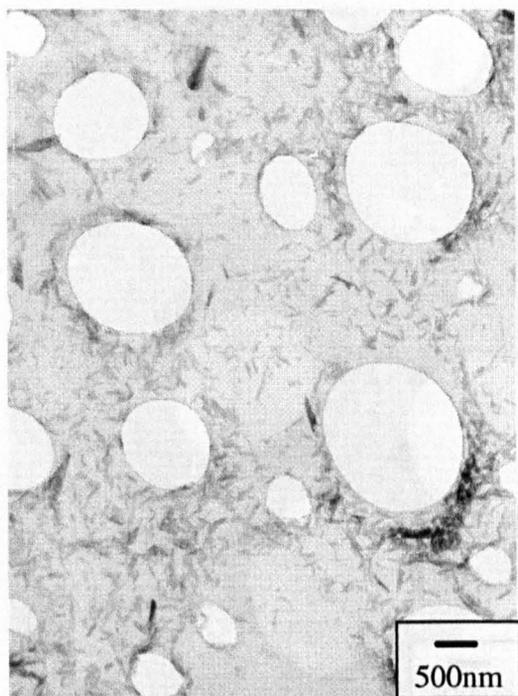
Figure 4.18 : PM055 - 20% nitrobenzene

PM051 - Particle Size Distribution
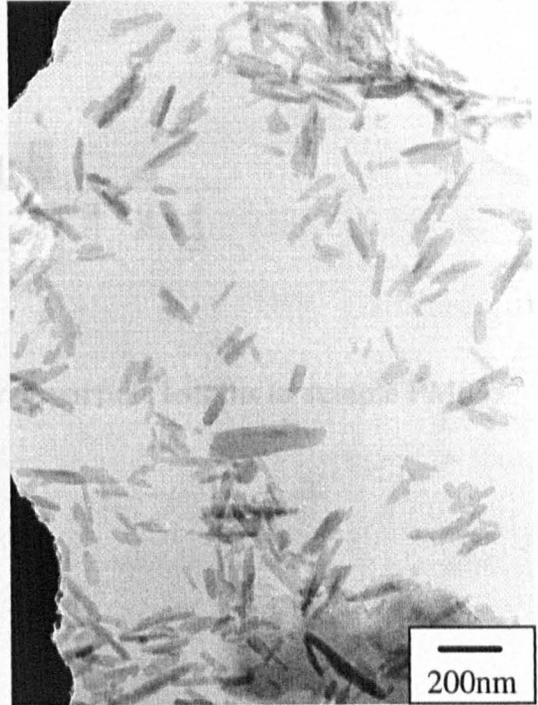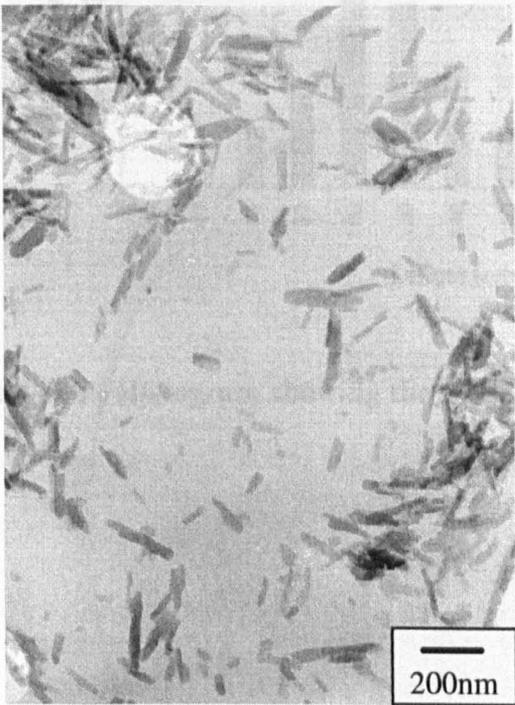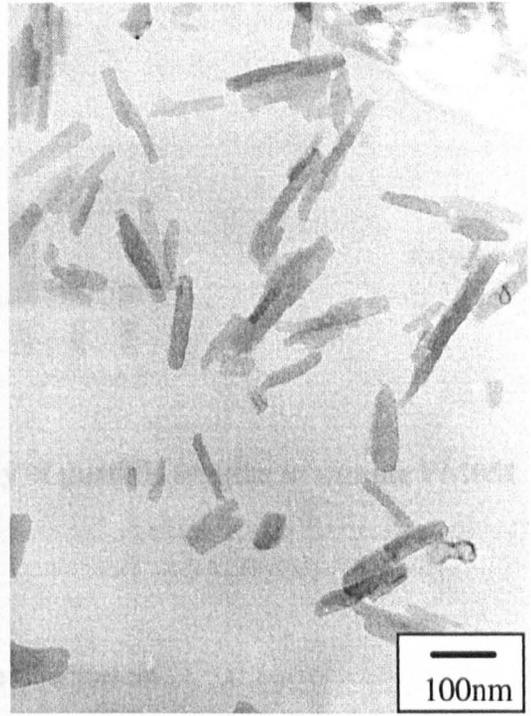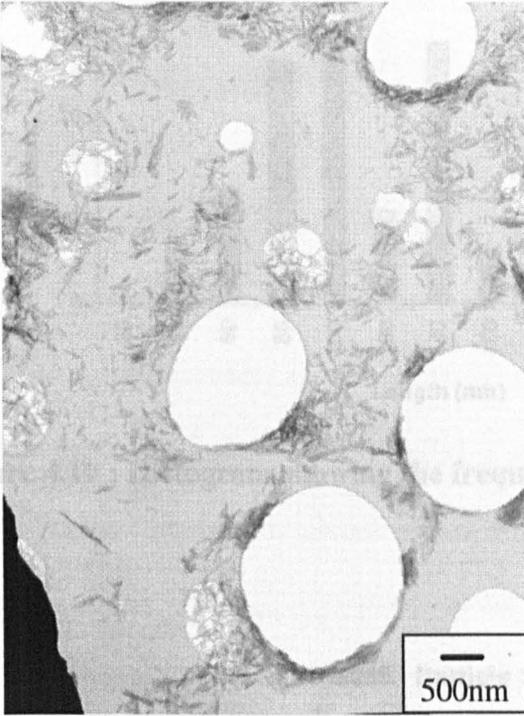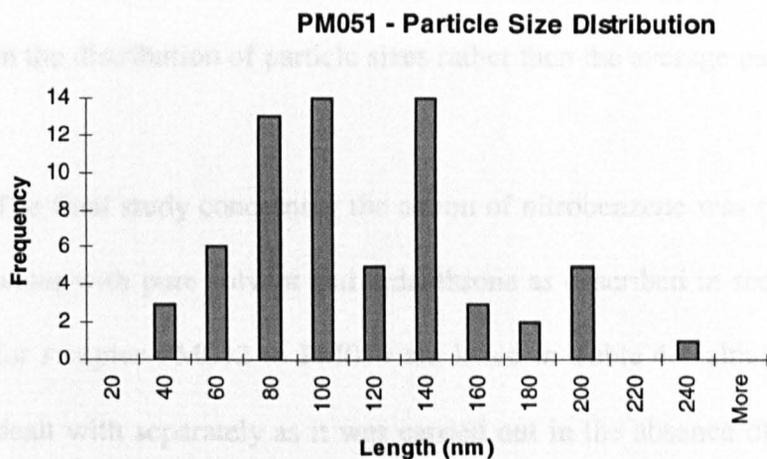
Figure 4.19 : Histogram showing the frequency of particle lengths in sample PM051

PM055 - Particle Size Distribution
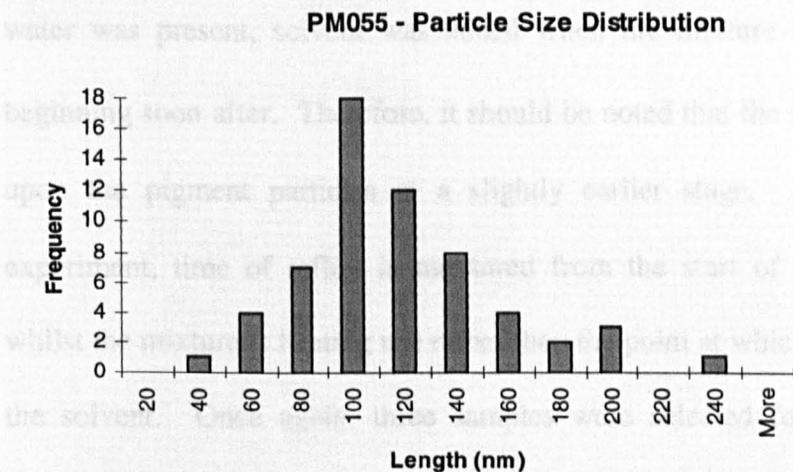
Figure 4.20 : Histogram showing the frequency of particle lengths in sample PM055

of growth at this stage. The reason behind longer reflux times would thus appear to lie in the distribution of particle sizes rather then the average particle size.

The final study concerning the action of nitrobenzene was carried out in the absence of water with pure solvent and indanthrone as described in section 2.6. The surface areas for samples PM032 to PM039 are listed in Table 4.1 although sample PM039 will be dealt with separately as it was carried out in the absence of heat. These samples were obtained in a similar way to PM051-55 by sampling at time intervals throughout reflux. However, in this case solvent was present during the heating of the mixture as water was not present to act as a carrier medium for the pigment particles. In the cases where water was present, solvent was added when the mixture reached 85°C with reflux beginning soon after. Therefore, it should be noted that the solvent has a chance to act upon the pigment particles at a slightly earlier stage. For the purposes of this experiment, time of reflux is measured from the start of the experiment (including whilst the mixture is heating up) rather than the point at which reflux began after adding the solvent. Once again, three samples were selected for more detailed study by microscopy. PM032 (20 minutes), PM034 (45 minutes) and PM037 (240 minutes) are shown in figures 4.21, 4.22 and 4.23. It can be seen from these images that excessive growth has occurred during the course of this experiment. It would appear that water is not necessary to facilitate growth of indanthrone particles during solvent treatment. Once again, table 4.1 shows decreasing surface areas as growth proceeds and we see surface areas which are a great deal lower than those found for samples refluxed in

Figure 4.21 : PM032 - No water present in prep. 10:1 nitrobenzene : indanthrone ratio. Sample removed when prep reached 80°C.

400nm

(a) 25K image of PM032

100nm

(b) 100K image of PM032

200nm
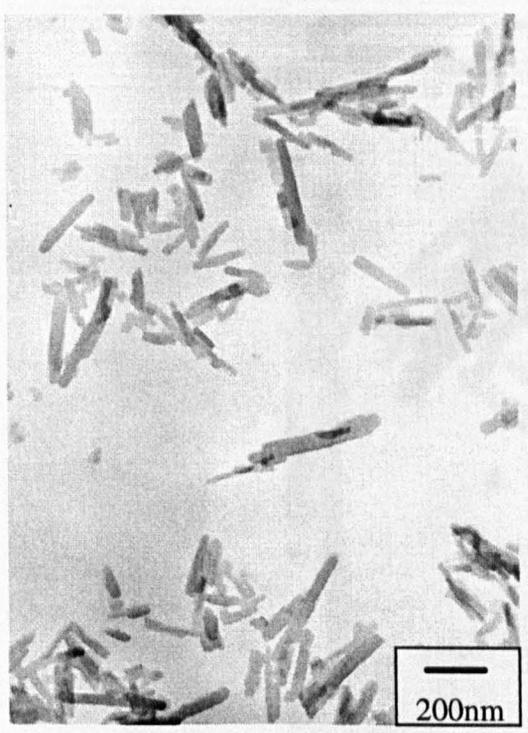
(c) 50K image of PM032

200nm
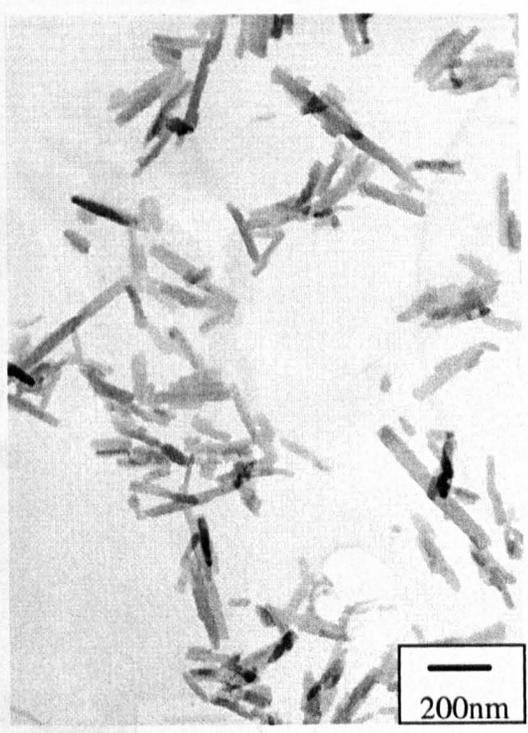
(d) 50K image of PM032

Figure 4.22 : PM034 - No water present in prep. 10:1 nitrobenzene : indanthrone ratio. Sample removed 10 minutes after mixture reached 96°C.

(a) 10K image of PM034
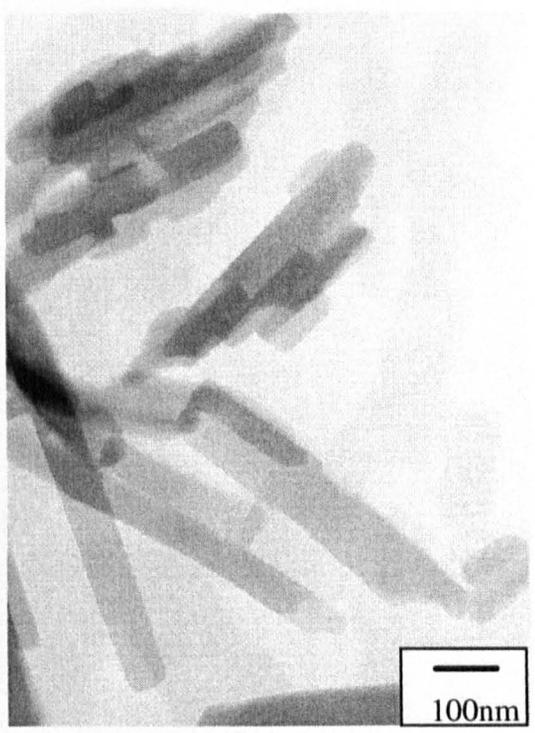
(b) 100K image of PM034
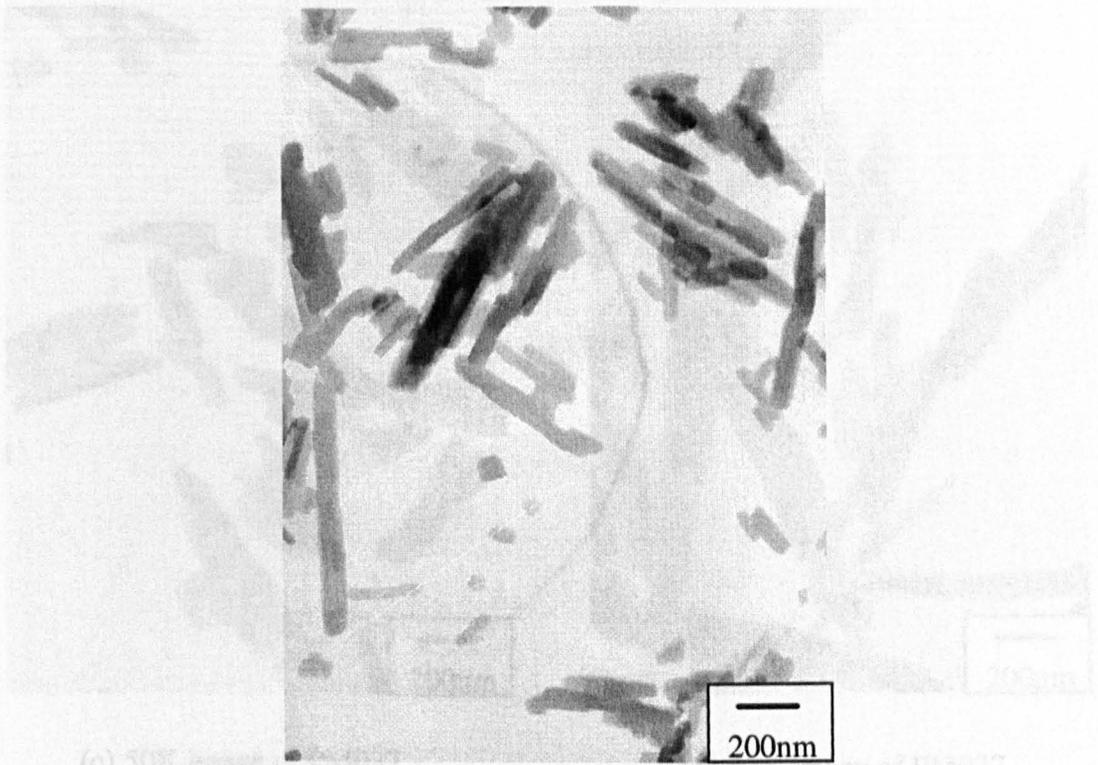
(c) 50K image of PM034

Figure 4.23 : PM037 - No water present in prep. 10:1 nitrobenzene : indanthrone ratio. Sample removed 3hrs 25 mins after mixture reached 96°C.

500nm

(a) 10K image of PM037

100nm

(b) 100K image of PM037

200nm
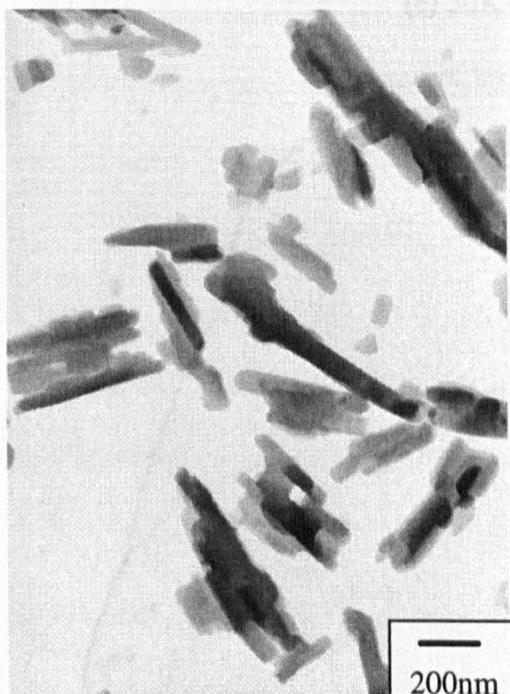
(c) 50K image of PM037

200nm

(d) 50K image of PM037

Figure 4.23(e) : PM037 - No water present in prep. 10:1 nitrobenzene : indanthrone ratio. Sample removed 3hrs 25 mins after mixture reached 96°C.

200nm

(e) 50K image of PM037

water. Average particle lengths were measured for PM032, 34 and 37 and were found to be 138nm, 204nm and 228nm respectively showing that growth was continuing although the rate of growth was decreasing. It is worth noting the level of growth which has occurred in sample PM032 after only 20 minutes and considering the sample had not even reached the usual reflux temperature of 96°C.

Finally, images of sample PM039 are shown in figure 4.24. This particles were grown in 100% nitrobenzene without the application of heat - simply drowned out indanthrone placed in a beaker with nitrobenzene and stirred regularly for five hours. It can be seen from the images and also from the surface area value of $80.6m^2g^{-1}$ that a relatively high degree of growth has taken place. However, the degree of growth is similar to sample PM032 which had spent only 20 minutes in the solvent but which had been heated from room temperature to 80°C during this period. This emphasises the importance of heat in improving the rate at which growth occurs. It is likely this is due to two main factors; heat increases the solubility of the system allowing more indanthrone molecules to go in and out of solution and increases the probability that they will then attach themselves to a growing indanthrone particle resulting in further growth. Secondly, heat and agitation increases the mobility of the molecules which will again increase the possibility that they will play a part in growth of indanthrone particles.

In an attempt to further understand the behaviour of this system during crystal growth, some of the data obtained has been collated and displayed graphically. In order that true

Figure 4.24 : PM039 - No water present in prep, no heat applied. 10:1 nitrobenzene : indanthrone ratio. Sample removed after 5 hours at room temperature.
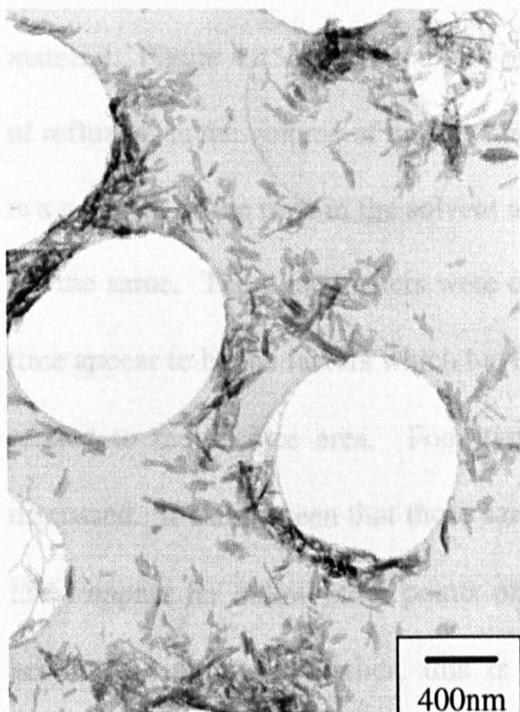
(a) 25K image of PM039
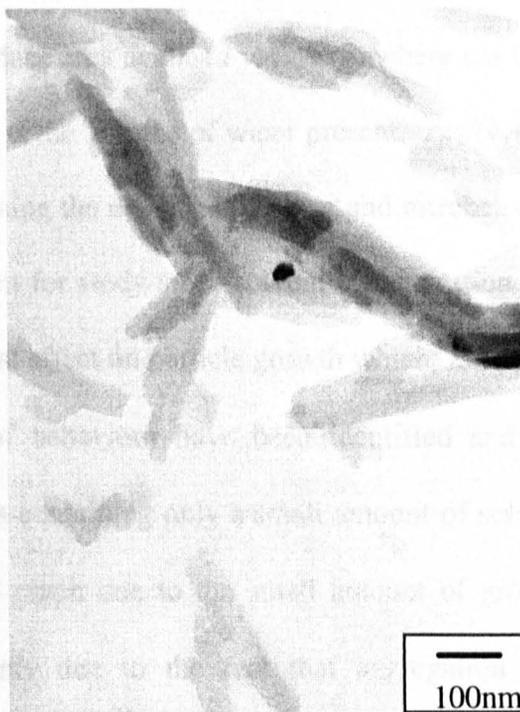
(b) 100K image of PM039

(c) 50K image of PM039

(d) 50K image of PM039

comparisons can be made, the data shown has been gathered only from samples refluxed in nitrobenzene, and only from samples produced from a single batch of drown out material. Figure 4.25(a) shows a plot of surface area against $t\, v_s/(v_s+v_w)$ where t is time of reflux, v_s is the volume of solvent and v_w is the volume of water present. $t\, v_s/(v_s+v_w)$ is a measure of the time in the solvent assuming the densities of water and nitrobenzene are the same. These parameters were chosen for study since solvent concentration and time appear to be the factors which have most effect on particle growth which, in turn, is related to the surface area. Four types of behaviour have been identified and are discussed. It can be seen that those samples containing only a small amount of solvent (5%) appear far below other points on the graph due to the small amount of growth achieved. As stated earlier, this is mainly due to the fact that aggregation and flocculation are prevalent in such samples leading to an apparently small surface area. This suggests that there is just enough solvent present to begin breaking the flocculates apart, but not enough to promote crystal growth. Nitrobenzene is less than 1% soluble in water and so the system will exist as a two phase medium with pockets of solvent distributed throughout the water based mixture provided agitation is continuous. The pigment and solvent have an affinity for one another as they are both organic in nature. The particles will, however, simply go in and out of the solvent phase continuously but with very little growth taking place, no matter how long they are held in this low solvent concentration. As they leave the solvent phase they may well re-flocculate in the aqueous phase requiring them to be broken down again on re-entering the solvent phase. However, the points for samples refluxed in 20% nitrobenzene show a large increase in
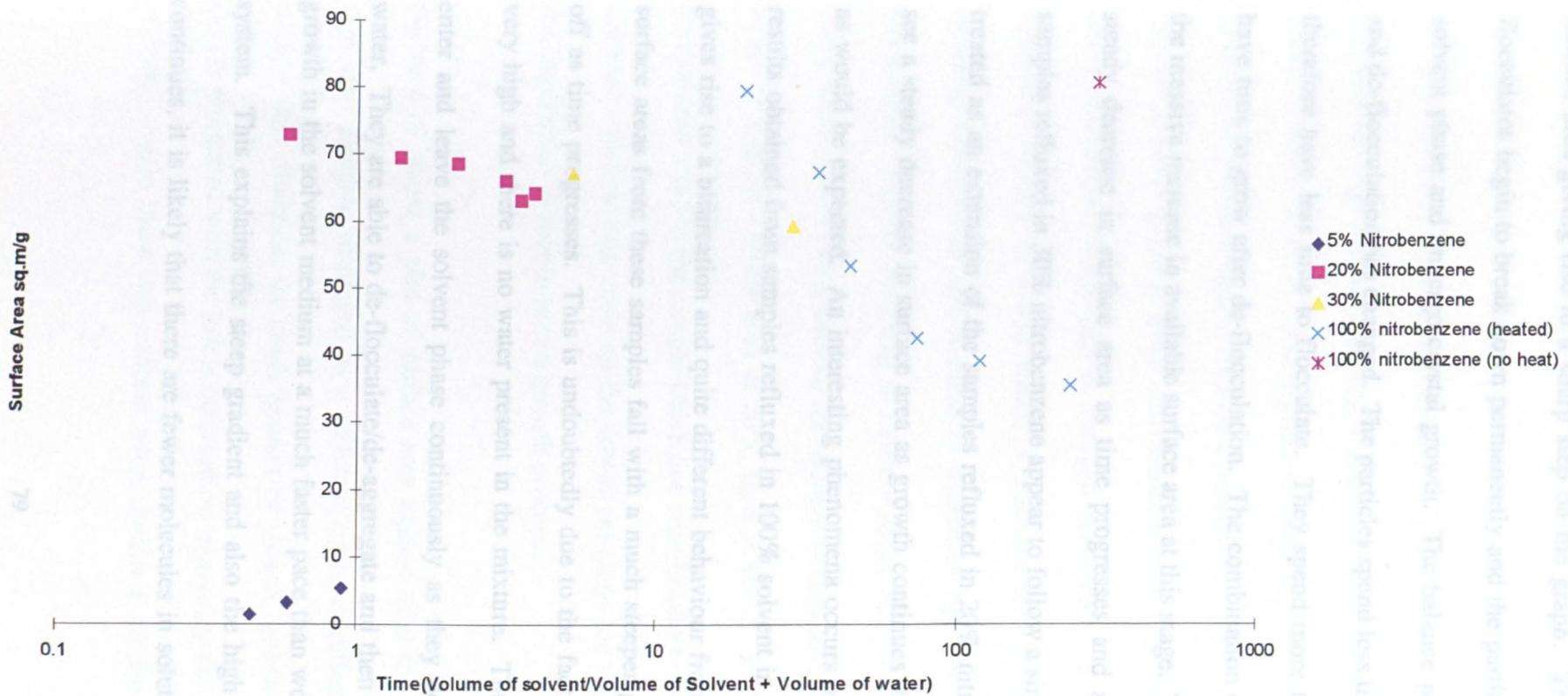
Figure 4.25(a) : Plot of Surface Area against Time of Reflux(Volume of Solvent/Volume of Solvent + Volume of Water) for samples solvent treated with nitrobenzene

surface area giving rise to a sharp step on the graph. This occurs as aggregates and flocculates begin to break down permanently and the particles can go in and out of the solvent phase and undergo crystal growth. The balance point between re-flocculation and de-flocculation has changed. The particles spend less time in the aqueous phase and therefore have less time to flocculate. They spend more time in the solvent and thus have time to grow after de-flocculation. The combination of these factors accounts for the massive increase in available surface area at this stage. These samples then follow a steady decrease in surface area as time progresses and as they grow further. The samples refluxed in 30% nitrobenzene appear to follow a similar path and can almost be treated as an extension of the samples refluxed in 20% nitrobenzene. Once again, we see a steady decrease in surface area as growth continues due to prolonged reflux time as would be expected. An interesting phenomena occurs however, when we study the results obtained from samples refluxed in 100% solvent in the absence of water. This gives rise to a bifurcation and quite different behaviour from that seen previously. The surface areas from these samples fall with a much steeper gradient initially, but levels off as time progresses. This is undoubtedly due to the fact that the level of solvent is very high and there is no water present in the mixture. Thus, particles do not have to enter and leave the solvent phase continuously as they do with samples containing water. They are able to de-flocculate/de-aggregate and then undergo continuous crystal growth in the solvent medium at a much faster pace than would occur in a water based system. This explains the steep gradient and also the high level of growth. As time continues, it is likely that there are fewer molecules in solution available to aid crystal

growth and so the rate slows down. This theory is consistent with the Ostwald ripening growth mechanism discussed earlier in chapter 2. Also, the first point (at 80°C) lies off the smooth curve formed by the next five which were at 96°C. It does not quite generate the high surface area which would be expected by extrapolation of the smooth curve. Turning to these 100% solvent samples in more detail, Figure 4.25(b) shows a graph of surface area against time on a logarithmic scale. As before, the slope seen here appears to have a gentle slope downwards initially which is most likely to be due to some flocculation which inhibits nitrogen penetration. The surface area begins to fall somewhat quicker in a way which is characteristic of ripening. This evens off as ripening slows down and is possibly overtaken by coalescence as the main growth mechanism. Finally, returning to figure 4.25(a), the point representing the sample in 100% solvent for 5 hours without the addition of heat illustrates that it takes a lot longer to get to a given surface area at 20°C than at 96°C. In fact, this sample is close in surface area value to the sample which had been heated from 20°C to 80°C over only 20 minutes - the first blue cross on the downward slope for 100% solvent. This underpins the importance of heat in such a growth process.

Figure 4.26 shows a plot of surface area against time for nitrobenzene samples with each concentration displayed as a different series enabling comparisons to be drawn easily. This illustrates the small amount of growth achieved in the low concentration sample compared with the levels obtained on increasing the solvent concentration to 20 or 30%. Again these two concentrations follow a similar path as illustrated by the

Graph of Surface Area against time for sample refluxed in 100% nitrobenzene
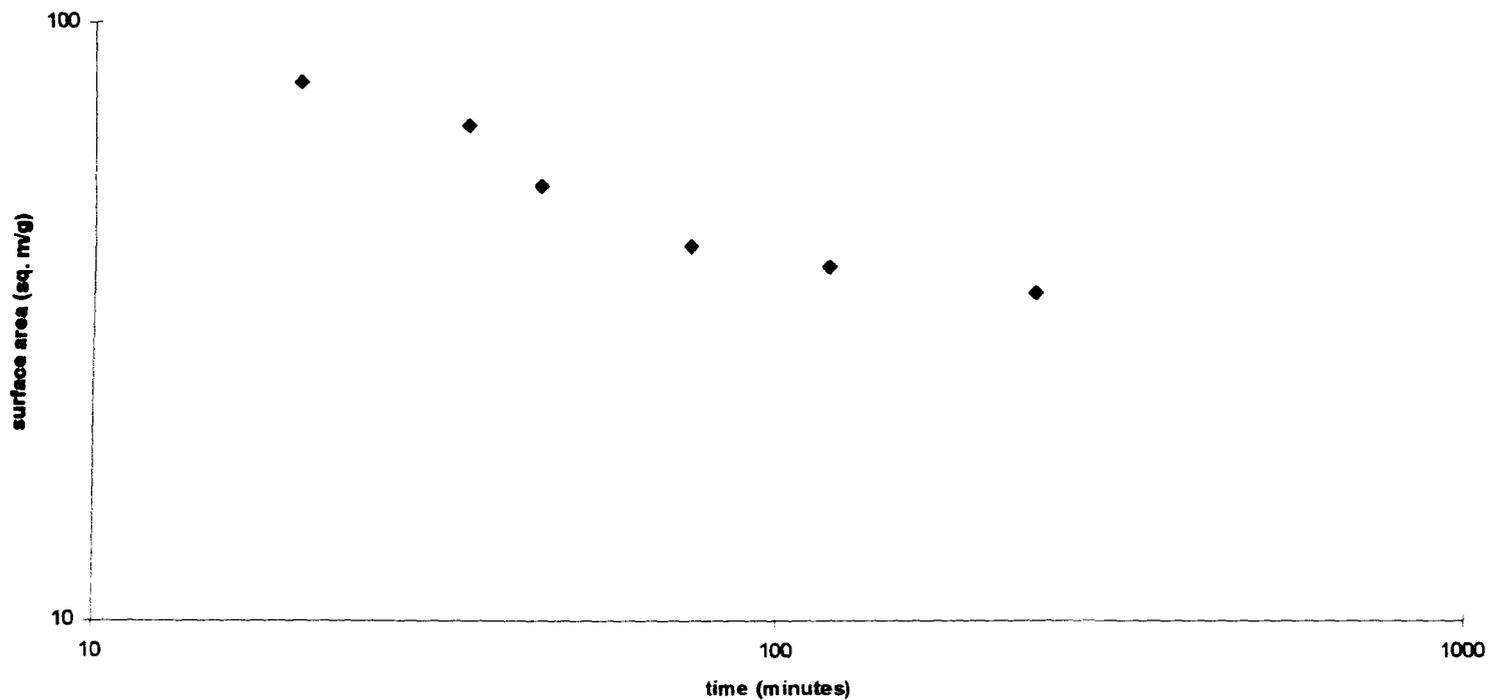
Figure 4.25(b) : Surface area against time on a logarithmic scale for samples treated with 100% nitrobenzene
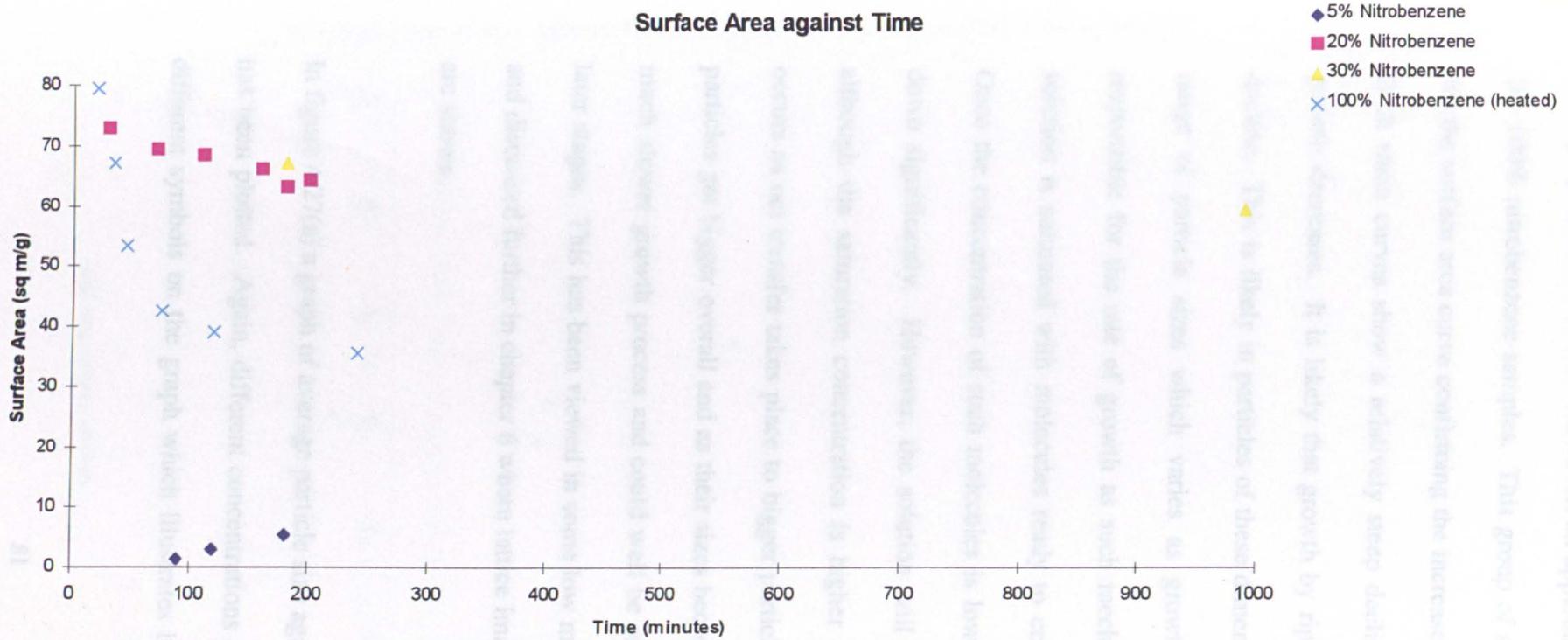
Figure 4.26 : Surface area against time of reflux plot for different concentrations of nitrobenzene

micrographs shown earlier. However, an apparent difference is clear between these and the 100% nitrobenzene samples. This group of samples shows a much steeper decline for the surface area curve confirming the increased rate at which growth has proceeded. Both main curves show a relatively steep decline then a leveling off as the rate of growth decreases. It is likely that growth by ripening is the main cause of this steep decline. This is likely in particles of these dimensions and the micrographs do show a range of particle sizes which varies as growth progresses. This could also be responsible for the rate of growth as such mechanisms can occur quickly where the solution is saturated with molecules ready to contribute to the growth of a particle. Once the concentration of such molecules is lowered, this ripening process will slow down significantly. However, the solution will continue to be saturated throughout although the saturation concentration is higher around smaller particles. Ripening occurs as net transfer takes place to bigger particles. This process slows down as the particles get bigger overall and as their sizes become closer together. Coalescence is a much slower growth process and could well be responsible for growth taking place at later stages. This has been viewed in some low magnification images and is illustrated and discussed further in chapter 6 where lattice images of apparently coalesced particles are shown.

In figure 4.27(a) a graph of average particle size against $t\, v_s/(v_s+v_w)$ for selected samples has been plotted. Again, different concentrations of solvent have been displayed with different symbols on the graph which illustrates how those samples containing water

Average Particle Size against Time (Vol of Solvent / Vol of solvent + Vol of water)

Legend:
- ◆ 20% Nitrobenzene
- ■ 30% Nitrobenzene
- ▲ 100% Nitrobenzene

Y-axis: Average Particle Size (nm)

X-axis: Time(Vol of solvent/Vol of solvent + Vol of water)
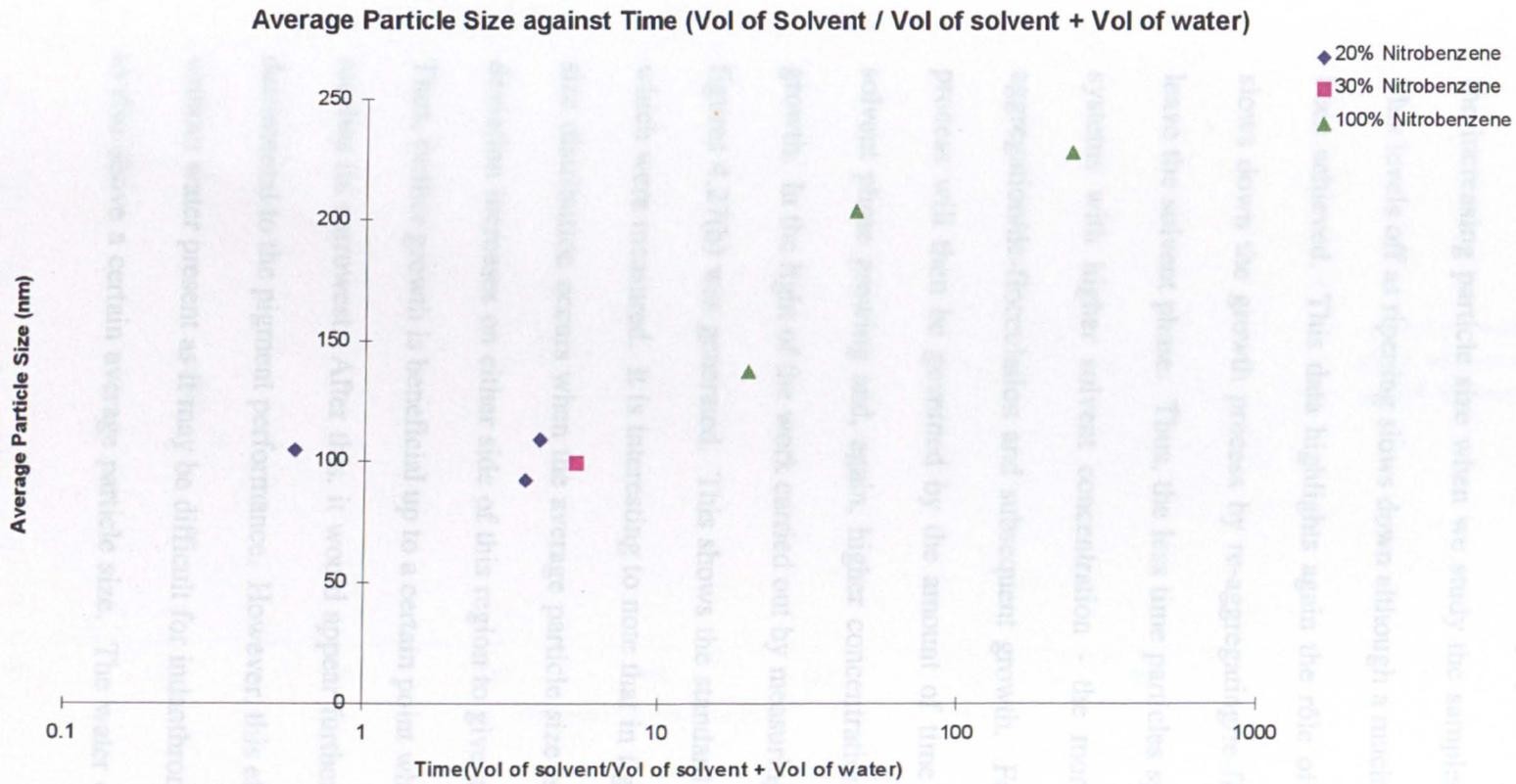
Figure 4.27(a) : Graph showing average particle size against time of reflux(volume of solvent/volume of solvent + volume of water) for selected nitrobenzene samples

appear to vary little in average particle size once a certain stage of growth has passed. This was discussed earlier when it was noted that the particle size distribution of such samples can be changing although the average particle size does not. Notice, however, the increasing particle size when we study the samples refluxed in pure nitrobenzene. This levels off as ripening slows down although a much greater average particle size has been achieved. This data highlights again the rôle of water in such systems. Water slows down the growth process by re-aggregating/re-flocculating the particles as they leave the solvent phase. Thus, the less time particles spend in the water phase - i.e. in systems with higher solvent concentration - the more opportunity there is for de-aggregation/de-flocculation and subsequent growth. Following this stage, the growth process will then be governed by the amount of time the particles can spend in the solvent phase growing and, again, higher concentrations will obviously lead to faster growth. In the light of the work carried out by measuring the particle sizes, the graph in figures 4.27(b) was generated. This shows the standard deviations of the particle sizes which were measured. It is interesting to note that in figure 4.27(b) the tightest particle size distribution occurs when the average particle size is around 110nm. The standard deviation increases on either side of this region to give a wider spread of particle sizes. Thus, further growth is beneficial up to a certain point when the particle size distribution reaches its narrowest. After this, it would appear further growth may well prove to be detrimental to the pigment performance. However, this effect may be limited to systems without water present as it may be difficult for indanthrone in aqueous solvent mediums to rise above a certain average particle size. The water could effectively be a limiting

82
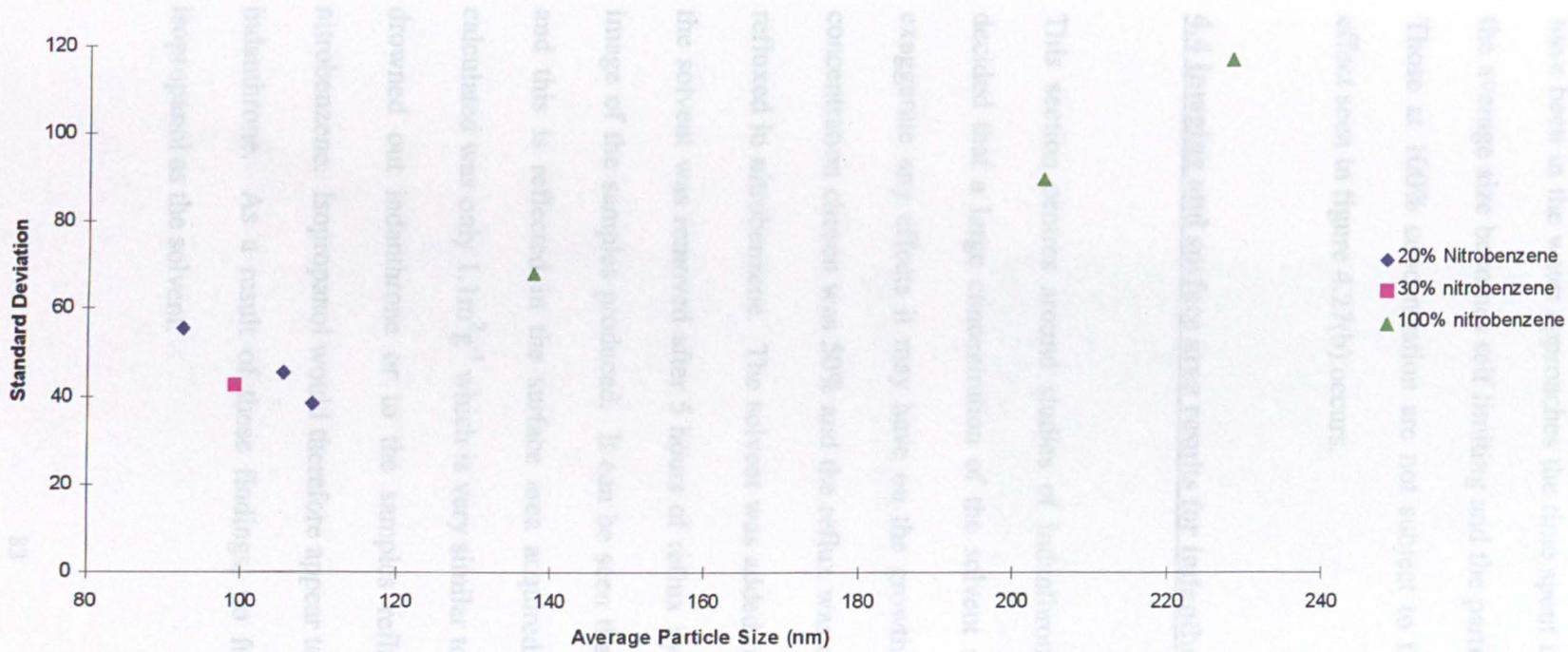
Figure 4.27(b) : Standard deviation for particle size against average particle size

factor on the growth. In a 20-30% solvent concentration case for example, after the particles have grown to a certain size, the time taken to de-flocculate them after they have been in the water approaches the time spent in the solvent in any one pass. Thus the average size becomes self limiting and the particle size distribution simply narrows. Those at 100% concentration are not subject to this water based effect and thus the effect seen in figure 4.27(b) occurs.

4.4 Imaging and surface area results for indanthrone refluxed in isopropanol

This section centres around studies of indanthrone refluxed in isopropanol. It was decided that a large concentration of the solvent should be used initially in order to exaggerate any effects it may have on the growth of the indanthrone particles. The concentration chosen was 50% and the reflux was carried out in a similar way to those refluxed in nitrobenzene. The solvent was added upon the mixture reaching 80°C and the solvent was removed after 5 hours of reflux by distillation. Figure 4.28 shows an image of the samples produced. It can be seen that very little growth has taken place and this is reflected in the surface area acquired by the BET method. The value calculated was only $1.1 \text{m}^2\text{g}^{-1}$ which is very similar to values associated with a sample of drowned out indanthrone or to the samples refluxed in very low levels (5%) of nitrobenzene. Isopropanol would therefore appear to be a very poor growth promoter in indanthrone. As a result of these findings, no further work was carried out using isopropanol as the solvent.
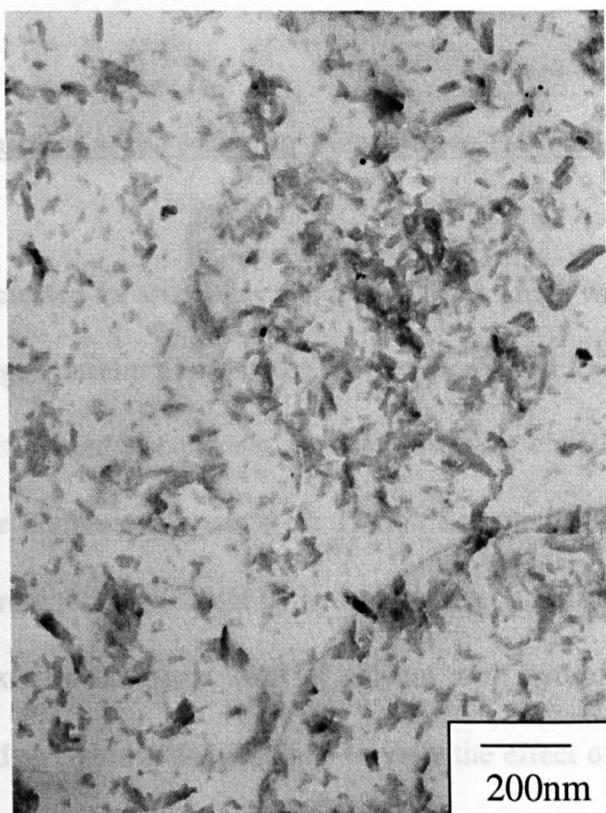
Figure 4.28: Indanthrone refluxed in isopropanol

4.5 Imaging and surface area results for indanthrone refluxed in methyl benzoate

The final solvent selected for study was methyl benzoate which was described in chapter 2. Once again, large concentrations of the solvent were used to exaggerate any growth effects. In the initial methyl benzoate studies, 80% was chosen as the concentration after consulting the literature (Gerson et al, 1993). Sample PMO24 was refluxed for 3 hours and solvent removal carried out by hydrolysis over a four hour period. Similarly, PMO25 was refluxed in the same level of solvent with hydrolysis removal although reflux was allowed to continue for 15 hours to view the effect of extended reflux time. Figures 4.29 and 4.30 show micrographs of these samples. The surface areas for PMO24 and PMO25, listed in Table 4.2, were found to be $50.1m^2g^{-1}$ and $47.8m^2g^{-1}$ respectively. It was apparent that further, but not significant, growth had taken place during the extra 12 hours allowed for reflux. As with nitrobenzene, the bulk of the growth takes place in the earlier stages of reflux. Having studied the effect of extended time, a further parameter was chosen for study. Methyl benzoate has the advantage that removal is possible by two methods - hydrolysis and distillation. The aim with this next study was to investigate the difference between these methods with respect to crystal growth. Sample PMO26 was prepared by refluxing indanthrone with 80% methyl benzoate for 3 hours and solvent removal by distillation. We will therefore be comparing this to the previous 3 hour sample - PMO24 which was illustrated in figure 4.29. A low magnification image of sample PMO26 is shown in figure 4.31. The

200nm

Figure 4.29: Indanthrone refluxed in 80% methyl benzoate
for 3 hours - solvent removed by hydrolysis

200nm

Figure 4.30: Indanthrone refluxed in 80% methyl benzoate
for 15 hours - solvent removed by hydrolysis

Table 4.2 - Surface areas for samples prepared using methyl benzoate

Sample	Solvent present*	Time	Solvent removal	Surface area $(m^2g^{-1}) \pm 0.2$
PM024	80% Methyl benzoate	3 hours	Hydrolysis	50.1
PM025	80% Methyl benzoate	15 hours	Hydrolysis	47.8
PM026	80% Methyl benzoate	3 hours	Distillation	48.7
PM042	100% Methyl Benzoate	Sampled at 80°C after 25 minutes	Filtration	76.6
PM043	100% Methyl Benzoate	Sampled at 80°C after 35 minutes	Filtration	73.3
PM044	100% Methyl Benzoate	Sampled at 80°C after 45 minutes	Filtration	64.3
PM045	100% Methyl Benzoate	Sampled at 80°C after 75 minutes	Filtration	48.9
PM046	100% Methyl Benzoate	Sampled at 80°C after 125 minutes	Filtration	40.1
PM047	100% Methyl Benzoate	Sampled at 80°C after 245 minutes	Filtration	33.3
PM048	100% Methyl Benzoate	Sampled at 80°C after 335 minutes	Filtration	31.7

Figure 4.31: Indanthrone refluxed in 80% methyl benzoate for 3 hours -solvent removed by distillation

overall impression from the micrographs was that more growth had occurred when solvent removal was carried out by distillation. This was confirmed when surface area studies were carried out. The surface area for this sample was found to be $48.7m^2g^{-1}$ compared to $50.1m^2g^{-1}$ for PM024. In terms of growth, the PM026 (3 hours reflux, removal by distillation) appears to be midway between the samples refluxed for 3 and 15 hours with solvent removal by hydrolysis. However, this can be explained by the fact that chemically, it can be assumed that hydrolysis of the solvent occurs immediately. Therefore, even though hydrolysis is allowed to continue for 4 hours, growth by solvent treatment should have terminated immediately. Distillation however, takes place over approximately 50 minutes and the amount of solvent present in the mixture steadily decreases over this time. Therefore, solvent is still present in the reaction vessel for a longer period than was originally assumed and some crystal growth will inevitably occur. This information is useful when dealing with any solvent which can be removed by distillation as it illustrates the fact that growth will be taking place during distillation. This will obviously have a more significant effect proportionately for shorter reflux times.

As methyl benzoate had been shown to be an effective growth promoter in indanthrone an experiment was carried out with pure solvent and no water present in the reaction mixture. This is similar to the pure solvent experiment carried out on nitrobenzene. The results of this experiment can be viewed by studying the surface area values in Table 4.2 for the series PM042 to PM048. This shows a very similar pattern to the

results achieved for nitrobenzene which were shown in Table 4.1. Clarity is gained by plotting the surface areas for all the methyl benzoate samples together as shown in figure 4.32. This shows a similar bifurcation between pure solvent samples and those which contain water as was observed with the nitrobenzene plot. The curve following the progress of the 100% samples has a steep downward trend which levels off as the time spent in the solvent increases. This reflects the behaviour of the indanthrone particles in nitrobenzene and implies that a similar growth mechanism is taking place. To check the similarity between the two solvents, the next section will study the combined information from both solvents.

4.6 Combining results from methyl benzoate with nitrobenzene

Figure 4.33 shows the combined results from the surface area data for both nitrobenzene and methyl benzoate. It can be seen that they fit together relatively well and follow similar paths. The point that does not fit with either line is the sample for which no heat was applied and so can be considered to have been grown under different conditions. It is in the early stages of both 100% samples that the strongest deviation from the rest of the samples occurs. This is most likely to be due to the supersaturation of indanthrone in the pure solvent at this time, with ample opportunity for the particles to grow. This results in speedy initial growth and de-aggregation which, in turn, results in an inflated surface area value. As growth slows down due to the solution being less saturated and

Surface Area Plot for Methyl Benzoate Samples

Legend:
- ◆ 80% methyl benzoate
- ■ 100% methyl benzoate

Y-axis: Surface Area sq. m/g

X-axis: Time(Volume of solvent/Volume of solvent + Volume of water)
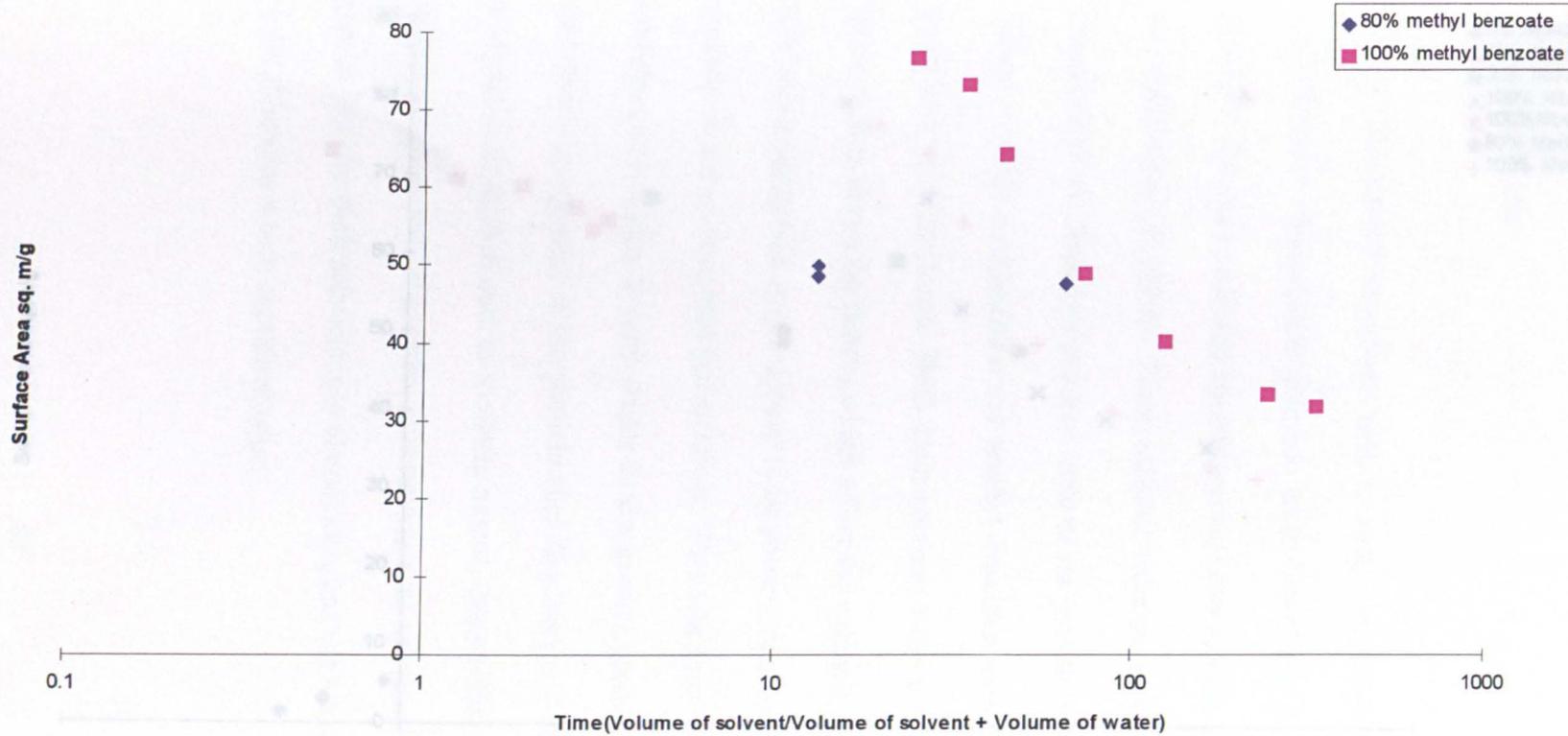
Figure 4.32 : Plot of Surface Area against Time in Solvent(Volume of Solvent/Volume of Solvent + Volume of Water) for samples solvent treated with methyl benzoate.

Surface Area Plot for Nitrobenzene and Methyl Benzoate Samples

Legend:
- ◆ 5% Nitrobenzene
- ■ 20% Nitrobenzene
- ■ 30% Nitrobenzene
- × 100% Nitrobenzene (heated)
- ✳ 100% Nitrobenzene (no heat)
- ● 80% Methyl Benzoate
- + 100% Methyl Benzoate

Y-axis: Surface Area sq.m/g

X-axis: Time(Volume of solvent/Volume of Solvent + Volume of water)
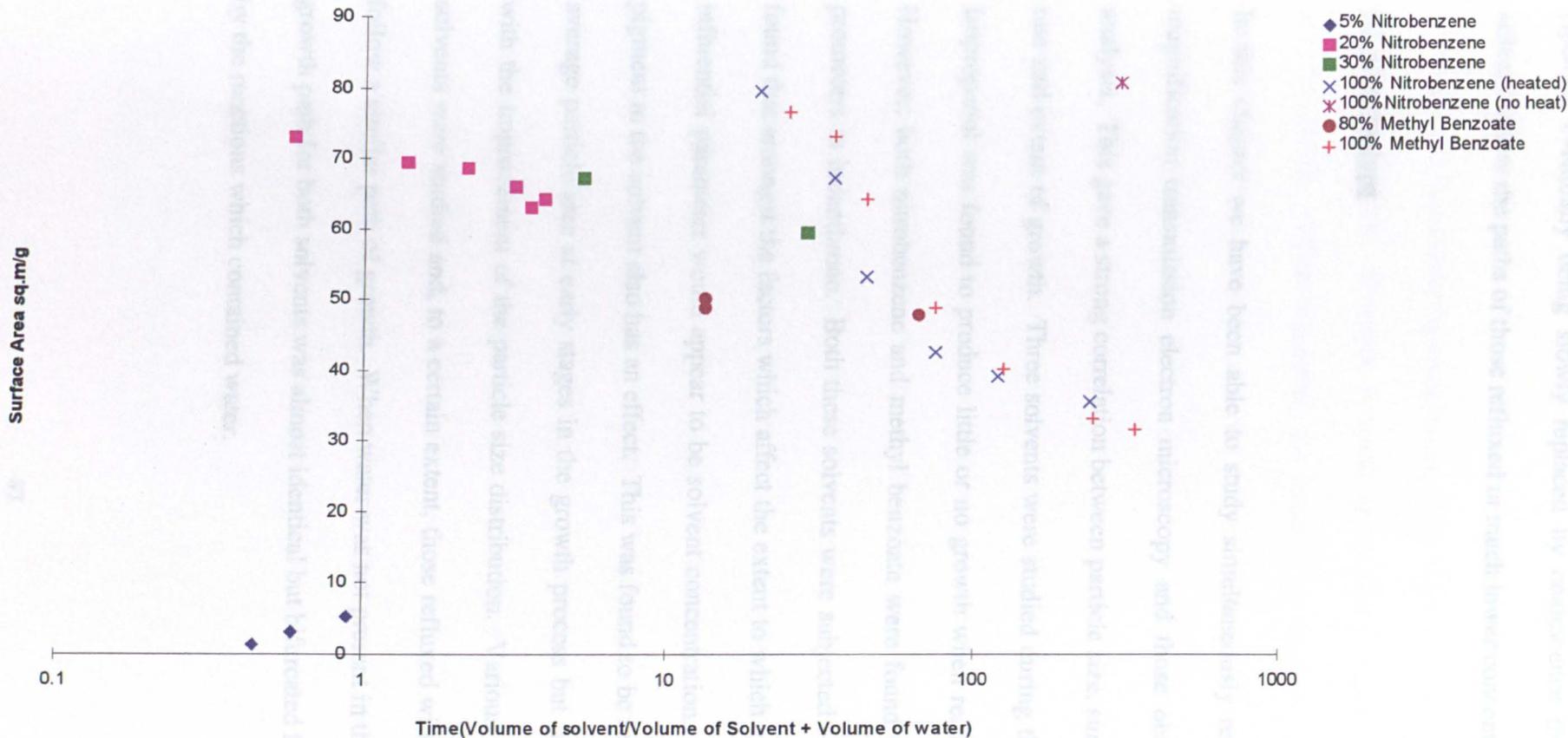
Figure 4.33 : Plot of Surface Area against Time in Solvent(Volume of Solvent/Volume of Solvent + Volume of Water) for samples solvent treated with nitrobenzene and for those treated with methyl benzoate.

ripening eventually being slowly replaced by coalescence the samples from 100% solvent follow the paths of those refluxed in much lower concentrations.

4.7 Conclusions

In this chapter we have been able to study simultaneously results obtained via low magnification transmission electron microscopy and those obtained by surface area analysis. This gave a strong correlation between particle size, surface area and of course rate and extent of growth. Three solvents were studied during the course of this work. Isopropanol was found to produce little or no growth when refluxed with indanthrone. However, both nitrobenzene and methyl benzoate were found to be effective growth promoters in indanthrone. Both these solvents were subjected to further study. It was found that amongst the factors which affect the extent to which growth occurs, the most influential parameter would appear to be solvent concentration. The time spent by the pigment in the solvent also has an effect. This was found to be related to the increase in average particle size at early stages in the growth process but later is more concerned with the improvement of the particle size distribution. Various concentrations of both solvents were studied and, to a certain extent, those refluxed with the addition of water follow a similar path of growth. When water was not present in the reaction mixture the growth path for both solvents was almost identical but bifurcated from the path followed by the reactions which contained water.

The growth mechanism for indanthrone crystal growth suggested by these results is that of ripening followed later by coalescence. This hypothesis will be studied further in the chapters that follow. However, it would appear that ripening is the primary source of growth initially. When this occurs the smallest particles are able to go into solution when they come into contact with the solvent as they will posses a higher solubility level than larger particles. When combined with water, due to their low solubilities these solvents exist as small separate areas or 'globules' of solvent which are dispersed evenly throughout the reaction mixture when sufficient agitation is present. Obviously when no water is present there is even more opportunity for particles to come into contact with solvent and so the rate at which this occurs is increased significantly. As these small particles dissolve, the solvent becomes saturated with indanthrone which then precipitates onto larger particles thereby increasing their size. It would appear however that ripening is not the sole growth mechanism but that it is followed by coalescence where particles 'fuse' together. Coalescence occurs after ripening and its effects would cause little change in terms of surface area. This fact combined with the remission of ripening explains the way in which the overall growth rate slows down when viewed with respect to both surface area and average particle size as determined by microscopy. In the chapters which follow, these mechanisms will be investigated further together with other aspects of crystal growth in indanthrone.

Chapter 5

Diffraction studies of indanthrone pigment

5.1 Introduction

Diffraction patterns provide information on the internal structure of the pigment particles and the orientation of the crystal structure. The methods by which these patterns were obtained is described in section 5.2 and the results of this work are presented and discussed in section 5.3. Finally, in section 5.4 conclusions are drawn from the results of this work.

5.2 Diffraction studies of indanthrone

As discussed in chapter 3, the minimum area from which diffraction patterns arise using selected area diffraction (SAD) is still too large for the purposes of studying pigment

particles. In order to study one particle using this method, the particle density on the carbon film would have to be low. McColgan (1990) studied high density areas of pigment particles using SAD. Using this method, most of the particles contributed to the background intensity whilst there was a possibility that one particle might be in the correct orientation to present a prominent reciprocal lattice to the incident beam. However, as was also described in chapter 3, convergent beam electron diffraction (CBED) enabled diffraction patterns to be obtained from areas with dimensions of the order of a single particle even from samples with a high density of pigment particles.

As with all microscopy studies of indanthrone, measures were taken to reduce the electron dose administered to the sample. Using a condenser aperture with a diameter of $40\mu m$ and the smallest spot size, it was possible to focus the electron probe down to an area of approximately 50nm in diameter whilst in imaging mode using the JEOL 1200EX. As the average indanthrone particle is ~80-120nm long by ~20-40nm wide, it was then relatively easy to place the probe on a single particle and switch to diffraction mode to record the diffraction pattern. Ideally, this technique would have been followed for all diffraction patterns. However, once again radiation damage meant that by the time a particle had been selected and diffraction mode was selected, much of the crystallinity was lost and the diffraction pattern had faded. Diffraction patterns were prone to fading within 4-6 seconds. To overcome this, most of the diffraction patterns were obtained by simply moving the sample around in diffraction mode and recording clear patterns which appeared to arise from single particles. The relevant area could subsequently be viewed in imaging mode after the diffraction pattern had been recorded.

Initially standard photographic film (such as Kodak 4489) was used to record the patterns. However, in view of the fast deterioration of the patterns due to radiation damage, a fast photographic emulsion was often used to allow shorter exposure times to be employed. In such cases, Reflex-15 x-ray (or RX) film was used.

As the spot spacings on the micrographs of diffraction patterns can be used to determine the lattice parameters, an accurate measurement of the camera length was required. This was done by analysis of a diffraction pattern at different camera lengths for a specimen of known lattice parameter. The specimen chosen in this case was thallous chloride (ThCl). Calculation of the camera lengths gave values of 47.2cm $\pm$ 0.5cm and 31.7cm $\pm$ 0.5cm for nominal values of 50cm and 30cm respectively.

Although effective in obtaining diffraction patterns of indanthrone and very useful for obtaining general information about the pigment, convergent beam diffraction is very difficult to control and it is also difficult to determine from which part of the specimen the pattern came from. In an attempt to overcome these problems another method was employed. This was devised by Smith (1997) and involved operation of the TEM microscope in a scanning mode. With the image displayed on a TV screen one is able to select a suitable area of pigment for study and view the diffraction pattern on the microscope screen. By selecting a suitably small reduced area scan, diffraction patterns can be recorded in steps across either a large particle or an aggregate. However, the scanning image of the specimen is usually very poor and gave little or no information on

the sample. Also, the diffraction spots are prone to fading even faster than under convergent beam diffraction due to the intensity of the probe. Despite the limitations, the technique was used for selected samples to investigate whether particles had sub-structure. The camera length was for the scanning unit was also calibrated using thallous chloride and was found to be 40.3cm ± 0.5cm.

The "Diffract" software package (© Virtual Laboratories, Ukiah, CA 95482, USA) in version 1.5a was used to generate diffraction patterns for indanthrone for various zone axes. By entering the atomic co-ordinates from the literature (Bailey, 1955), the simulated diffraction patterns were obtained as shown in figure 5.1 (a) to (c). These show the diffraction patterns for the [100], [010] and [001] orientations respectively.

5.3 Results of diffraction studies of indanthrone

Diffraction patterns were recorded for all the samples which were prepared. Over 90% of the diffraction patterns obtained showed the same zone axis. This was found to be true regardless of variations in the crystal growth process. By comparing the patterns to those predicted by "Diffract" and by measuring the spacings between the spots on the diffraction pattern, this was found to be the [001] zone axis and we are therefore looking down the c-axis of the crystal. The pattern for this orientation is illustrated in figure 5.2 and can be compared with the "Diffract" simulation for this zone axis shown in figure 5.1(a). This pattern, in common with most of those viewed, arose from a single particle. Identification of the zone axes may be complicated by streaking present on the outer line
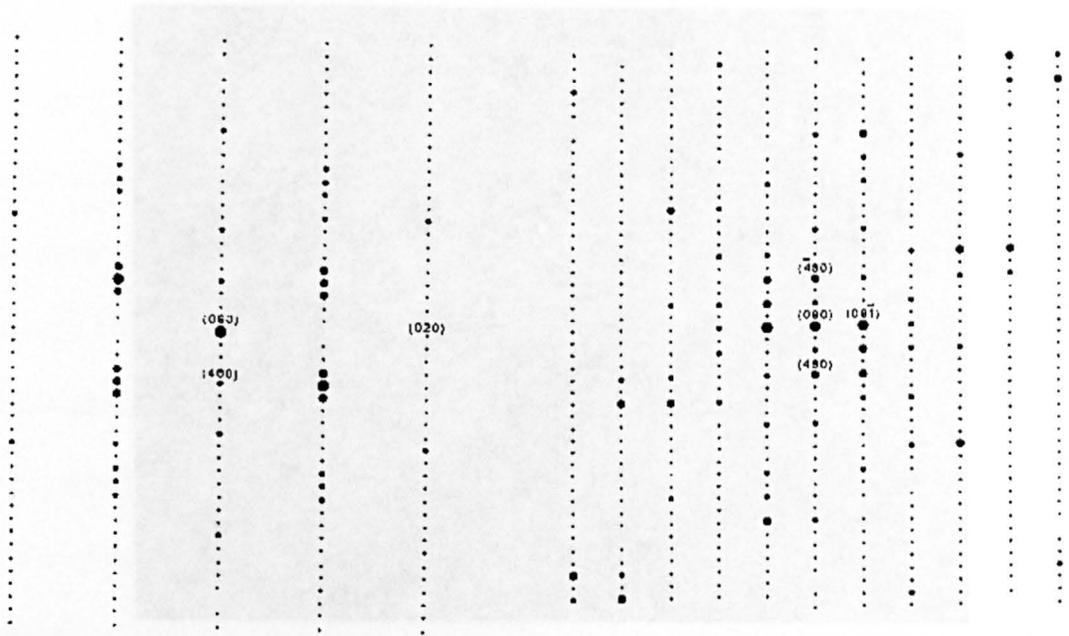
Figure 5.1(a) - "Diffract" simulation for [001] zone axis

Figure 5.1(b) - "Diffract" simulation for [010] zone axis
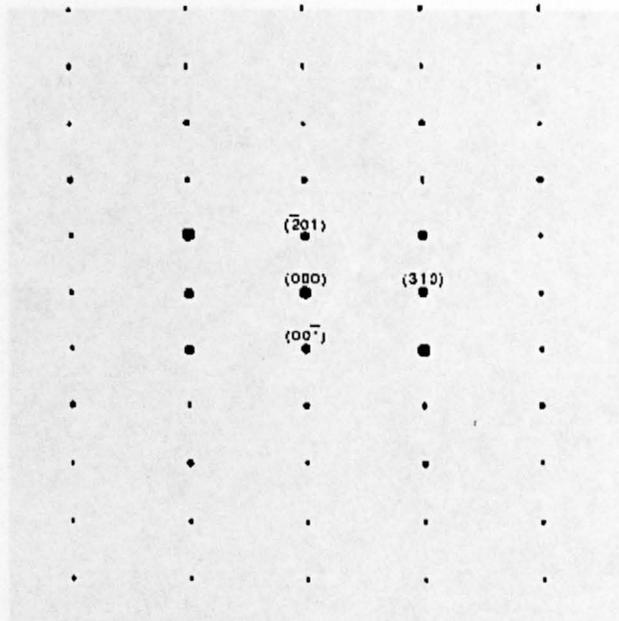
Figure 5.1(c) - "Diffract" simulation for [100] zone axis

of spots in s

patterns are

and the perp

ratio between

spacing. Th

identification

be measured

5.1 shows the

It should be noted that in certain micrographs the line spot ratio was found to be half that

predicted

a change in the short range order.

under the beam as periodic disorder occurred along the columns of molecules.

present both in measurement and in determining the centre of the spot but it was clear

from the data that the

matched with that of

Figure 5.2 : Diffraction pattern from solvent treated indanthrone
showing [001] zone axis. Line spot ratio is given by a/b.

A few examples we

5.3. These compare

figure 5.1(e). This

treatment to control

particle aligning itself

from samples which had not undergone growth control treatment.

would appear to
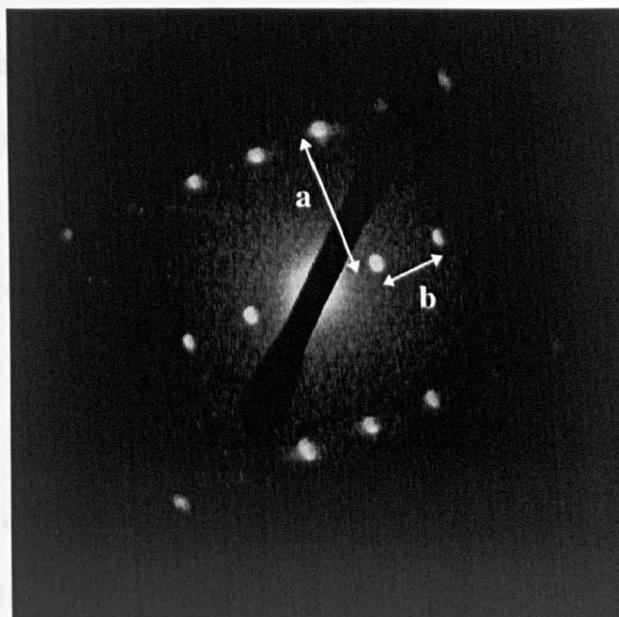
Figure 5.3 : Diffraction pattern from solvent treated indanthrone showing
[100] zone axis. Line spot ratio is given by a/b.

of spots in some diffraction patterns. The most easily determined parameters on the patterns are the spacings of the spots along the centre (i.e. the centre line spot spacing) and the perpendicular separation of the lines. The line spot ratio is determined as the ratio between the perpendicular distance to the outer line and the centre line spot spacing. Thus determination of the line spot ratio is the simplest way of starting the identification of the zone axis of the recorded patterns. As the predicted ratios can also be measured using the 'Diffract' simulations, a direct comparison can be made. Table 5.1 shows the values for these measurements which correspond to the [001]orientation. It should be noted that in certain micrographs the line spot ratio was found to be half the predicted value due to the fading of every second spot on the central line. This is due to a change in the short range order. Generally, the centre line was always the first to fade under the beam as periodic disorder occurred along the columns of molecules. Errors are present both in measurement and in determining the centre of the spot but it was clear from the data that the line spot ratio for the majority of the diffraction patterns obtained matched with that of the diffract simulation for the (001) orientation.

A few examples were found which showed the [100] zone axis as illustrated in figure 5.3. These compare well with the "Diffract" simulation for this orientation shown in figure 5.1(c). This pattern was taken from a sample that had undergone additional treatment to control crystal growth and this could have enhanced the possibility of the particle aligning itself in this orientation. Such patterns were also obtained infrequently from samples which had not undergone growth control treatment. The pattern shown would appear to have occurred in one of two possible situations. The first is when the

[001]	Perpendicular distance to the outer line (±0.02)	Centre line spot spacing (±0.02)	Line spot ratio (a/b)
'Diffract'	1.65cm	0.21cm	7.9
Typical micrograph	1.65cm	0.21cm	7.9
Central line fading has occurred (every second spot)	1.65cm	0.42cm	3.9

Table 5.1 : Line spot ratios for calculated and experimentally obtained diffraction patterns along the (001) orientation

[100]	Perpendicular distance to the outer line (±0.02)	Centre line spot spacing (±0.02)	Line spot ratio (a/b)
'Diffract'	1.90cm	0.89cm	2.1
Typical micrograph	1.90cm	0.89cm	2.1

Table 5.2 : Line spot ratios for calculated and experimentally obtained diffraction patterns along the (100) orientation

particle is supported by other particles and is able to lie in this orientation which is geometrically less favourable. The second is when growth along the c-axis (thickness) has exceeded the growth along the a-axis (width). Either of these situations would then make it geometrically favourable for the particle to orient itself in this way. The line spot ratios for this pattern and its corresponding 'Diffract' simulation are shown in Table 5.2 and illustrate a direct correlation.

The [010] orientation has never been viewed but this is to be expected due to the geometry of the particles. Such an orientation would require the particle to be positioned rather like a needle standing on its end and would therefore not be favoured.

Although the majority of the patterns recorded were indeed spot patterns, some showed complex arrays of spots which built up into what appeared to be a ring pattern superimposed on the single crystal pattern. An example of such a pattern is shown in figure 5.4. This was particularly common with samples which had undergone little growth but also featured in many other samples where the pattern arose from an area featuring many particles. It was particularly important to use RX film with such samples as any crystallinity was destroyed even faster than with standard solvent treated indanthrone samples making any interesting features on the diffraction pattern barely discernible. In view of this, the pattern chosen to illustrate this deviation from the single crystal pattern arose from a sample that had undergone considerable growth. The diffraction pattern is very bright in the centre and is particularly interesting as it shows a strong central line as well as the array of spots which form arc-like shapes around the
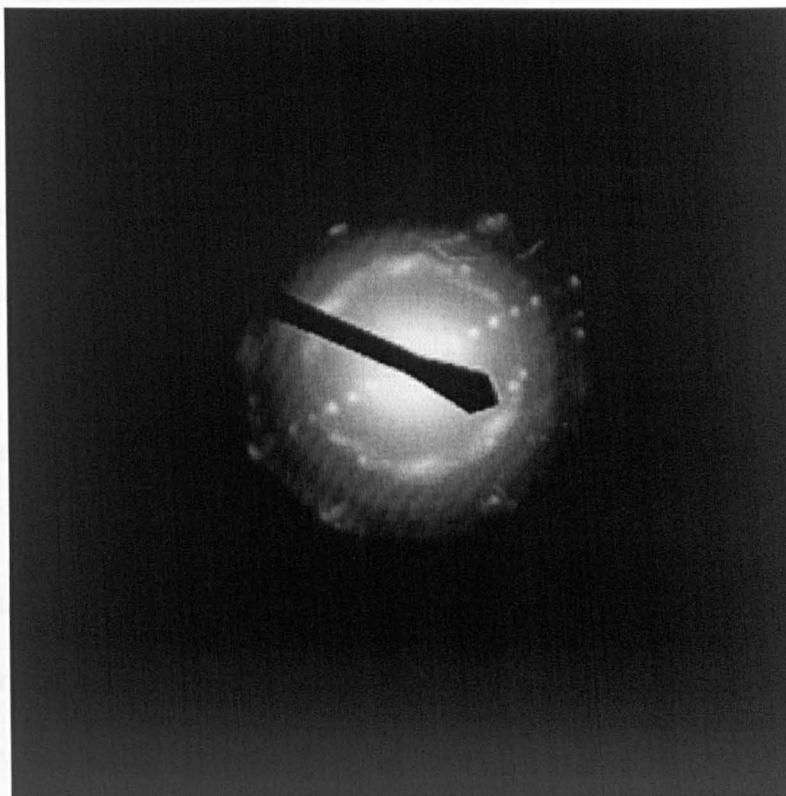
Figure 5.4 : Diffraction pattern from area containing many indanthrone particles

central spot. The ring pattern probably occurred due to the diffraction pattern being recorded from an area containing several overlying particles which are randomly oriented with respect to each other and thus contribute to the background intensity. The strong central line suggests the presence of a large particle with smaller particles on the surface. Another reason for the combination of spots and streaked areas could be the presence of faults such as random 'twinning' of the stacks of plate-like molecules. The line spot ratio for this pattern was calculated to be 4 ± 0.5. This agrees with the [001] orientation where the central line has been prone to fading.

Diffraction studies were then continued using the TEM in conjunction with a scanning attachment as described earlier. Examples are shown in figure 5.5(a) to (f) of diffraction patterns obtained in this manner. The sample used for this study had been refluxed in 30% nitrobenzene for 3 hours and could therefore be considered to have undergone a reasonable degree of growth. These particular patterns were obtained from 6 points across an area of indanthrone which appeared to be one particle when viewed on the scanning unit. The patterns were recorded at 15-20nm intervals and figure 5.5(g) shows a representative illustration of the particle. However, as can be seen in the transition from (c) to (d), a change in the orientation of the particle is visible as viewed with respect to the pointer. The crystal normal of the diffraction pattern at (d) is the same as the previous patterns but there has been some rotation about it. This would suggest that this area was in fact composed of more than one particle. This could be due to a number of factors including aggregation or coalescence of more than one particle. Streaking of the pattern in well defined crystallographic directions is evident in all of the patterns
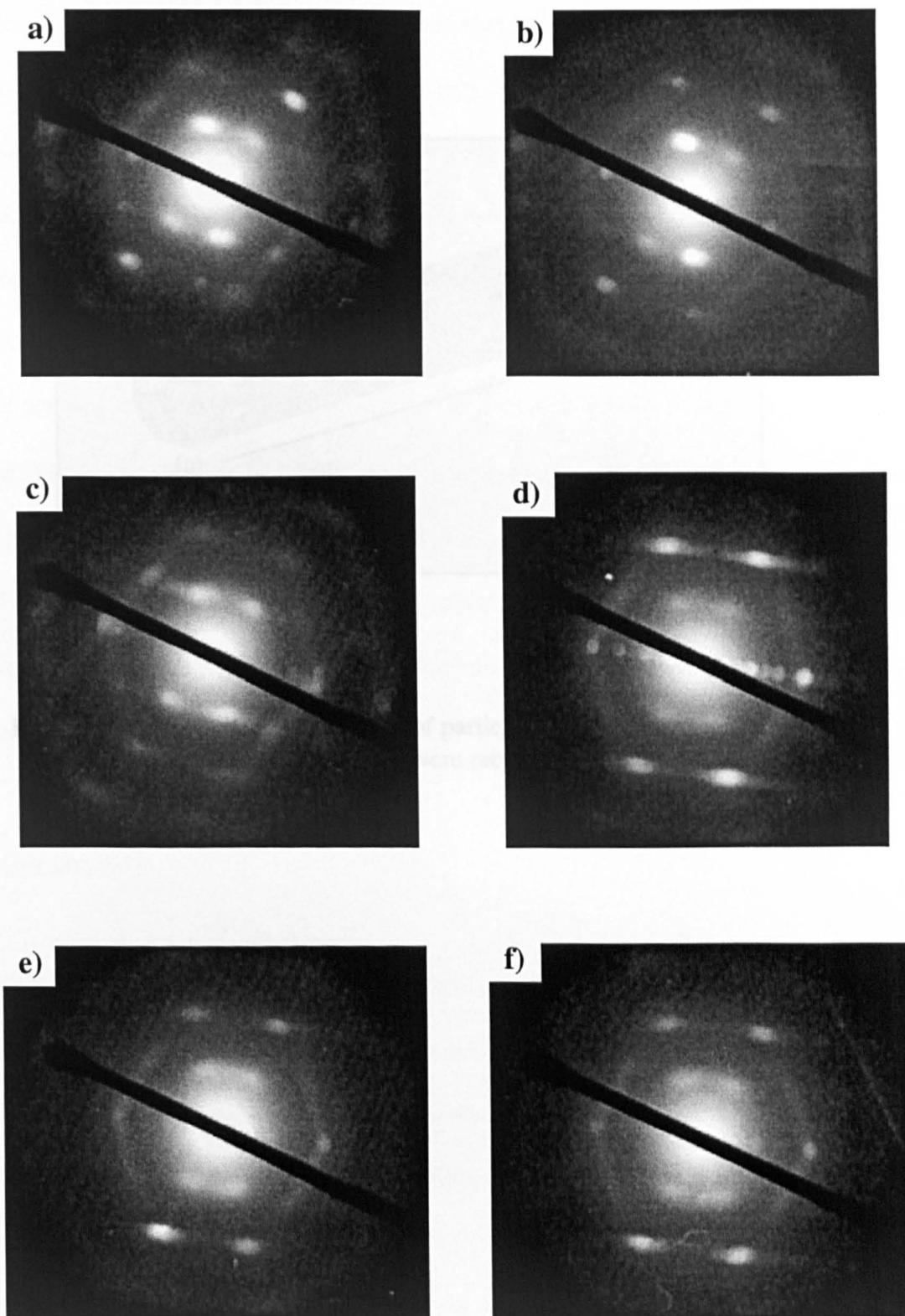
Figure 5.5(a) to (f) : Diffraction patterns obtained using the scanning unit on the TEM
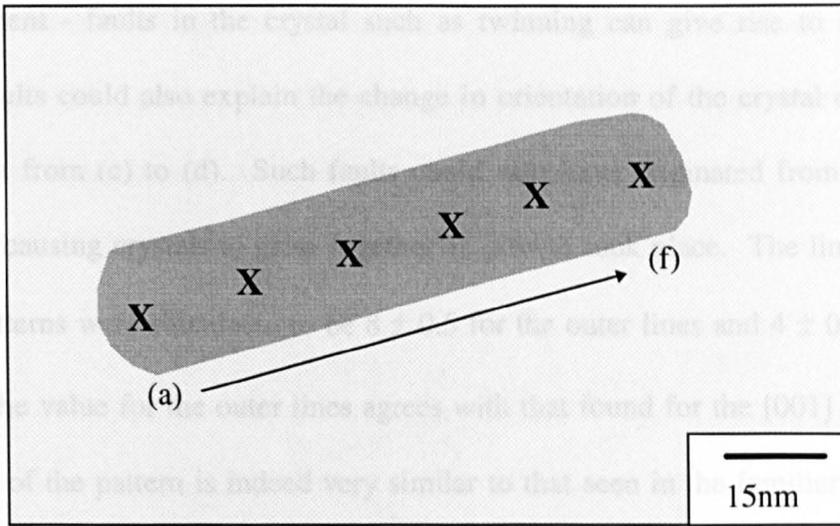
Figure 5.5(g) : Schematic diagram of particle showing points at which diffraction patterns were recorded.

shown in figure 5.5 giving rise to a polygon arrangement. Possible reasons for this are the same as those stated for the earlier sample which deviated from the single crystal arrangement - faults in the crystal such as twinning can give rise to such streaking. These faults could also explain the change in orientation of the crystal observed in the transition from (c) to (d). Such faults could also have originated from the drown-out material causing crystals to grow together as growth took place. The line spot ratio for these patterns were calculated to be 8 ± 0.5 for the outer lines and 4 ± 0.5 for the inner lines. The value for the outer lines agrees with that found for the [001] orientation and this part of the pattern is indeed very similar to that seen in the familiar [001] patterns. Unfortunately this technique proved to be rather problematic due to drift which caused difficulty in ascertaining the exact location of the probe and so extensive study was not undertaken.

5.4 Conclusions

Diffraction studies of indanthrone have shown most of the particles to be single crystals which are orientated so that the electron beam was parallel to the c-axis of the crystal. Geometrically this is the most favoured orientation with the largest face in contact with the application medium for maximum stability. This orientation is illustrated in figure 5.6.
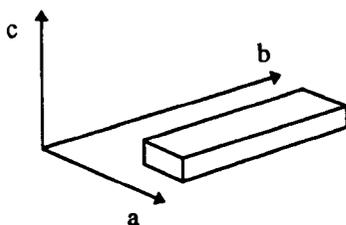
Figure 5.6

A small number were found where one is in effect looking down the a-axis of the crystal. This is illustrated in figure 5.7. It can be seen that this is geometrically less favourable but still possible, particularly if the particle has undergone further growth in the 'a' direction or if the particle is supported by other pigment particles.
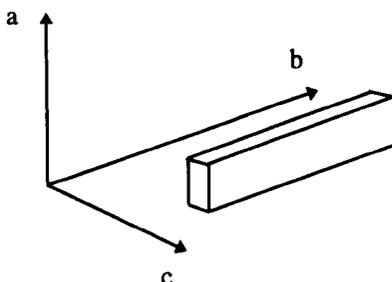
Figure 5.7

No evidence was found of particles with their b-axis pointing upwards which would be geometrically very unfavourable.

Most of the patterns originated from single crystals but a small number of patterns appeared to originate from a number of crystals. This could be due to aggregates or faults such as twinning in the crystal. However, the majority of particles appeared to have good crystal structure prior to damage caused by the electron beam. The crystallinity of the particles is investigated further in chapter 6.

Chapter 6

Lattice Imaging in the CTEM

6.1 Introduction

High magnification lattice images, although difficult to obtain in a radiation sensitive sample like indanthrone, provide good information about the internal structure of the particles. The quality and extent of the lattice images indicate the degree of order in the pigment particles. The aim of this chapter is to describe how these lattice fringes are formed and to investigate their significance in the study of indanthrone. Section 6.2 provides information on the formation of lattice fringes in the CTEM whilst section 6.3 shows some of the lattice images of indanthrone obtained during the course of this work. These images are then interpreted and discussed and finally, in section 6.4, conclusions are drawn from the information revealed by this work.

6.2 Lattice Imaging in the CTEM

Lattice images are formed when the transmitted beam and one or more of the diffracted beams are allowed to pass through the objective aperture. A schematic diagram of lattice image formation is shown in figure 6.1. This illustrates the three beam case of the undeflected beam and one Bragg reflection. The angle between the transmitted beam and the Bragg reflected beam is $\alpha = 2\theta_B$. The transmitted and diffracted beams can be made to recombine in the image plane forming interference fringes. These fringes are separated by a distance dM, where d is the interplanar spacing in the crystal and M is the magnification of the electron optics. The illumination incident on the specimen must be highly coherent in order to obtain high contrast lattice fringes.

This work was carried out in the JEOL 1200EX using the smallest condenser aperture combined with the smallest objective aperture at a spot size of 5. This ensured that the electron dose administered to the specimen was kept as low as possible to preserve the crystallinity. A further important factor in being able to resolve the lattice fringes is the correction of objective lens astigmatism. This was carried out at 150-200Kx by studying the edge of holes in the carbon film. The lattice fringes in indanthrone were usually viewed at around 100-120Kx but disappeared usually within 2-4 seconds due to radiation damage. As the electron dose was already as low as possible, little else could be done to extend the lifetime of the fringes. The lattice fringes thus had to be recorded using fast photographic emulsions which allow low exposure times to be used. The film in use for this
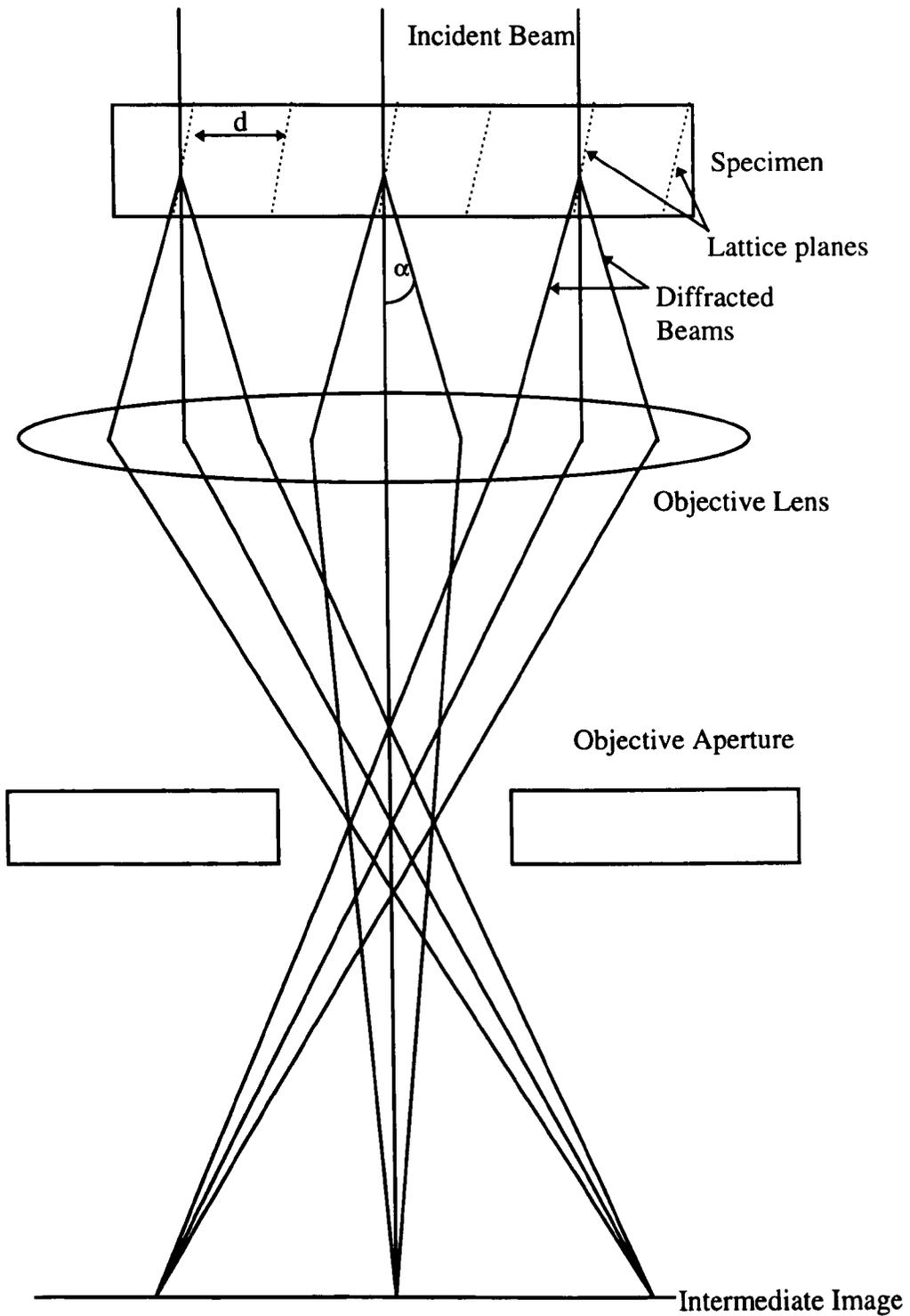
Figure 6.1 : Schematic diagram showing formation of a lattice image.

project was CEA Reflex-15 x-ray film which allowed the lattice images to be recorded with an exposure time of 1-2 seconds.

6.3 High magnification results

Lattice images from solvent treated indanthrone samples are shown in figures 6.2 to 6.3. By entering the unit cell dimensions (Bailey, 1955) into the "Diffract" software package, values were obtained various lattice spacings. These were then compared with those values obtained measuring fringe separation on the high magnification images. Figures 6.2 and 6.3 show lattice images of single particles with well defined sides and clear lattice fringes. The microscope used for this work had previously been calibrated at this magnification using a cross grating. These show lattice fringe spacings of 1.51nm ± 0.05nm which correspond to the (200) plane spacing which was predicted by "Diffract" to be 1.54nm. This was by far the most common spacing seen, although the (100) spacing measuring 3.08nm was often viewed. We would not expect to see the (001) spacing due to its direction and the (010) spacing would be damaged very quickly by radiation due to its small size of 0.38nm. Also, due to the fact that the smallest objective aperture was used it is unlikely that these fringes could be resolved with the stated operating conditions. In both images, there are areas of darker contrast indicating areas of different thickness. There is also rounding of the edges and fading of the lattice fringes at these ends of the particles. It is possible that this phenomenon is due to radiation damage by the electron beam. These changes in structure and composition are thought to be dependant on the diffusion of highly reactive radicals following bond breaking. Radiation damage is discussed more fully in section 3.11. In figure 6.3, the width of the particle can be

20nm

Figure 6.2

a

25nm
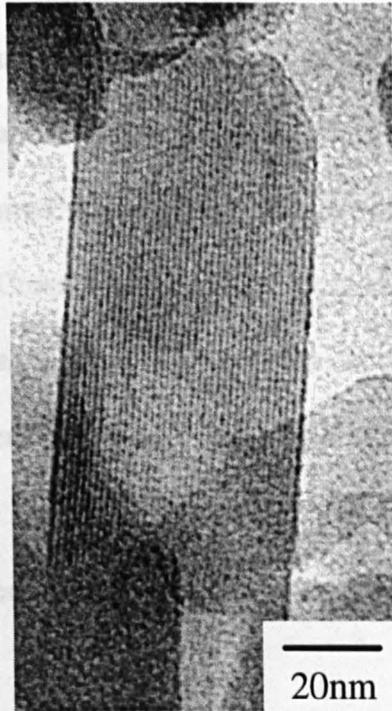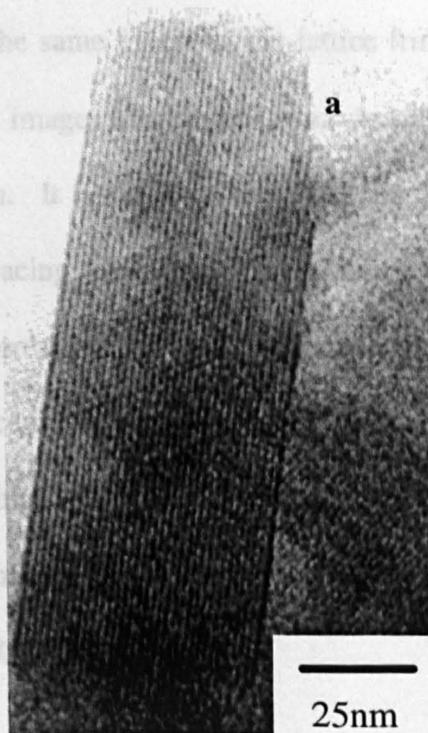
Figure 6.3

seen to change in "steps" at position **a**. As the lattice fringes extend right to this edge it is unlikely that this was caused by radiation damage. This variation in the width of the particle would appear to have occurred during the growth process and indicates that something has occurred to prevent crystal growth from continuing evenly up to the end of the particle. Crossed lattice fringes as a result of overlapping particles can also be seen in this image. This is a vynamon sample - drowned-out indanthrone refluxed in 50% nitrobenzene for 20 hours. This type of sample gave rise to some particularly good lattice images. This was probably due to the fact it had undergone more growth than other samples and the crystallinity took slightly longer to be destroyed by the beam.

Figure 6.4 shows a number of particles with lattice fringes. These also originate from a vynamon sample. The same fading of the lattice fringes at the edges of particles viewed in the previous images can be seen at **a**. At position **b**, fringes with a wider separation can be seen. It is possible that these are Moiré fringes caused by two crystals of different spacing overlapping to produce a double periodicity. However the dark fringes at **c** correspond to the (100) plane spacing. At position **d**, the crystal is highly strained, as can be seen by the bending of the lattice fringes in this area. This was not a particularly common phenomenon in indanthrone particles but has been viewed in the pthalocyanines (Fryer, 1980), (Fryer, 1981). All the fine fringes corresponded to the (200) plane spacing.

Figure 6.5 shows what would initially appear to be two indanthrone particles side by side. However, on closer examination, especially at position **a**, we can see that the lattice fringes across the particles are completely continuous indicating that these
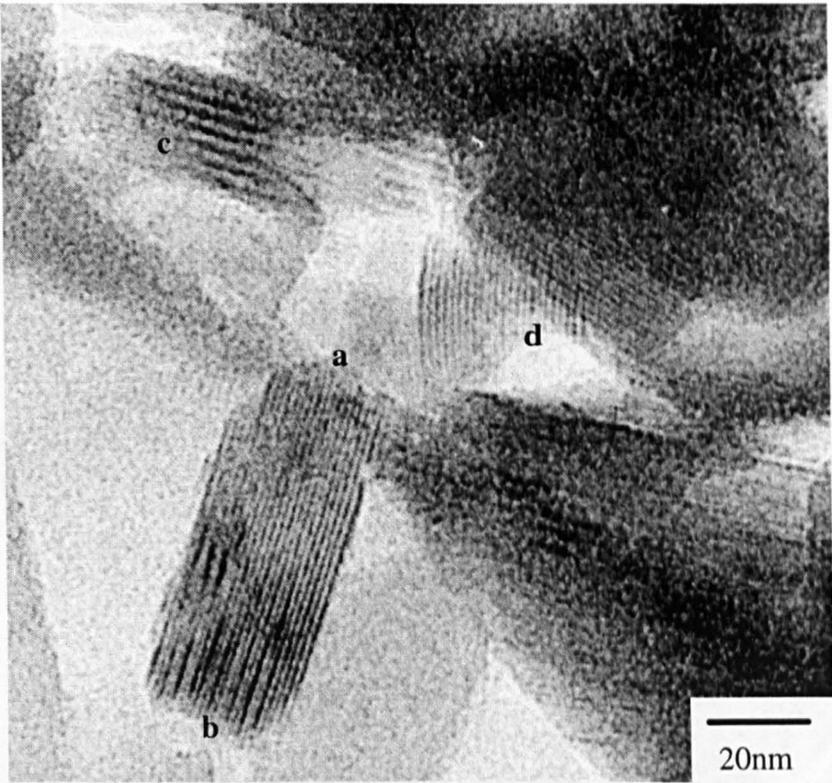
Figure 6.4

Figure 6.5

30nm
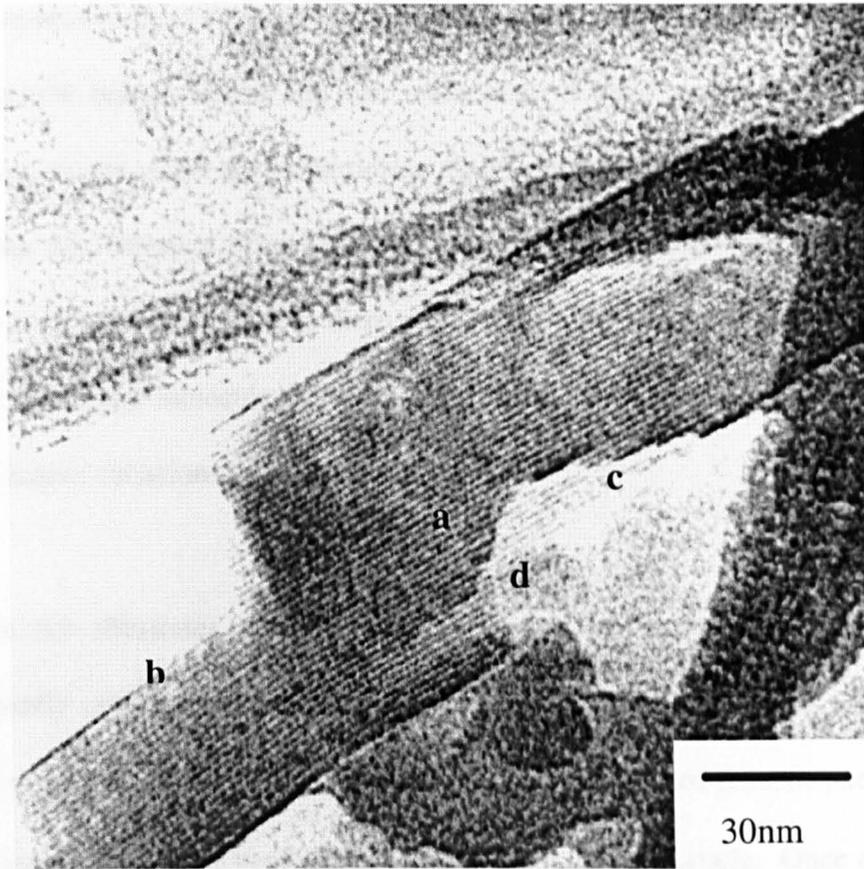
particles have coalesced during the growth process. This sample was grown in 30% nitrobenzene for 3 hours. Also, part of the crystal is strained as the lattice fringes again appear to bend slightly on going from **a** to **b**. At position **c** and **d** the edges of the particle being studied and one underneath it have a stepped nature causing a variation in the width of the particles. As the fringes here represent the (200) plane spacing, this variation occurs in 1.5nm steps. This corresponds to half the unit cell width in this direction and, as there are two molecules in the unit cell, a reduction in the width of one molecule at a time. Variations in the contrast indicate the presence of thickness variations in the particle.

Figure 6.6 illustrates another example of two or more of the largest particles apparently coalescing to produce continuous lattice fringes. This is a particularly large indanthrone particle and is from a vynamon sample of indanthrone. The fringes are clear at **a** but have been destroyed elsewhere in the particle. Once again, damage appears to have started at the far ends of the particle leaving only the fringes near the centre intact. However, it could also be the case that the particle is bent in some way leading to stronger diffraction in the centre. Overlapping particles at **b** can be clearly seen and give rise to crossed fringes in this area. All fringes in this images correspond to the (200) spacing. "Stepping" can be seen at **c** but this is obviously not occurring molecule by molecule, but in rather larger increments. This is likely to be the edge of one of the coalesced particles whilst other areas are probably due to overlapping particles.

Figure 6.7 is a particularly interesting image as it shows a lattice spacing not viewed in previous images. At **a** and **b** the common (200) spacing can be seen. However, on
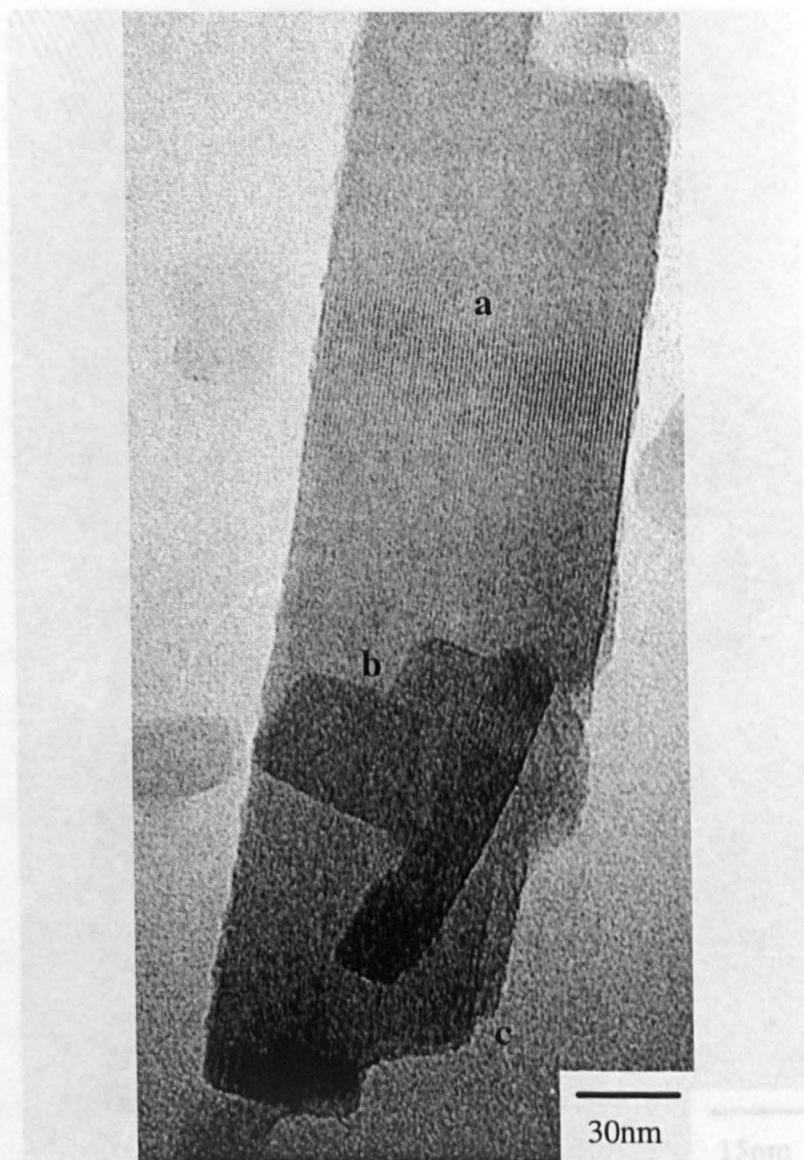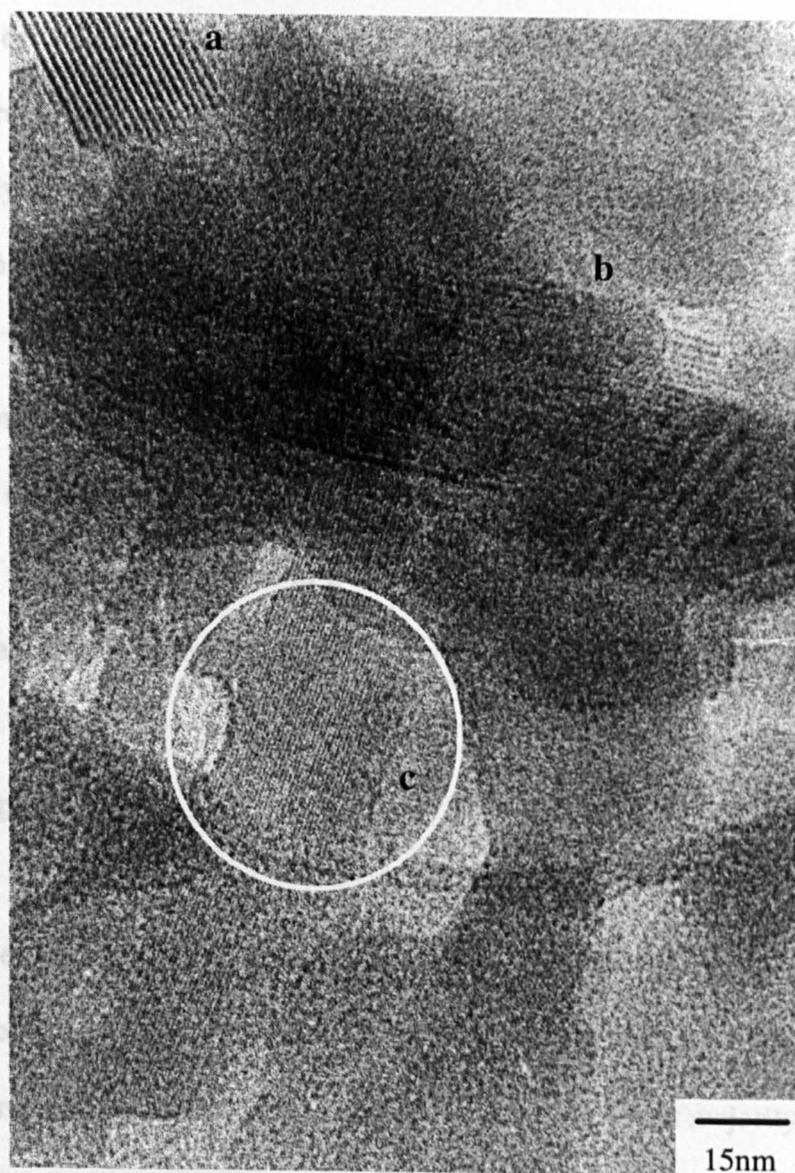
a

b

c

30nm

Figure 6.6

close examination of the image, the fringes at c were discovered. These were subsequently measured to be 0.72nm ± 0.5nm which corresponds to the basal spacing ... ... other particles elsewhere ... ... This image was obviously ... ... ently and with optimum ... ... In fact sample SD1654 ... ... which had undergone ... ... This may have affected ... ... These were the smallest ... ... It was fortunate that such sma... ... ...

15nm

Figure 6.7

It has be... ... ... and b-axis along the carbo... ... ... particles and the measure... ... ... of particles.

Many of the particles show that c... ... ... has been lost, especially at the ends of the particles. This is most likely to be due to radiation damage and was unavoidable.

Some particles appeared to have coalesced during the growth process causing lattice fringes to be continuous across what appeared to be more than one particle. These were viewed in samples which were refluxed in relatively high solvent

close examination of the image, the fringes at c were discovered. They were subsequently measured to be 0.72nm ± 0.5nm which corresponds to the (400) spacing of 0.77nm. There were other examples of these fringes on other particles elsewhere on the negative from which this image was taken. This image was obviously recorded before the area of interest was damaged significantly and with optimum imaging conditions for lattice imaging. This sample was in fact sample SD1654 which was a standard solvent treated indanthrone sample which had undergone additional treatment to control the growth of the particles. This may have affected the ability of the crystal to withstand electron irradiation. These were the smallest fringes viewed - and in a sample such as indanthrone it was fortunate that such small fringes were resolved.

6.4 Conclusions

It has been shown that the indanthrone particles lie with their elongated b-axis along the carbon support film. It is clear from the images of the pigment particles and the measurement of the lattice fringes that this is true for the vast majority of particles.

Many of the particles show that crystal detail has been lost, especially at the ends of the particles. This is most likely to be due to radiation damage and was unavoidable.

Some particles appeared to have coalesced during the growth process causing lattice fringes to be continuous across what appeared to be more than one particle. These were viewed in samples which were refluxed in relatively high solvent

concentrations (>30%) but not in samples refluxed in lower concentrations of solvent. This could be simply due to the fact that samples refluxed in lower concentrations of solvent and for relatively short times had poorer crystallinity which was destroyed by the electron beam in a shorter space of time. However, it could also be the case that coalescence happens later in the growth process after ripening has terminated, or both processes occur simultaneously after a certain amount of growth has taken place.

It is clear that growth is not continuous across all particles - both from the "stepping" seen causing width variations in some particles and from the contrast changes indicating thickness variations. The width variations which occurred "stepwise" indicated that the width was changing by the minimum amount possible - by one molecule at a time. This has obviously occurred during the growth process and was seen in various samples. It indicates that growth in these areas is incomplete and was possibly inhibited in some way.

Bending of the lattice fringes was relatively uncommon and therefore few of the crystals appear to be strained.

Finally, it is very difficult to view small fringes with a sample such as indanthrone. The 0.7nm fringes which were viewed backed up the conclusion that the particles lie in the orientation which was originally suggested. It was also interesting that fringes of this size were resolved irrespective of the problem of radiation damage and confirms that the maximum amount of information possible was extracted from the samples studied using this technique.

Chapter 7

STEM studies of indanthrone pigment

7.1 Introduction

This chapter aims to present the theory and results obtained from work carried out on the

VG HB5 STEM which was described in detail in chapter 3. The theory behind parallel

electron energy loss spectroscopy (PEELS) is given in section 7.2 including details of

how such spectra can be used to yield information on the specimen thickness. In section

7.3 the results from this technique are shown alongside the corresponding images of

indanthrone. Section 7.4 gives a very brief account of DPC imaging and is followed in

section 7.5 by the images obtained using this technique. Finally, in section 7.6,

conclusions are drawn from the information obtained using the STEM.

7.2 Parallel Electron Energy Loss Spectroscopy (PEELS) of indanthrone

When fast electrons are transmitted through a solid specimen they interact elastically and inelastically with the atoms in the specimen (Egerton, 1992). Electron energy loss spectroscopy (EELS) measures the energy distribution of electrons which have been transmitted through such a specimen. The resulting energy loss spectrum is a plot of the intensity as a function of the energy lost.

A typical energy loss spectrum can be seen on figures 7.1(a) and (b). Figure 7.1(a) spectrum shows a zero loss peak (ZLP) which represents electrons which have been transmitted through the specimen without any appreciable loss of energy. This includes electrons which are 'unscattered' having passed through the specimen with no loss of energy and are undeflected. The next most intense feature is the first plasmon peak where electrons have lost energy via plasmon excitations. This is highly visible in figure 7.1(b) which gives a closer view of the spectrum in 7.1(a). Plasmons are quantised collective excitation of valence electrons. Second and higher plasmon peaks arise from those electrons which have excited two or more plasmons. The region of the spectrum from the zero loss peak to ~50eV is known as the low loss region and can be very useful for determining information about the thickness of a specimen (Egerton, 1986, 1989 & 1992). The thickness information comes from measurement of the probability of inelastic scattering. The probability P_0 of no elastic scattering is represented by the area I_0 under the zero loss peak, relative to the total area I_t beneath the complete spectrum.
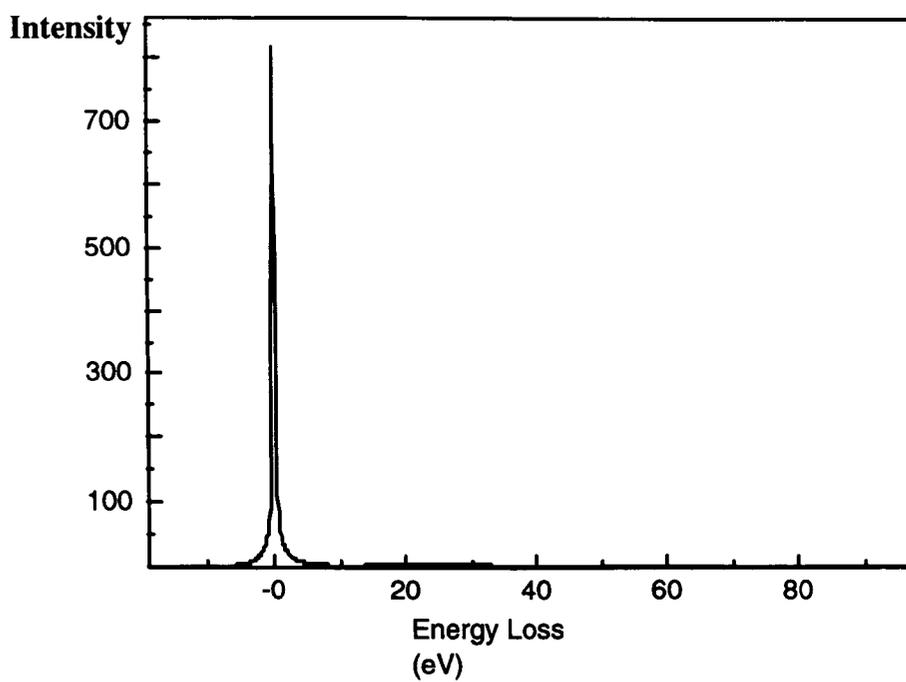
Figure 7.1(a) : Electron energy loss spectrum showing intense zero loss peak (ZLP)
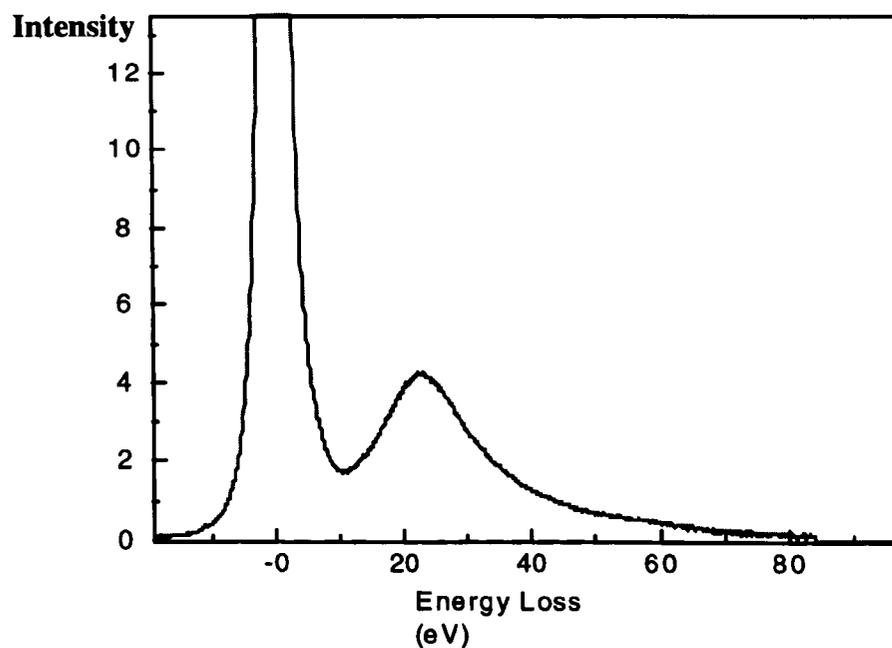
Figure 7.1(b) : Electron energy loss spectrum showing zero loss peak and subsequent plasmon peak

This probability is also given by Poisson statistics, in terms of the total mean free path for inelastic scattering, λ.

$$P(n) = (1/n!)(t/\lambda)^n exp(-t/\lambda)$$ (7.1)

Setting n=0 in this equation we get

$$P=I_0/I_t=exp(-t/\lambda)$$
$$\Rightarrow\ t/\lambda=ln(I_t/I_0)$$ (7.2)

λ is the total inelastic mean free path whose value depends on the incident electron energy E_0 and the collection semi-angle β (Egerton, 1992). λ is given (in nm and to an accuracy of +/- 20%) by

$$\lambda = \frac{0.106T}{E_m \ln(2\beta E_0 / E_m)}$$ (7.3)

where $E_m=7.6\ Z^{0.36}$, with Z being the mean atomic number of the specimen and T is the 'relativistically corrected' incident energy (in eV). With the standard PEELS set-up on the HB5, β is equal to 12.5mrad and T can be calculated from the following equation:

$$T = \frac{E_0(1+E_0/2m_0c^2)}{(1+E_0/m_0c^2)^2}$$ (7.4)

where E_0=100keV and m_0c^2=511keV. This gave a value of 120nm for the mean free path of indanthrone, whilst the mean free path of the carbon film was calculated to be similar to this at 110nm.

Although this method may not be totally accurate for calculation of absolute thickness, it is an excellent method for comparing the relative thickness of certain areas of sample.

The HB5 STEM was aligned for PEELS as described in section 3.10. Usually two iterations of the alignment procedure were necessary to ensure correct positioning of the relevant components within the column. Having obtained a zero loss peak, the microscope was ready for spectroscopy. The specimen was studied using the annular dark field detector. A major problem during this technique was finding areas of the specimen which were suited to detailed study. It was necessary to find particles which were isolated as far as possible from other particles to ensure there was no overlap of particles. It was also essential that individual particles overlapped holes in the carbon film. Such positioning of the particles enabled spectra to be acquired from indanthrone particles at points where they were unsupported by the carbon film. It was however acceptable for the particle to be supported at one or more points along the particle as long as the majority of the particle was unsupported. This ensured thickness values obtained corresponded to the indanthrone particle alone and all spectra could be recorded in this same way. It would have been far easier to record spectra from individual

particles on the carbon film, but non-uniformities in the carbon film would have contributed to errors and so this was avoided.

Having aligned the microscope and selected a generally good area of the specimen, it was then necessary to remove all the apertures and flood the specimen as described in section 3.10. The apertures could then be re-inserted and their position checked prior to recording spectra. This procedure had to repeated as often as appeared necessary. The signs of contamination are discussed in the next section of this chapter.

The spectra were recorded by positioning the probe on the desired area of sample and moving the specimen into the required position. Large movements were carried out using the mechanical shifts whilst small adjustments to position were made by use of the electrical shifts. Since such fine tuning had to be carried out at high magnification, this was carried out as quickly as possible to minimise contamination. The magnification was quickly lowered and the beam blanking system described in section 3.10 was switched on. The magnification could then be increased to the pre-determined level and a spectrum was recorded from the point of interest. It should be noted that the 'area' mode was used rather than the 'spot' mode for these acquisitions. This procedure was repeated for each of the desired points along a particle or group of particles. For each such set of spectra obtained, a dark current spectrum was also recorded. This can then be subtracted from the low loss spectra for subsequent analysis. An image of the area from which spectra were recorded was taken via a Link eXL digital imaging system.

Images were always recorded after spectra were taken for two main reasons. The first is that this avoids any unnecessary contamination being deposited on the sample until after the important information has been obtained. The second is that any contamination caused by the probe when recording the spectra will be easily viewed on the image. If there is sufficient evidence of such probe contamination, the data obtained during the suspect acquisition must subsequently be treated with severe caution. However, with regular flooding and care regarding the time spent on any one area, this was avoided in most instances.

After the spectra and corresponding images had been recorded, it was necessary to analyse the spectra. This was done with the aid of the same Gatan EL/P software used when collecting the spectra. The relevant dark current spectrum was subtracted from the low loss spectrum and using this 'corrected' low loss spectrum the t/λ value could be computed. Using the mean free path values stated earlier, a value for the thickness of the area of interest was then calculated. In the results that follow, the thicknesses of the areas of interest are tabulated below the corresponding image showing the points from which the spectra were taken.

7.3 Images and results from PEELS studies

As previously discussed, contamination was a major problem during acquisition of spectra. This was even more prevalent during earlier studies before regular flooding was

carried out. In these studies, the thickness of indanthrone appeared to be greater than its width. This did not fit in with previous thinking of how indanthrone particles orientated themselves in the application medium as shown earlier in Figure 1.2. This was found to be due to carbon build-up on the particle and the real thickness was thought, in general, to be smaller than the width of the particle. Also, the thickness of an indanthrone particle on the carbon film, was often a great deal smaller than the thickness of this same particle over a hole plus the thickness of an adjacent piece of carbon film. Alternatively, to find the thickness of a particle situated over a hole, the t/λ value for the adjacent piece of carbon could be subtracted from the t/λ value obtained from the particle over the film. Ideally one should then be left with a t/λ value equal to that of an indanthrone particle overlying a hole. The reason for this discrepancy between the values is most likely to be the fact that contamination was occurring in each of the measurements, and by adding the thickness of the indanthrone to the thickness of the carbon, contamination is being incorporated into the result twice. Similarly if the carbon t/λ is subtracted from the t/λ value for a particle on the carbon film, then the effect of contamination is cancelled out whereas contamination which has occurred on a particle over a hole cannot be removed in this way. It should be noted that particles selected for such study were those which appeared to have a relatively uniform thickness. Damage which occurred at higher magnifications (500K and above) during spectrum acquisition appeared as a small circular bright area on the sample. At lower magnifications this damage is characterised as a bright square area, equal in size to the area being scanned. However, after adopting the technique of regular flooding combined with vigilant observation of the sample for

any signs of contamination, this problem was greatly reduced. The t/λ values proved to be reproducible within approximately 5% margin for error.

This is illustrated in figure 7.2, which shows particles of a typical solvent treated indanthrone sample. The particle chosen for study appears to have uniform contrast along its length which indicated that this particle was of relatively uniform thickness. The image also showed no visible signs of damage or contamination by the probe after acquisition of the spectra. Table 7.1 shows that the data corroborates this fact. The addition of indanthrone thickness at position 2 with the carbon film at position 4 gives a value of 55.4nm which is very close to the combined thickness of 55.3nm measured at position 1. A second value of indanthrone thickness was measured at position 3 and demonstrated that the thickness of the particle was indeed relatively constant.

However, the purpose of using this technique to study indanthrone was to gain information on any thickness variations across particles. The majority of the subsequent particles chosen for study were those which showed signs of contrast variation in the ADF image in an attempt to understand what form these thickness variations take.

Figure 7.3 and 7.4 shows a particle which has not taken the lath-like form of the usual indanthrone particles. It is supported on holey carbon film, which can be seen by the increase in brightness and therefore increased thickness at these points. However, with the small probe size available, it is possible to work around these areas to gain

Figure 7.2

100nm
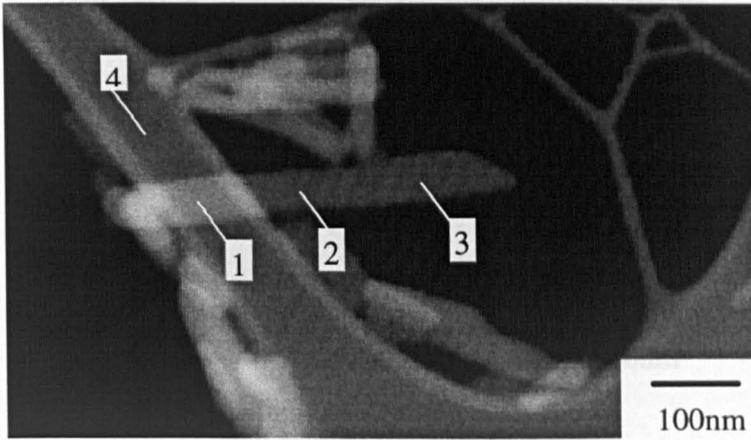
Table 7.1

	t/λ	thickness (nm)
1. ind on carb	0.5045	55.3
2. indanthrone	0.2187	25.1
3. indanthrone	0.2225	25.6
4. carbon	0.2763	30.3

Figure 7.3

50nm

Figure 7.4

30nm

Table 7.2

	t/λ	thickness (nm)
1	0.2096	24.2
2	0.2238	25.7
3	0.2861	32.9
4	0.2471	28.4

information on the indanthrone particle alone. Images were recorded at two magnifications to fully illustrate the change in contrast across the particle. At the more tapered left hand side, the brightness is somewhat lower than the rest of the particle. The brightness then increases in the middle area and is reduced on reaching the far end. The data in Table 7.2 shows a gradual increase in thickness initially, which then rises to almost 33nm, falling back down to 28.4nm at the right hand side. This indicates a particle which is wedge shaped at both ends of the length of the particle, although this wedge would appear to be somewhat asymmetric. It is difficult to ascertain exactly how these thickness variations are produced. However, the absence of sudden contrast changes on the image combined with the data obtained from this and similar images suggests that the thickness changes probably occur due to small steps or ledges rather than large changes associated with two particles lying on top of one another.

Having studied changes in particle thickness along the length of particles, it was thought that thickness values across the width of particles might also be of interest. One of those areas studied in this was the particles shown in figure 7.5. Spectra were recorded along the length of each particle and this was followed by a run of acquisitions spanning across the width of both particles. Once again, care must be taken with contamination, since detailed study such as this requires the probe to be focused on the sample for a longer total time. The particles can be seen to be of a particularly elongated nature and small changes in contrast can be viewed along the length of the particles. From Table 7.3 we can see that the narrower particle shows a variation in thickness of more than 13nm -

Figure 7.5

50nm
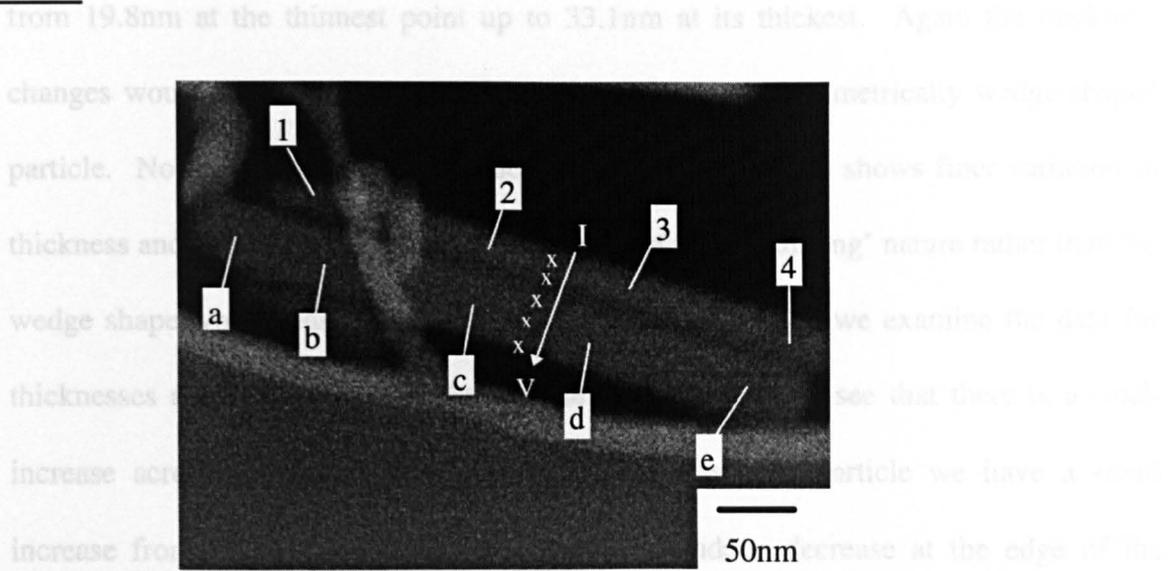
Table 7.3 : Across the length of the particles:

	t/λ	thickness (nm)
1	0.1719	19.8
2	0.2424	27.9
3	0.2874	33.1
4	0.2424	27.9
a	0.2655	30.6
b	0.2556	29.5
c	0.2696	31.1
d	0.2518	24.9
e	0.2707	31.2

Table 7.4 : Across the width of the particles:

	t/λ	thickness (nm)
I	0.234	27.0
II	0.2492	28.7
III	0.2476	28.5
IV	0.2543	29.3
V	0.1958	22.6

from 19.8nm at the thinnest point up to 33.1nm at its thickest. Again the thickness changes would appear to be gradual and this is another asymmetrically wedge-shaped particle. Notice that the wider particle situated directly below shows finer variation in thickness and would appear to be have a surface of an 'undulating' nature rather than the wedge shape which was studied previously. However, when we examine the data for thicknesses across the width of the particle in Table 7.4, we see that there is a small increase across the narrower particle but across the wide particle we have a small increase from 28.5nm to 29.3nm followed by a sudden decrease at the edge of the particle to 22.6 nm. Once again this forms a wedge shape although this time spanning the width of the particle rather than its length. As previous studies with the beam on the STEM eliminated mass loss caused by damage from the electron beam it is unlikely that this thinning at certain edges is due to radiation damage.

This can be further discounted when we examine images such as that shown in figure 7.6. It can be seen from the scale that these particles are relatively small. Table 7.5 shows that their corresponding thickness values, which fall within the 13nm to 20nm range, are also smaller than average indanthrone thickness measurements. The upper particle shows an increase as we track across the particle but no decrease in thickness at the far end. This particle would therefore appear to a one-sided wedge with 50% increase in thickness between the farthest ends. If radiation damage was causing thinning of the particle edges, we would surely expect both sides of the same particle to react in the same way to the electron beam. The thinning phenomena would therefore

Figure 7.6

appear to be solely due to processes prior to study by electron microscopy. The surface, however, the particle below is of perfectly even thickness and has therefore suffered damage by the [...] during manufacture or specimen preparation.

Another example [...] image and data shows that for particle take the [...] dimensions of the particle are somewhat larger than those illustrated in figure 7.6. The surface of this particle would appear to undergo a much more sudden increase in thickness on going from the area of

Table 7.5

the particle situated above the carbon film in the image to the area below. Although the carbon support causes difficulty there are [...] the image to indicate that this

	t/λ	thickness(nm)
1	0.1134	13.1
2	0.1571	18.1
3	0.1715	19.8
4	0.1697	19.6
5	0.1704	19.6

increase is caused by two separate particles sitting on top of one another. Coalescence of particles at some point in the growth process could cause such a variation as could a large ledge or step on the surface of the particle.

During collection of spectra from particles with thickness variations, the thinnest end of the particle was usually studied first since any contamination occurring would be immediately visible on areas of low contrast such as these. However, it was necessary to show that the increase in thickness which was observed was not as a result of additive effects of contamination as the probe traversed the particle. It was therefore important that a number of spectra were acquired from particles starting at what appeared to be the thickest end. An example of one such acquisition is shown in figure 7.8 and table 7.7.

appear to be solely due to processes prior to study by electron microscopy. In contrast however, the particle below is of perfectly even thickness and has therefore suffered no damage by the beam nor has any variation occurred during manufacture or specimen preparation.

Another example of this is shown in figure 7.7. The image and data show that this particle take the shape of a wedge. However, all dimensions of the particle are somewhat larger than those illustrated in figure 7.6. The surface of this particle would appear to undergo a much more sudden increase in thickness on going from the area of the particle situated above the carbon film in the image to the area below. Although the carbon support causes difficulty, there are no signs in the image to indicate that this increase is caused by two separate particles sitting on top of one another. Coalescence of particles at some point in the growth process could cause such a variation as could a large ledge or step on the surface of the particle.

During collection of spectra from particles with thickness variations, the thinnest end of the particle was usually studied first since any contamination occurring would be immediately visible on areas of low contrast such as these. However, it was necessary to show that the increase in thickness which was observed was not as a result of additive effects of contamination as the probe traversed the particle. It was therefore important that a number of spectra were acquired from particles starting at what appeared to be the thickest end. An example of one such acquisition is shown in figure 7.8 and table 7.7.

Figure 7.7

30nm
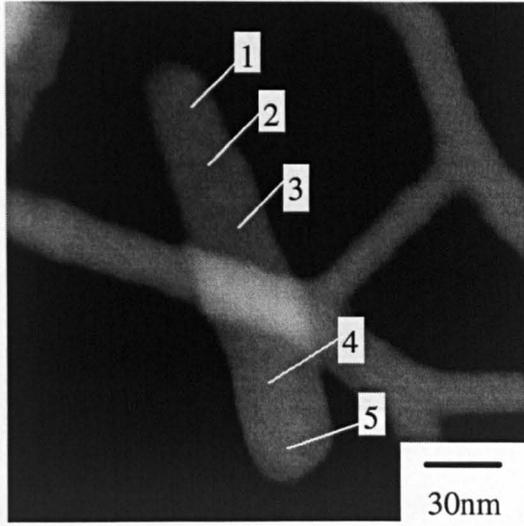
Table 7.6

	t/λ	thickness (nm)
1	0.2026	23.3
2	0.2119	24.4
3	0.2104	24.2
4	0.2715	31.3
5	0.2790	32.1

Figure 7.8
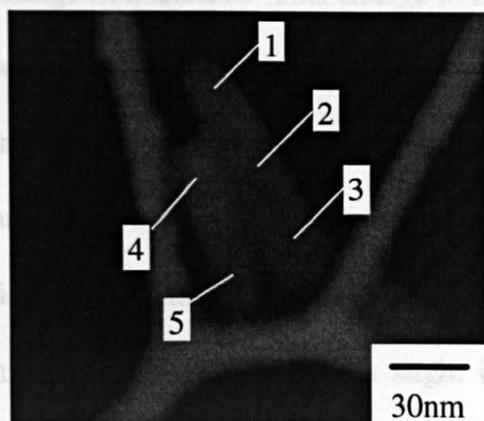
Table 7.7

	t/λ	thickness(nm)
1	0.1682	19.4
2	0.1484	17.1
3	0.1543	17.8
4	0.1925	22.2
5	0.1306	15.0

Both particles show a decrease in thickness with the smaller particle showing a particularly rapid change in thickness. This change in contrast can be easily seen on the image and suggests coalescence of two particles at an earlier stage in the growth process. This has resulted in a change in thickness in the region of 7nm and indicates the profile of the particle would show a single ledge or step rather than the gradual slope which would be present in a wedge shaped particle. The particle on the right exhibits a less dramatic fall in thickness and there is even a slight increase at the lower end. The contrast changes indicate a more gradual change in thickness than seen in the smaller particle. The thickness range for these particles falls between 15-22nm as would be expected for particles of this size and width.

In contrast to this, the particle shown in figure 7.9 is relatively long and wide although the contrast in the ADF image suggested it was rather thin. The surrounding particles and supporting carbon film are all much brighter and the contrast in the image had to be enhanced to make the particle more easily visible. Also, there would appear to be little in the way of contrast variation along the particle length and width. Spectra were taken at the points shown along the particle. Table 7.8 shows that the particle is indeed very thin considering the length and width. This would indicate that indanthrone particles have no fixed aspect ratio. As suspected, the thickness only varies by around 6% as we traverse the length of the particle. Such variations can be considered to be negligible and the upper surface of this particle is almost perfectly flat.

Figure 7.9
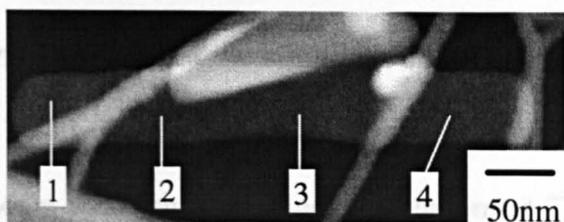
Table 7.8

	t/λ	thickness(nm)
1	0.1509	17.4
2	0.1465	16.8
3	0.1501	17.3
4	0.1548	17.8

Figure 7.10
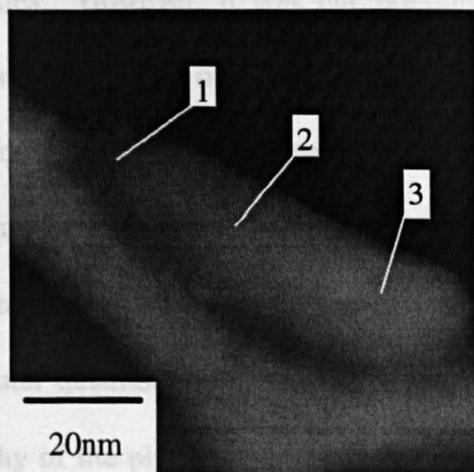
Table 7.9

	t/λ	thickness (nm)
1	0.1574	18.1
2	0.2108	24.2
3	0.2324	26.8

Finally, figure 7.10, which was recorded at higher magnification than most other images, gives a closer view of contrast variation in a small particle. It shows a small tapered particle cradled by a section of the holey carbon film. The particle thickness increases from 18nm to 24nm and then further increases to almost 27nm. This is reflected in the increased brightness shown at the relevant areas in the image and there does not appear to be any obvious probe damage.

7.4 Differential Phase Contrast Imaging of Indanthrone

CTEM images of indanthrone provided information on the size and distribution of indanthrone pigment particles. They also suggested that the particles might have some sort of thickness variation. This was confirmed using PEELS to give the thickness at points along particles. However, it was not possible to confirm the form of these thickness variations from the data obtained. A technique based on the differential phase contrast (DPC) mode of microscopy can provide simultaneous topographic information and also high contrast lattice images assuming that the dose required is sufficiently low. This imaging technique was described in sections 3.8 and 3.9. Using the difference signals from the outer quadrants of the detector, it is possible to obtain images which show the topography of the pigment particles. Ideally, the difference signals from the inner quadrants should give the lattice information on the pigment particles. However, this proved problematic due to the radiation sensitivity of indanthrone. Any lattice fringes which did appear faded almost instantaneously making acquisition of such

images almost impossible. Attempts were made to improve this situation including altering the resolution at which the images were recorded and reducing the magnification. Even with such measures, only a small number of lattice images were obtained and these are of poorer quality than was originally hoped. However, numerous topographic images were obtained and these provide more information on thickness variations along particles and indicate the presence of any ledges, steps or coalescing particles.

7.5 Images and Results from DPC studies

Figure 7.11 shows a topographic image of an area of solvent treated indanthrone. The topography is illustrated by the changes in contrast. This can be likened to the effect obtained by shining a light from a given direction onto the sample. The edges of the particles are clearly discernible and there would appear to be several overlaying particles and possibly some which have coalesced or are aggregates. At point **a,** two particles appear to have fitted almost exactly on top of one another causing a ledge on the surface. However, notice further down at **b** how there is a line of contrast running down the side edge. This tapers off and would appear to be a ledge on the upper particle. This kind of morphology would give rise to the thickness variations observed in the previous section as it shows a change in contrast along both the width and the length of the particle. Notice also, at point **c,** how the particles shape also tapers off and thinning of the dark line of contrast would indicate that the thickness is decreasing at this point also. At
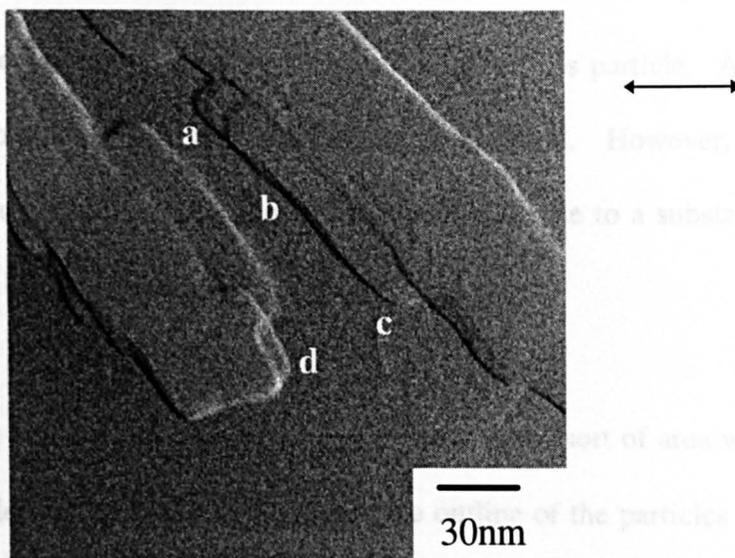
Figure 7.11 : DPC image showing topography of solvent treated indanthrone particles
Arrows show the direction of differentiation.
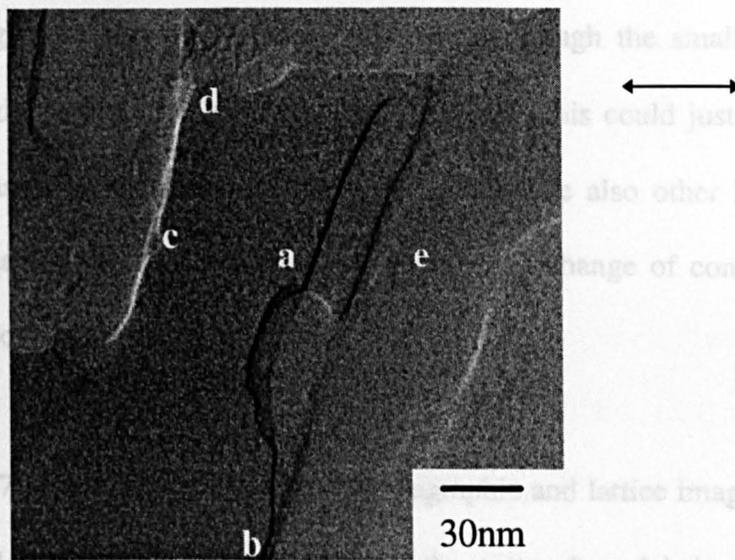
Figure 7.12 : DPC image showing topography of solvent treated indanthrone particles

point **d** we can see an interesting curve-shaped ledge on this particle. Again, if this is two overlaying particles, they are almost exactly matched. However, this does not explain the curious shape of the ledge which would give rise to a substantial thickness variation judging by its intensity.

In figure 7.12 we can see similar overlaying particles. This sort of area would probably not have been selected for PEELS study since the outline of the particles would suggest that this was almost certainly a group of particles. However, the way in which these particles have come together is interesting particularly at point **a**. This would appear to show two small particles and a longer tapered particle which is attached underneath an even larger particle. On closer study, it could be argued that one of the smaller particles is above the long one whilst the other is below even though the small particles are matched exactly down their left hand side. Alternatively this could just be one small particle which has a ledge feature at this point. There are also other ledge features visible in this image at **b, c** and **d**. Also at **e** there is a change of contrast which is indicative of an isolated area of reduced thickness.

Figures 7.13 and 7.14 are high magnification topographic and lattice images for an area of solvent treated indanthrone. These illustrate the curve-shaped ledges seen earlier, particularly at **a** and at area **b** there is another particularly strong ridge which has a rounded edge. This area is even more interesting when we turn to the corresponding lattice image. The lattice fringes running across this area are continuous across the
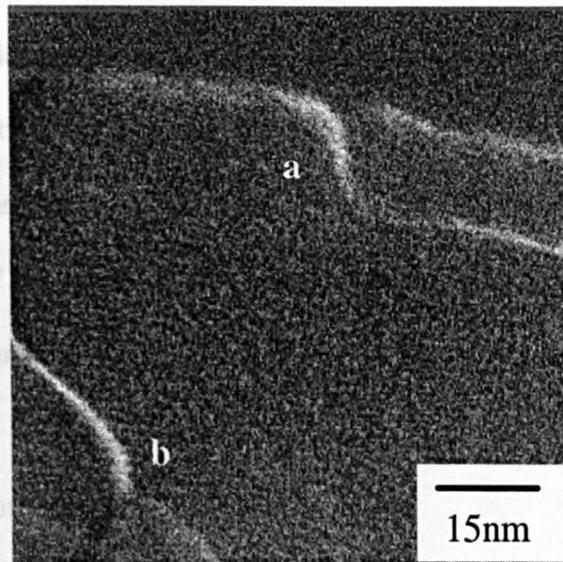
Figure 7.13 : DPC image showing topography of solvent treated indanthrone particles
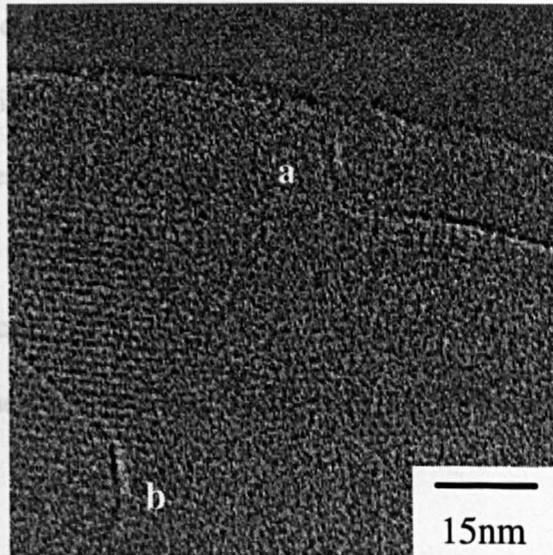

Figure 7.14 : DPC image showing corresponding lattice image of figure 16dec41

ledge. This would strongly indicate that this was not two separate particles on top of one another, but particles which coalesced during the growth process or a ledge on the surface of the particle. It must also be considered however that these fringes could be due to fringes of the particle underneath with the over-laying particle not showing any fringes. However, the intensity of the fringes would suggest that this is not the case and that the previous theory holds. This sort of surface phenomena could indeed cause the thickness variations found during PEELS studies.

Figure 7.15 is an example of a particle with ledges and steps which are almost certainly a characteristic of this one particle rather than suspecting the contrast variation was caused by other particles attaching themselves. On the surface of the particle at **a**, a ledge can be seen running diagonally across the particle but stopping short of the edges. This suggests this variation in thickness was caused during the solvent treatment growth process and indicates that something has occurred to prevent growth from continuing along this part of the particle. Another ledge can be seen at **b** where something similar has happened to cause this step down in thickness. Again, these surface characteristics would explain the data obtained during PEELS and ADF studies of solvent treated indanthrone.

In this section...

Figure 7.15 : DPC topographic image of solvent treated indathrone

7.6 Conclusions
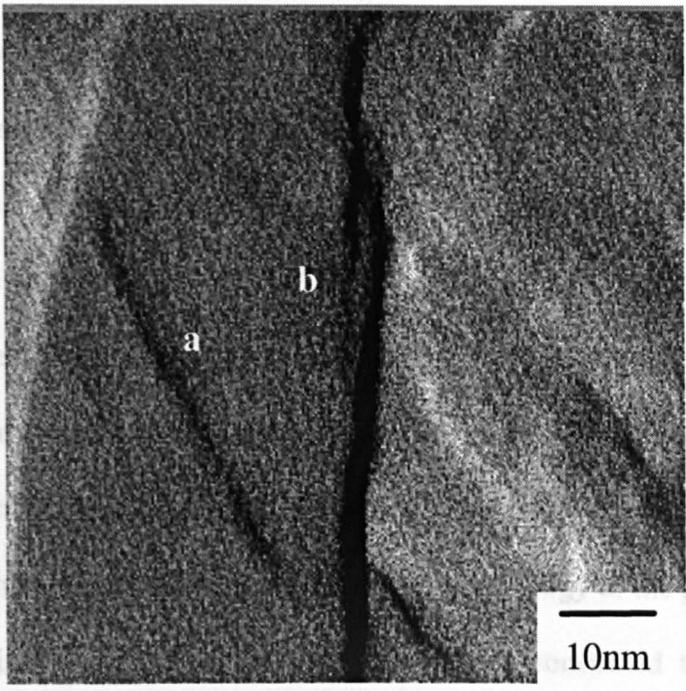
In this section, results obtained from PEELS and DPC studies of indanthrone pigments have been presented. A selection of samples were studied to ensure that a range of particle sizes were studied and also to ensure that characteristics which appeared were not confined to any one particular sample. These studies confirmed that thickness variations are indeed present along many particles. Since spectra were recorded along the particle from points a finite distance apart, it was difficult to determine exactly what form these thickness variations take. However, from the information gained from the spectra, estimates were made as to the surface morphology of the pigment particles. The images obtained in the DPC imaging mode have confirmed this suspicion. Some particles do indeed appear to have ledges and steps on their surfaces, both along the length and at the side edges. This gives some particle edges a terraced appearance and would lead to thickness variations along the particles. There is also evidence to suggest that particle coalescence is occurring and that particles can situate themselves on top of one another but aligned along the edges giving the appearance of a single particle in ADF imaging mode. This too would lead to the thickness variations observed the previous results section. To conclude, many of the indanthrone particles are not as smooth or regular in shape as first thought and the surfaces of the particles posses irregular features in the form of ledges and steps with less evidence to support a more gradual thickness variation.

Chapter 8

Conclusions and further work

8.1 Introduction

The aim of this work was to study the crystal growth of indanthrone during the pigmentation process. In this chapter the observations and conclusions from the preceding chapters are reviewed and discussed in terms of the study as a whole. Finally some ideas are given for possible further work.

8.2 Discussion

It has been shown that a number of parameters have an effect on the extent to which growth takes place in indanthrone. These include the choice of solvent, solvent concentration, time spent in the solvent, temperature, the method by which the solvent

was removed and the presence/absence of water in the reaction mixture. In terms of the actual particles, it was considered to be of interest to study their form and crystallinity by various techniques. The work carried out in this project is discussed in this section and conclusions are drawn.

The choice of solvent has been shown to be a significant parameter in these studies. From the low magnification studies, it was seen that isopropanol generated very little growth and was therefore not studied any further. Methyl benzoate and nitrobenzene both promoted growth in indanthrone although methyl benzoate studies were limited to relatively high concentrations of solvent. This implies that the ring structure plays an important part in the growth promotion stage and in particular that polarity may be an important factor. This is discussed in section 8.3.

After choice of solvent, the most influential parameter was found to be solvent concentration. This was particularly noticeable with the nitrobenzene studies where a range of concentrations were studied and the effects plotted graphically in terms of particle size and/or surface area. As discussed in chapter 4, there would seem to be three main types of behaviour with respect to the solvent concentrations studied. A solvent concentration that is too low results in a system where pigment particles are de-flocculated by the solvent particles, but do not get the chance to undergo growth. The second type of behaviour noticed is that used in normal pigment production where the pigments undergo growth over a period of a few hours at 20-30% concentration. From the surface area studies it was seen that a sudden initial increase in surface area indicating de-flocculation and initial growth was followed by a decrease in surface area as growth progresses. When water was not present in the

reaction mixture, a third type of behaviour was seen. This involved very sudden initial increase in surface area (again due to de-flocculation) followed by a much steeper decrease in surface area as growth. When these results were plotted together it could be seen that there was indeed a bifurcation in the plots which represented the addition or omission of water. From these studies we can conclude that the solvent does indeed exist in droplet form when in a water-rich mixture and that the pigment particles pass through these droplets to undergo growth and to de-flocculate. When there is water present however, they have the chance to re-flocculate on re-entering the water phase. The time spent in this water phase will obviously have a great impact on the amount of growth that is achievable. This also highlights the need for constant agitation during the solvent treatment stage.

Another parameter which relates to this is the time the pigment particles spend in the solvent mixture. The studies on this area also confirmed the above theory. Extended time in solvent is only of benefit if there is enough solvent for the particles to undergo growth in. A low level of solvent for an extended time will simply result in the particles passing in and out of the solvent phase where they undergo de-flocculation and possible a little growth. However, by spending longer periods of time in the water phase of the mixture the simply re-flocculate and the benefit of extending reaction time is non-existent. One of the studies did show however, that extended time had the effect of tightening the particle size distribution without causing a significant increase in the average particle size.

Solvents were removed from the mixtures by three different methods:- distillation, hydrolysis and filtration. The effects of each of these were studied in terms of growth

of the sample. It was found that distillation caused added growth when compared with hydrolysis. This would appear to be due to the fact that hydrolysis negates the solvents effectiveness immediately whereas distillation occurs over a period of almost one hour. Over this time, the level of solvent is decreasing steadily and so there is opportunity for further growth during this time.

Studies into the effect of temperature were carried out for samples treated with pure nitrobenzene. It was found that it took 5 hours for a mixture which was unheated to reach the same level as growth as a sample treated for 20 minutes as it was heated from room temperature to 80°C. This illustrates the importance of heat combined with constant agitation. The unheated mixture was stirred by hand at regular intervals rather than constantly agitated. Both of these are important in maintaining high mobility of the particles which will contribute to steady growth. The fact that such a strong effect was noticed in a mixture with pure solvent indicates that the same or even stronger effect would be seen in a water rich mixture and could be an area worthy of further study.

The trends identified by the low magnification and surface area studies strongly suggest that ripening is the primary mechanism for crystal growth in indanthrone particles. This has been illustrated via particle size distributions, average particle size measurements and standard deviations of particle size. The trends in growth with respect to time using various solvent concentrations also indicate that this is the case. However, some evidence has also been found for growth by coalescence particularly in samples grown for longer periods of time in a relatively high level of solvent. This was illustrated in the lattice fringe images seen in chapter 6. It would therefore be

reasonable to assume that initial growth takes place by ripening and as this process slows down due to a lower saturation of molecules available in the solution, coalescence may commence between particles which have already undergone a reasonable amount of growth.

The physical form of the crystals was an area studied in detail by this work. It had been thought previously that the crystals were even, regular and took a cuboid form. However, PEELS studies on the VG HB5 showed that there were in fact significant variations in the thickness of the crystals across both the length and breadth of the particles. Thickness values ranged from 13nm to 33nm across the range of samples studied whilst variations of up to 13nm were found in individual particles. This indicated that growth is not necessarily uniform and it was important to ascertain the nature of these thickness variations. DPC studies showed the topography of the particles and verified the presence of ledges and steps on the surface.

As the sample preparation technique was designed to mimic the application medium, it can be assumed that the particles take on a form similar to that viewed on the carbon film when applied to a paint or resin system. When the orientation of the crystals was studied by diffraction it was found that the b-axis had undergone most growth in almost all cases. The damage caused to the crystallinity by the electron beam caused serious problems when obtaining diffraction patterns. Nevertheless, the required information was obtained by using X-ray film and by taking various measures to reduce the amount of damage suffered by the specimen.

The crystallinity came under scrutiny again during high resolution studies. Generally, prior to electron beam damage, the lattice fringes which were resolved were straight, evenly spaced with any abnormalities being attributable to radiation damage. It has been shown however that a few were strained with bending of the fringes whilst other images depicted coalesced particles. This adds weight to the argument that ripening was not the sole growth mechanism in place.

8.3 Possibilities for further work

There are clearly some experiments which could be done for completion of the above studies. Some of those considered will be discussed in this section.

Further studies should be carried out relating to trends in growth. It is believed that average particle size measurements and standard deviations relating to these measurements could establish further trends particularly when combined with the corresponding surface area measurements. This information could then be used to optimise both pigment production and pigment performance simultaneously. Of particular interest would be a study relating to the limitation of particle size by the solvent concentration. This was touched on briefly in chapter 7 and would also yield further information relating to the water/solvent relationship during the solvent treatment process. This would involve further low magnification work using the JEOL TEM. For more detailed information on the extent of face-to-face packing of crystals, the ratio S_{BET}/S could be studied where S_{BET} is the specific surface area of the pigment powder and S is the specific surface area of the crystals determined from electron micrographs (McKay, 1989).

Continuing with further TEM work, additional lattice imaging studies would prove useful in the light of information gained regarding the growth mechanisms. Such studies could give crystallographic detail particularly with particles at opposite ends of the growth spectrum. It is not thought that diffraction would be an especially suitable technique for further study in this particular project.

The differential phase contrast (DPC) imaging work is obviously incomplete and a more thorough study would have been desirable. This would have led to more information on the surface topography. A greater understanding of the ledges and steps which appear on the surface of the particles would be beneficial combined with lattice fringes relating to the same area. Research should be carried out to quantify the steps and ledges by theoretical studies of the contrast variation. It would then be possible to determine whether the changes in thickness were occurring in one molecule stages or in multi-molecular steps. This imaging technique proved difficult due to a number of difficulties including radiation damage. However, with further experience in this technique it is believed that further surface knowledge would be obtained.

Solvent concentration has been shown to be an important parameter in the study of this pigmentation process. Therefore, dynamic effects should be studied to gain a better understanding of the solvent/water interaction. The size of the solvent droplets could be of particular importance as a limiting factor. The question arises as to whether this size varies with change in concentration or agitation method. One possible way of examining this in more detail would be by shining a laser through a

water/solvent mixture to determine the size of the solvent droplets. The time spent in the droplet of solvent by each particle must also be a significant contributing factor to the growth.

Finally, to fully understand how certain solvents promote growth whilst others do not, a more detailed study of a range of solvents could be carried out. This would enable the key factors such as structure, polarity and active sites during growth to be identified and could lead to the use of a superior solvent in terms of concentration required and environmental impact.

List of References

Alberty and Silbey, 1992, 'Physical Chemistry', First Edition, John Wiley and Sons Inc.

Bailey, M., 1955, Acta.Cryst., **8**, 182

Carr, W., 1978, JOCCA*, **61**, 397-410

Carr, W., 1982, JOCCA, **65**, 373-383

Chapman, J.N., McFadyen, I.R., McVitie, S., 1990, IEEE Transactions on Magnetics, **26**, 1506-1511

Cowley, A.C.D., 1987, JOCCA, **70**, 207-213

Dekkers, N.H., De Lang, H., 1974, Optik, **30**, 352

Dekkers, N.H., De Lang, H., 1977, Philips Tech. Rev., **37**, 1

Drummond, 1985, PhD Thesis, University of Glasgow

* Journal of Oil and Colour Chemistry Association

Dunning, W.J., 1972, Proceedings of the Symposium in Particle Growth in Suspensions, 3-28, Academic Press 1973, Society of the Chemical Industry no.38, Edited by A.L. Smith

Egerton, R.F., 1992, 'Quantitative Microbeam Analysis: Proceedings of the Fortieth Scottish Universities Summer School in Physics - Dundee', pp145-168, Co-published Scottish Universities Summer School in Physics and IOP Publishing, Bristol and Philidelphia.

Egerton, R.F., 1989, Ultramicroscopy, **28**, 215-225

Egerton, R.F., 1986, Electron Energy Loss in the Electron Microscope, First Edition, pp291-297, Plenum Press: New York and London

Fryer, J.F., McKay, R.B., Mather, R.R., Sing, K.S.W., 1981, J.Chem.Tech.Biotechnol., **31**, 371-387

Fryer, J.R., 1993[1], J. Phys. D: Appl. Phys. **26**, B137-B144

Fryer, J.R., 1980, J.Microscopy, **120**, 1-14

Fryer, J.R., 1993[2], MSA Bulletin, **23**, 44-56

Fryer, J.R., 1996, Private Communication

Gerson et al, 1993, United States Patent, Patent no. 5,248,336, Sept.28th

Honigmann, B., Horn, D., 1972, Proceedings of the Symposium in Particle Growth in Suspensions, 283-297

Honigmann, B., 1966, J.Paint.Tech., **38**, 77-84

Isaacson, M., 1979, Ultramicroscopy, **4**, 193-199

MacKenzie, M., 1997, PhD Thesis, University of Glasgow

Mather, R.R., 1981, Chemistry and Industry, 5th September, pp600-605

McColgan, P., 1989, Ph.D. Thesis, University of Glasgow

McKay, R.B., 1988, JOCCA, **71**, pp7-10

McKay, R.B., 1989, JOCCA, **72**, 89-93

McKay, R.B., 1993, JOCCA, **76**, 292-297

McVitie, S., 1997, Private Communication

Murphy, L.J., 1995, Private Communication

Myers, 1990, 'Introductory Solid State Physics', Taylor and Francis, London

Rideal, Sir E., 1972, Foreword to Proceedings of the Symposium on Particle Growth in Suspensions, Academic Press 1973, Society of the Chemical Industry no.38, Edited by A.L. Smith

Sappok, R., 1978, JOCCA, , **61**, 299-308

Shoemaker, Garland and Nibler, 1989, Experiments in Physical Chemistry, Fifth Edition, McGraw-Hill Book Company

Smith, J.M., 1997, Ph.D. Thesis, University of Glasgow

Swan and Felton, 1957, 'The Chemistry of Heterocyclic Compounds, Phenazines 11th Volume, Interscience Publishing Inc.

Wehr, Richards and Adair, 1984, 'Physics of the Atom', pp 220-224, Fourth Edition, Addison-Wesley Publishing Company.

Williams and Carter, 1996,'Transmission Electron Microscopy I,II & III', Plenum Press, New York

Wright, J.D., 1995,'Molecular Crystals', Second Edition, Cambridge University Press

Wyman, G.M., 1956, J.Am.Chem.Soc., **78**, 4599